1952

Gamma ray dosimetry with a scintillation counter

Prestwich, George Downes.

Massachusetts Institute of Technology

GAMMA RAY DOSIMETRY WITH A SCINTILLATION COUNTER

G. D. PRESTWICH AND T. H. COLVIN

GAMMA RAY DOSIMETRY

with a

SCINTILLATION COUNTER

by

GEORGE DOWNES PRESTWICH
B.S., U. S. Naval Academy
(1943)

and

TED HOWARD COLVIN
B.S., U. S. Naval Academy
(1944)

SUBMITTED IN PARTIAL FULFILLMENT OF THE
REQUIREMENTS FOR THE DEGREE OF
MASTER OF SCIENCE

at the

MASSACHUSETTS INSTITUTE OF TECHNOLOGY
(1952)

ABSTRACT

Title: "Gamma Ray Dosimetry with a Scintillation Counter"

Authors: George Downes Prestwich and
Ted Howard Colvin

Submitted to the Department of Physics on May 16, 1952 in partial fulfillment of the requirements for the degree of Master of Science.

ABSTRACT

Title: "Games Ray Tracing with a Pointillation Counter"

Author: George Thomas Prestwich and
Ted Howard Colvin

Submitted to the Department of Physics on May 12,
1982 in partial fulfillment of the requirements for
the degree of Master of Science.

In this paper we evaluate the worth of a scintillation counter as an instrument to measure gamma ray dosage; i.e., the energy absorption per unit mass. Data are obtained by calculations from differential pulse height spectra obtained with nearly monoergic sources in the 0.2 to 3 Mev range; and comparisons of average secondary electron energy with that theoretically expected are made. Also dosages calculated from the crystal output are compared with that obtained from an ion chamber.

It is concluded (on theoretical grounds) that organic crystals are much better suited for dosage measurements than inorganic types; and (on experimental grounds) that as the gamma ray energy is increased the finite size of the crystal causes the average secondary electron energy (and therefore the expected dosage) to decrease. This is explained by "leakage"; i.e., edge effects of the crystal. One can decrease this effect by surrounding the crystal in an air-equivalent medium such as lucite which reflects the secondary electrons back into the crystal.

Other experimental conclusions are: (a) Lucite light pipe and reflectors associated with the scintillator

In this paper we evaluate the merits of a scintillation counter as an instrument to measure beams for dosage; i.e., the energy absorption per unit mass. Data are obtained by calculations from differential pulse height spectra obtained with nearly monoenergetic neutrons in the 0.2 to 3 Mev range; and comparisons of average secondary electron energy with those theoretically expected are made. Also charges calculated from the crystal output are compared with that obtained from an ion chamber.

It is concluded (on theoretical grounds) that organic crystals are much better suited for dosage measurements than inorganic types and (on experimental grounds) that as the gamma ray energy is increased the finite size of the crystal causes the average secondary electron energy (and therefore the expected dosage) to decrease. This is explained by "leakage", i.e., edge effects of the crystal. One can decrease this effect by surrounding the crystal in an if-equivalent medium such as lucite which reflects the secondary electrons back into the crystal.

Other experimental considerations are: (a) Lucite light pipe and reflectors covered with the scintillator

have little effect on dosage. (b) Removal of photons from the beam, though an appreciable effect, can easily be computed and thus corrected. (c) Plural scattering effects in the crystals used are shown to be relatively unimportant. (d) Dosage determinations with the scintillation counter using our experimental set-up are somewhat indeterminate due to the difficulty in determining th window width of the differential discriminator. However values of dosage obtained are in reasonable agreement with those obtained from the conventional ion chamber. (e) A value of the gamma energy of radium which is a weighted average of the various energies according to abundance is experimentally determined. If meaningful it indicates that the gamma spectrum of radium is somewhat more energetic than indicated by the spectrum commonly accepted. It is felt, however, that these results are not too significant, due to the heterogeneity of the radium spectrum.

Thesis Supervisor: Robley D. Evans

Title: Professor of Physics

Thesis Supervisor: Dudley S. Evans

Title: Professor of Physics

TABLE OF CONTENTS

TABLE OF CONTENTS

LIST OF FIGURES

List of Figures

B-8	Secondary Electron Spectrum: Co^{60}; crystal con."B".
B-9	Secondary Electron Spectrum; Na^{24}; crystal con."A".
B-10	Secondary Electron Spectrum; Na^{24}; crystal con."B".
B-11	Secondary Electron Spectrum: Ra; crystal con."A".
B-12	Secondary Electron Spectrum: Ra; crystal con."B".
B-13	Calibration of Keleket Dosimeter No. X-3358.
B-14	Correction Factor for Keleket Dosimeter.

I. INTRODUCTION

A. Statement of Problem and Interest Therein.

All measurements of gamma ray dosage have, for years, been based on the air ionization chamber, for it can be simply made and rather easily calibrated to read dosage in roentgens. Of course, there are many survey instruments in current use which ostensibly read dosage rate, but these are usually counter tubes with output connected to an RC integrating circuit so as to give a DC current roughly proportional to the intensity of the radiation incident thereon. These are usually calibrated with the heterogeneous gamma spectrum of a standard radium source and are therefore of little value in obtaining an accurate estimate of roentgen dosage for sources other than radium.

A more comprehensive treatment of the meaning of "dosage" makes the reason for the preceding statement obvious and is to be found in Section II-A-2.

Many of the usual requirements of medical and other research physics are incompatible with the inherent characteristics of ionization chambers. Small size ion chambers are desired in order that "good" geometry may

I. INTRODUCTION

A. Statement of Problem and Interest Thereto.

All measurements of ionic ray dosage rate, for years, have been based on the air ionization chamber, for it can be simply made and rather easily calibrated to read dosage in roentgens. Of course, there are many survey instruments in current use which ostensibly read dosage rate, but these are usually complex tubes with circuits connected so as to interpret circuit so as to give a DC current roughly proportional to the intensity of the radiation reading thereon. These are usually calibrated with the ionization chamber response of a standard radium source and are therefore of little value in obtaining an accurate estimate of roentgen dosage for purposes other than reading.

A more comprehensive treatment of the meaning of "dosage" makes the reason for the preceding statement obvious and is to be found in Section II-A-2.

Many of the usual requirements of medical and other research physics are incompatible with the inherent characteristics of ionization chambers. Small size ion chambers are desired in order that "spot" geometry may

be obtained, or that a quantitative measure of activity localized in a small area, and the exact position of that small area, be obtained. However, when we try to meet the small size requirements, we find that the exposure time must be very long in order to get an accurate reading of dosage and to obtain dosage rate therefrom. For example, the small Victoreen chamber is a very convenient size, but reads 250 roentgens full scale. For the usual tracer dose in medical physics where the dosage to be measured is of the order of 10 mr/hr or less, it is clear that the length of time to obtain a reasonable scale reading is prohibitive. If one finds a chamber which has a reasonable scale, i.e., 200 mr full scale or less, the physical dimensions are apt to be ten times larger than the area to be localized.

Thus we see that a need exists for a small yet efficient instrument for dosage measurements. The use of a scintillation counter for this purpose was suggested to the authors by Dr. Gerald J. Hine of the Radioactivity Center, M.I.T., and with his advice and encouragement, this investigation was begun. The smallness of the scintillation crystal would permit good "localization"

be obtained, or that a quantitative measure of activity
localized in a small area, and the exact position of
that small area, be obtained. However, when we try to
meet the small size requirements, we find that the
exposure time must be very long in order to get an
accurate reading of charge and to obtain charge rate
therefrom. For example, the small fluctrons employed
in a very convenient size, be it route 000 transform
full scale. For the usual trader dose in medical
service simply the charge to be measured is of the order
of 10 mr/hr or less. It is clear that the length of
time to obtain a reasonable scale reading is prohibitive.
If one finds a chamber which has a reasonable scale,
i.e., 000 or full scale or less, the physical dimensions
are apt to be ten times larger than the area to be
localized.

Thus we see that a good optic for a small pet
efficient instrument for dosage measurements. The use
of a scintillation counter for it is improved via suggested
in this opinion by Dr. Gerald J. Hine of the Brookhaven
Center, B.N.L., and with his advice and encouragement,
this investigation was begun. The sensitivity of the
scintillation crystal would permit good "localization"

of an activity, or its use in a "good" geometry experiment, while its density, which is many times that of air, would render much more efficient sampling of the radiation incident thereon, permitting more rapid measurements of dosage and dosage rate with small activities.

Recent authors[1] have stated that organic scintillators "should be relatively 'air-equivalent'" in the region above 500 Kev, i.e., the domain of most gamma emitters. We shall show that the statement is easier said than demonstrated. The meaning of the term "air-equivalence" and its significance for this problem are discussed in Section II.

B. Methods of Approach.

It would be very convenient to have a compact instrument which would cause a needle to deflect an amount proportional to the dosage rate at the instrument probe's position. The initial efforts of the authors were along this line, and led deeper and deeper into an electronic morass, until the electronic complications threatened to obscure the physical principles involved in obtaining a dosage measurement from a scintillator. At length it was rather conclusively shown that the

of an activity, or its use in a "game" geometry
environment, with its density, which is every class
that of air, would render such more efficient qualifying
of the radiation treatment systems, necessitating more
rigid measurements of energy and density rods with
small activities.

Recent authors[1] have stated that ozonide
ultrafiltrate "should be relatively 'air-equivalent'"
in the region above 800 Kev, i.e., for density of most
dense matters. We should show that the statement is
rather half than determination. The meeting of the
case "air-equivalence" and its significance for this
problem are discussed in Section II.

4. Methods of Measure.

It would be very convenient to have a compact
instrument which would enable a checks to deliver an
atomic proportional to the energy rate of the instrument
probe's position. The initial efforts of the writing
were along this line, and the device was deeper into
an electronic measure, until the electronic complication
discouraged to observe the current variations involved
in obtaining a dosage measurement from a scintillator.
At length it was rather conclusively shown that the

electronic equipment under experimentation would never be able to do the job with an error satisfactory for research work. A comprehensive evaluation of the circuitry involved is presented in Section III-A.

Therefore, in order to by-pass the electronic difficulties and investigate the physical feasibility of dosimetry with a scintillation counter, the troublesome parts of the electronic circuit were removed and replaced partly with other types of electronic equipment and partly with two human beings. The authors realize that this is a bit far afield from the original desire for a "needle deflection". However, the determinations made and results obtained are basic to the problem. We shall leave the development of electronic circuitry to the electronic experts if the experimental physical determinations prove favorable to scintillation dosimetry; the reader is referred to Section V for our conclusions. A complete discussion of the final equipment and its manner of operation is to be found in Section III-B; while the results obtained therewith are to be found in Section IV-A et seq. Before proceeding to the experimental side, however, we must review a considerable amount of theory regarding the gamma ray interactions with matter.

II. THEORETICAL BASIS FOR THE PROBLEM

A. Basic Considerations.

1. Effect of Gamma Rays on Matter.

In considering a problem involving the "dosage" due to gamma radiation, it is first necessary to review in general the mechanisms by which gammas interact with matter and how these interactions pertain in particular to the problem at hand. First of all, what is "dosage"?

Physically speaking, the end result of all gamma interactions in matter is ionization of the atoms therein. Physiologically speaking, the ionization of matter is a disruption of the constituents of the matter and in it is contained the danger to health; in it is the manifestation of "dose". This ionization requires energy supply, and the gamma beam is the source thereof. The production of ion-pairs is not, however, in one-to-one correspondence with gamma-electron collisions as one might naively think. Indeed, a single gamma-electron collision produces one ion-pair, but the electron member of the pair has a large energy, on the average roughly half that of the incident gamma

II. Dimensional Basis for the Problem

---

1. Basic Considerations.

I. Effect of Gamma Rays on Matter.

In considering a problem involving the "dosage" due to gamma radiation, it is first necessary to realize in general the mechanisms by which gamma rays interact with matter and how these interactions depend in particular to the problem at hand. First of all, what is "dosage"?

Physically speaking, the end result of all gamma interactions in matter is ionization of the atoms therein. Physiologically speaking, the ionization of matter is a disruption of the constituents of the matter and in it is contained the danger to health; in it is the manifestation of "dose". This ionization requires energy simply, and the gamma does it the source thereof. The production of ion-pairs is [illegible], however, in one-to-one correspondence with photo-electron ejections at some higher energies this. Instead, a single gamma-electron collision produces one ion-pair, but the electron emits of the pair has a large energy, on the average roughly half that of the incident gamma

ray, or in the domain of thousands of electron-volts. Since the energy required for the production of an ion-pair in material such as air or tissue is of the order of tens of electron-volts, the energetic electron resulting from a single gamma-electron collision can and does produce many other ion-pairs, until its energy is fully expended. It is by this process, the step-by-step dissipation of the energy of the "secondary electrons" as the energetic fellows are termed, that the energy absorbed from the gamma ray beam is translated into ionization in the material.

2. The Roentgen.

The "roentgen" is the unit of dosage, and expresses the measure of gamma ray effect on matter in terms of the ionization discussed above. A roentgen is defined[3] as "that quantity of x- or gamma radiation such that the associated corpuscular emission per 0.001293 gm of air produces, in air, ions carrying one electrostatic unit of charge of electricity of either sign".

The corpuscular emissions referred to in the definition are the "secondary electrons" of our terminology. The quantity of air is 1 cc of dry air at 0° C and 760 mm Hg. Since 1 esu = 2.083×10^{9} ion-pairs, 1 roentgen produces 1.61×10^{12} ion-pairs per gram of air. If an

II. THEORETICAL BASIS FOR THE PROBLEM

A. Basic Considerations.

1. Effect of Gamma Rays on Matter.

In considering a problem involving the "damage" due to gamma radiation, it is first necessary to review in general the mechanisms by which gamma rays interact with matter and how these interactions pertain in particular to the problem at hand. First of all, what is "damage"?

Physically speaking, the end result of all gamma interactions in matter is ionization of the atoms therein. Physiologically speaking, the ionization of matter is a disruption of the compatibility of the matter and in it is contained the danger to health; in it is the annihilation of "dose". This ionization requires energy simply, and the gamma here is the source thereof. The production of ion-pairs is not, however, in one-to-one correspondence with gamma-electron collisions at the higher energies. Indeed, a single gamma-electron collision produces one ion-pair, but the electrons emitted at the peak use a large energy, on the average roughly half that of the incident gamma

ray, or in the domain of thousands of electron-volts. Since the energy required for the production of an ion-pair in material such as air or tissue is of the order of tens of electron-volts, the energetic electron resulting from a single gamma-electron collision can and does produce many other ion-pairs, until its energy is fully expended. It is by this process, the step-by-step dissipation of the energy of the "secondary electrons" as the energetic fellows are termed, that the energy absorbed from the gamma ray beam is translated into ionization in the material.

2. The Roentgen.

The "roentgen" is the unit of dosage, and expresses the measure of gamma ray effect on matter in terms of the ionization discussed above. A roentgen is defined[3] as "that quantity of x- or gamma radiation such that the associated corpuscular emission per 0.001293 gm of air produces, in air, ions carrying one electrostatic unit of charge of electricity of either sign".

The corpuscular emissions referred to in the definition are the "secondary electrons" of our terminology. The quantity of air is 1 cc of dry air at 0° C and 760 mm Hg. Since 1 esu = 2.083×10^{9} ion-pairs, 1 roentgen produces 1.61×10^{12} ion-pairs per gram of air. If an

average of 32.5 e.v. is expended [4,5] then 1 r corresponds to 5.24×10^7 Mev/gm of air. We shall have occasion to refer to this number later.

It should be noted that dosage is independent of time, due to the definition of the dosage unit of roentgens; therefore gamma ray dosage rates are given in roentgens/unit time; e.g., mr/hr = milliroentgens per hour. Also of importance is the concept of dosage rate as a measure of ionization intensity and <u>not</u> a measure of <u>gamma</u> intensity, for the reasons discussed above.

3. Production of Secondary Electrons.

The first process encountered then in the production of dosage by gamma radiation is the production of the secondary electrons. Here we encounter the well-known threefold process of importance in this problem by which gamma rays interact with electrons in matter: (a) Compton collisions, (b) photoelectric effect and (c) pair production. We have referred above to gamma-electron collisions, a term which is descriptive but not essentially true except for (a). In the Compton process, the gamma photon may be considered as a relativistic "cue ball" colliding with a free object ball at rest, with the usual consequences of billiard

ball collisions; i.e., transfer of energy with conservation of total mass-energy and momentum. In the photo-effect, the gamma may be considered as being swallowed whole by an atom, which then usually relieves itself by disgorging an electron with energy equal to that of the gamma ray minus the electronic binding energy. In pair production, an interaction explainable only in quantum terms occurs, in which a gamma ray, finding itself in the intense fields in the immediate vicinity of a nucleus, becomes so confused that it commits quantum suicide and is reincarnated as a positron-electron pair, which share an amount of energy equal to that of the gamma ray minus the rest energy of these particles (1.02 Mev).

All three of the above effects can and will occur in all materials, and (except for pair production with its mass-energy threshold of $2 m_0 c^2 = 1.02$ Mev) for <u>any</u> energy gamma ray. Happily, it frequently happens that one effect predominates to the near exclusion of the others, when one considers a <u>particular</u> material and a <u>particular</u> range of gamma energies. For example, for low gamma energies, in the domain less than 100 Kev for materials of moderate to high atomic number, the photoelectric effect predominates. For high gamma

energies, say above 3 Mev, and for high atomic number material, pair production predominates. Finally, for the great middle range of gamma energies and for materials of low atomic number such as air and tissue, the Compton effect predominates.

4. Secondary Electron Interactions.

Having seen in general how the energetic secondary electrons are produced, let us see how they produce the ionization, i.e., the real "dosage". At this point comes the basic stumbling block in our problem. In air, (that is, in the medium for which dosage units are defined) the energy of the secondary electrons is converted into ionization by a series of "soft billiard ball" collisions. That is, the cue ball (secondary electron) loses a little bit of its energy in each ionizing collision with a molecule, until it is all gone, after which we have a medium filled with ions, positive or negative, floating around. In an ionization chamber, the collecting electrodes then remove the charged particles. If no electrodes are present, recombination very shortly occurs. The total number of ion-pairs is proportional to the energy of the secondary electrons, since as pointed out above, the energy required for production of an ion-pair is roughly constant at about 32.5 e.v./ion-pair.

For this reason, one can make an air ionization chamber which collects the ion-pairs formed, measures their total charge and therefore has a measure of dosage.

In a scintillation crystal, however, one does not collect any charge and measure it. Indeed, the mechanism of the scintillator is complicated and has not been fully investigated [6]. Suffice it to say that the ionization which secondary electrons produce in the crystal causes a flash of visible light (or in the near ultraviolet range), which, in anthracene, has been shown to produce a photomultiplier voltage pulse proportional in amplitude to the energy of the secondary electron initiating it [7,8]. Thus we see that the final effect of gamma irradiation of a scintillator is entirely different from the effect in air, in terms of which dosage is defined. Nevertheless, if we can obtain a measure of the light intensity by the voltage pulses it produces, we have a measure of the rate of energy absorption from the gamma ray into the secondary electrons. If then the energy spectrum of the secondary electrons produced in the scintillator is the same as, or approximates the energy spectrum of the secondary electrons produced in air, we have a measure of the "dosage" which the same gamma intensity would produce

on a cc of air at the scintillator's position, for the ionization produced in air is also proportional to secondary electron energy. There are, of course, a few complications, which will be considered in due course of this paper.

We shall see later how one goes about measuring the number and amplitude of the pulses due to the light flashes and obtains a measure of dosage therefrom. Before that, there is a criterion to be applied which determines the type of scintillator appropriate for the stated purpose.

B. Average Energy of the Secondary Electrons.

1. Relation of Average Energy of Secondary Electrons to Dosage.

Since the energy of the secondary electrons produced by the photons in the scintillator is related to the energy absorbed from the gamma beam and thus to the dosage, it is of interest to calculate the variation in the average secondary electron energy produced in a given material by the variation of gamma energy. Because dosage is defined in terms of charge produced in air, we will determine this variation for air, anthracene, and sodium iodide. The choice of anthracene

and sodium iodide crystals for this determination is dictated by the fact that these are the two crystals most used in scintillation counting today; anthracene, the organic type; sodium iodide, the inorganic type. Anthracene being a hydrocarbon, one would expect that it would be "air-equivalent"; that is to say, over the range from 0.1 Mev to 10 Mev one would expect that the Compton effect greatly predominates over the photoelectric effect and pair production in materials of low atomic number. For such a condition, it will be shown that the average secondary electron energies are identical for the materials satisfying it. Conversely, since sodium iodide is inorganic and contains elements of moderate atomic number, one would expect such a crystal to be "air-equivalent" only over a much reduced range or not at all. It is anticipated that sodium iodide will be inherently unsuitable for gamma ray dosimetry because of its lack of "air-equivalence".

2. Formula for Average Energy of Secondary Electrons.

How then does one find the average energy of the secondary electrons? We shall consider first that the gamma energy is a continuous variable, producing secondary electrons in a small thickness. From such a determination we shall later show how an effective average secondary

electron energy can be obtained for a particular source and finite crystal thickness.

Let E_γ = gamma ray energy in Mev.

n = number of photons/cm^2-sec of energy E_γ incident on material considered.

A = effective area of incidence (cm^2).

σ = total Compton cross section in cm^2/electron.

σ_a = Compton absorption cross section in cm^2/electron.

σ = Compton linear attenuation coefficient in cm^{-1}.

σ_a = Compton linear absorption coefficient in cm^{-1}.

τ = photoelectric linear attenuation coefficient in cm^{-1}.

K = pair production linear attenuation coefficient in cm^{-1}.

μ = total linear attenuation coefficient in cm^{-1}

$= \sigma + \tau + K$.

μ_a = linear absorption coefficient in cm^{-1}

$= \sigma_a + \tau + K$.

W = binding energy of "K" electron.

Then the energy/sec absorbed in a thickness dx [10] = the total energy/sec of the secondary electrons = E_T:

electron energy can be obtained for a particular atomic and field crystal ionizer.

Let E_γ = photon ray energy in ev.

n = number of electrons/cm^3-mon of energy E_γ incident on material considered.

A = effective area of ionizer (cm^2).

σ_o = total Compton cross section in cm^2/electron.

σ_a = Compton Absorption cross section in cm^2/electron.

σ = Compton Linear attenuation coefficient in cm^{-1}.

σ_a = Compton linear absorption coefficient in cm^{-1}.

γ = photoelectric linear attenuation coefficient in cm^{-1}.

K = pair production linear attenuation coefficient in cm^{-1}.

μ = total linear attenuation coefficient in cm^{-1}

$= \sigma + \gamma + K$.

μ_a = linear absorption coefficient in cm^{-1}

$= \sigma_a + \gamma + K$.

δ = kinetic energy of e^- electron.

Then the energy/sec absorbed in a thickness Δr (cm) = the total energy/sec of the secondary electrons = E_γ

$$E_T = nAdx\left[\sigma_a E_\gamma + \tau(E_\gamma - W) + K(E_\gamma - 2m_o c^2)\right] \quad \text{(II-B-1)}$$

where $2m_o c^2$ = energy equivalent of 2 electron rest masses. Let the number of secondary electrons produced per sec = N; then

$$N = nAdx(\sigma + \tau + K) = \mu nAdx \quad \text{(II-B-2)}$$

Therefore the average electron energy is

$$E_{AV} = \frac{E_T}{N} = \frac{\sigma_a E_\gamma + \tau(E_\gamma - W) + K(E_\gamma - 1.02\ \text{Mev})}{\sigma + \tau + K} \quad \text{(II-B-3)}$$

It is of interest to consider the magnitude of W for the materials of interest, remembering our minimum E_γ = 0.1 Mev.

Table II-B-1

Element	W
H	Negligible
C	Negligible
N	Negligible
O	Negligible
Na	1.07 Kev
I	33.2 Kev

3. Calculation of Attenuation and Absorption Coefficients.

In order now to compute E_{AV} as a function of E_γ

$$E_{Ta}^{\lambda} = \max\left[Q\,\beta_{Ta}^{\lambda} + J\,(E_{Ta}^{\lambda} - E) + K(E_{Ta}^{\lambda} - 1.02\ \mathrm{Mev})\right] \qquad \text{(II-9-4)}$$

where β_{Ta}^{λ} = number multiplets of λ electrons resulting. Let the number of permissible electrons resulting be 3, then

$$E = \max(Q + J + K) = \text{multiplet} \qquad \text{(II-9-5)}$$

Therefore the electron binding energy is

$$E_{Ta} = \frac{E_{Ta}}{\lambda} = \frac{Q\,\beta_{Ta}^{\lambda} + J\,(E_{Ta}^{\lambda} - E) + K(E_{Ta}^{\lambda} - 1.02\ \mathrm{Mev})}{Q + J + K} \qquad \text{(II-9-1)}$$

It is of interest to consider the magnitude of E for the materials of interest, remembering for minimum $E_{Ta}^{\lambda} = 0.7$ Mev.

Table II-9-1

Element	E
Z	Negligible
Q	Negligible
R	Negligible
J	Negligible
Be	1.02 Mev
I	33.4 Mev

3. Determination of Ionization and Absorption Coefficients.

In order to compute E_{Ta} as a function of λ

for each material, one must first find or compute values of σ, σ_a, τ, K. See Appendix A for these computations and the results.

4. Comments on Computed Secondary Electron Average Energy.

Now having the required attenuation and absorption coefficients we can return to formula (II-B-1) and compute E_{AV} for E_γ in the range 0.1 Mev to 10 Mev. The results of these computations are displayed in Figure 1. Figure A-1, a plot of computed μ over the range of interest is included for use with later theory requirements. Here we see that anthracene is theoretically truly "air-equivalent" from 0.2 Mev to 8 Mev, while sodium iodide deviates widely from the air curve for $E_\gamma < 1$ Mev. We note that even down to 0.1 Mev, anthracene is theoretically substantially "air-equivalent".

From the above theoretical calculation, it was decided that sodium iodide and other inorganic crystals had average electron energies far greater than air for $E_\gamma < 1$ Mev, since the secondary electron energy for photoelectric absorption is $E_\gamma - W$ which is far greater than $\frac{\mu_a}{\rho}E_\gamma$ at low energies, (for $E_\gamma = 0.1$ Mev, $\frac{\mu_a}{\rho} = 0.14$) and would thus give too great a measure of dosage. Thus the remainder of our measurements and theory is based on

for each material, one must first find by numerous values of σ, σ_0, T, λ. See Appendix V for these computations and the results.

6. Comments on Computed Secondary Electron Average Energy.

See Table VIII for the required extrapolation and absorption coefficients to use values to formula (IX-4-j) and compute $\bar{E}^{\lambda}_{K}$ for E^{λ} in the range 0.1 kev to 10 kev. The results of these computations are displayed in Figure I. Figure 4-I, a plot of computed $\bar{\kappa}$ over the range of interest is included for use with later theory requirements. Here we see most noticeable is theoretically truly "air-equivalent" from 0.1 kev to 3 kev, while nothing inside deviates widely from the air curve for $E^{\lambda} < 1$ kev. We note east even down to 0.1 kev, substance is theoretically substantially "air-equivalent".

From the above theoretical exploitation, it was decided that nothing inside and other interesting crystals had average electron energies for ejection into air for $E^{\lambda} < 1$ kev, since the secondary electron energy for photoelectric absorption is $E^{\lambda} - B$ which is far greater than $\frac{dE}{dx}^{\lambda}$ at the energies, (for $E^{\lambda} = 0.1$ kev, $\frac{D}{d} \approx 0.14$) and would thus give too great a measure of change. Thus the remainder of our measurements and theory is based on

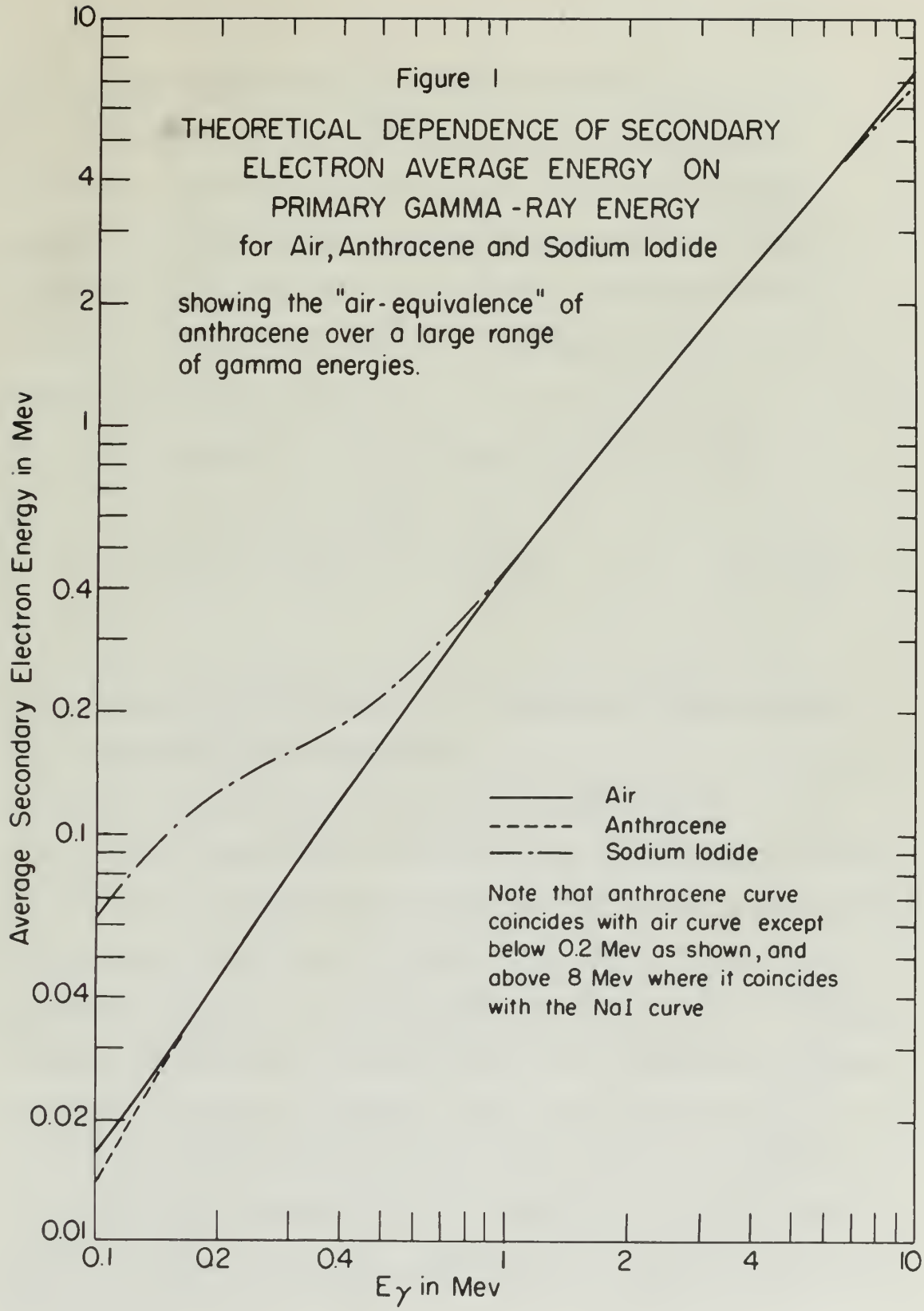
Figure 1
THEORETICAL DEPENDENCE OF SECONDARY ELECTRON AVERAGE ENERGY ON PRIMARY GAMMA-RAY ENERGY
for Air, Anthracene and Sodium Iodide
showing the "air-equivalence" of anthracene over a large range of gamma energies.
Air
Anthracene
Sodium Iodide
Note that anthracene curve coincides with air curve except below 0.2 Mev as shown, and above 8 Mev where it coincides with the NaI curve
Average Secondary Electron Energy in Mev
10
4
2
1
0.4
0.2
0.1
0.04
0.02
0.01
0.1
0.2
0.4
1
2
4
10
Eγ in Mev

the use of anthracene as a scintillator.

Since we will be dealing with anthracene from here on, and with 0.1 Mev $< E_\gamma <$ 8 Mev, we can make an obvious simplification of formulas (II-B-1) and (II-B-3). For carbon and hydrogen, W is negligible; also no pair production is observable. Therefore, these equations become

$$E_T = nAdx(\sigma_a + \tau)E_\gamma = n\mu_a E_\gamma A dx \qquad \text{(II-B-4)}$$

$$E_{AV} = \frac{\sigma_a E_\gamma + \tau E_\gamma}{\sigma + \tau} = \frac{\mu_a}{\mu} E_\gamma \qquad \text{(II-B-5)}$$

C. Theoretical Treatment of Quantities to be Measured in the Scintillation Crystal.

1. Average Electron Energy Significance.

We have seen that the absorption of energy from the gamma beam in the crystal results in the production of secondary electrons. We have also seen that each such electron gives a pulse of light which produces a voltage pulse proportional in amplitude to the electron energy. As will be shown in Section IV-A we can then obtain (1) a quantity expressing the total amount of energy per unit time received by the electrons in the crystal from the gamma ray, i.e., the rate of energy absorption

the case of multiprocess as a particle.

Since we will be dealing with multiprocess from here on, and with $0.1\ \mathrm{Mev} < E_\gamma < 3\ \mathrm{Mev}$, we can make no obvious simplification of formulas (II-3-1) and (II-3-2). For carbon and hydrogen, γ is negligible; also no pair- production is observed. Therefore, these equations become

$$E_\gamma^{\lambda} = \max(\alpha^{\beta} + \gamma)E_\gamma^{\lambda} = m\alpha^{\beta}{}_{\lambda}\alpha_{\beta} \qquad \text{(II-3-4)}$$

$$E_{\lambda\alpha} = \frac{\alpha^{\beta}{}_{\lambda} + \gamma\,\delta_{\lambda}^{\beta}}{\alpha + \gamma}\frac{p_\beta}{E_\gamma^{\lambda}} \qquad \text{(II-3-5)}$$

C. Theoretical Treatment of Quantities to be Measured in the Ionization Chamber.

1. Average Electron Energy Significance.

We have seen that the absorption of energy from the gamma beam in the crystal results in the production of secondary electrons. We have also seen that each such electron gives a pulse of light which produces a voltage pulse proportional in amplitude to the electron energy. As will be shown in Section IV-4 we can then obtain (1) a quantity representing the total amount of energy per unit time received by the electrons in the crystal from the gamma ray, i.e., the rate of energy absorption

in the crystal; and (2) a measure of the total number of electrons energized per unit time. Ostensibly, dividing (1) by (2) should give us a measure of the secondary electron average energy, for comparison with the theoretical curve obtained in B above (Fig. 1); while (1), since it represents the energy absorbed from the gamma beam, should be a measure of dosage and related to the "air-dose" in roentgens. That these conclusions are not quite so simple and direct but subject to modification in theory, disregarding experimental difficulties, is the purpose of this and the following divisions in Section II. (Authors' note: Immediately after the following theory was evolved, part I of a paper by Whitcher [17] was published, dealing with a very similar situation in liquids. Unfortunately, part II of the paper is to contain the calculations of interest and will not be available until after May 16, 1952. Attention is invited thereto when available.)

C. Relation between E_{AV} and Dosage.

To begin with, let us assume that each gamma photon has only one interaction in the crystal. The consequences of multiple interactions are considered later in Section II-D. Now from Section II-B we have the equations Total secondary electron energy/unit time produced in a thickness dx =

$$E_T = n\mu_a E_\gamma A dx \qquad \text{(II-B-4)}$$

$$I^{\beta} = \int \rho^{\beta}_{\gamma} E_{\gamma} dx \qquad (II\text{-}5\text{-}4)$$

Total number of secondary electrons produced/unit time in dx =

$$N = n\mu A dx \qquad \text{(II-B-?)}$$

For the moment we shall treat E_γ as single valued; i.e., a monoenergic source is being used:

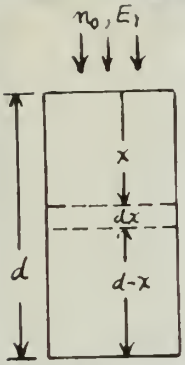

If the crystal is very thin, then n is constant and = n_o, the number of photons/ cm^2-sec incident on crystal face. Obviously for this case,

$$E_T = n_o \mu_a E_\gamma A d \qquad \text{(II-C-1)}$$

and $$N = n_o \mu A d \qquad \text{(II-C-2)}$$

Here $E_{AV} = \frac{\mu_a}{\mu} E_\gamma$ again and agreement should be obtained with the curve of Section II-B.

Also, suppose that one used two different monoergic sources E_{γ_1} and E_{γ_2}, for which there were the corresponding quantities n_{o_1}, μ_1, μ_{a_1} and n_{o_2}, μ_2, μ_{a_2}. If E_T is truly a measure of roentgen dosage rate as would be recorded by an ion chamber as rates R_1 and R_2, say, then the ratio

$$\frac{R_1}{R_2} = \frac{n_{o_1} \mu_{a_1} E_{\gamma_1}}{n_{o_2} \mu_{a_2} E_{\gamma_2}} \qquad \text{(II-C-3)}$$

Such a ratio holds strictly true for the "air-wall" ion chamber according to Evans [10] and Rossi and Staub [27]

Total number of secondary electrons produced/unit time
is Sx =

$$S = \text{delta} \tag{12-3-d}$$

For the moment we shall treat δ^{λ} as a single material i.e.,
a monoenergetic source is being used:

If the crystal is very thin, then n is
constant and = n^{0}, the number of electrons/
cm^{3}-sec incident on crystal face. Correspondingly
the flux rate,

$$\Phi^{\lambda} = n^{0} p_{\lambda} \epsilon_{\lambda} \lambda c \tag{12-c-1}$$

and $R = R^{0} e^{-\mu x}$ (12-c-2)

Here $R^{\lambda} = \frac{h}{h^{0}} \epsilon^{\lambda}$ again and agreement should be obtained
with the above of Section 12-c.

Also, suppose that one used two different monoenergetic
sources $\epsilon^{\lambda 1}$ and $\epsilon^{\lambda 2}$, for which there were the corresponding
quantities $n^{0 1}$, p_{λ}, $R^{\lambda 1}$ and $n^{0 2}$, p_{λ}, $R^{0 2}$. If δ^{λ} is truly
a measure of resulting doserate rate as would be received
by an ion chamber as rates S^{1} and S^{2}, say, then the ratio

$$\frac{S^{1}}{S^{2}} = \frac{n^{0 1} \nu^{\lambda} \epsilon^{\lambda 1} \delta^{\lambda}}{n^{0 2} \nu^{\lambda} \epsilon^{\lambda 2} \delta^{\lambda}} \tag{12-c-3}$$

Such a ratio ought directly serve for this rule-of-
thumb accounting as Evans [10] and Tuddal and Stone [27]

since dose rate $R = \frac{nE_\gamma \mu_a}{\rho}$ in Mev/min-gm air; and if we can satisfy the assumptions made to date then

$$\frac{E_{T_1}}{E_{T_2}} = \frac{R_1}{R_2} \qquad \text{(II-C-4)}$$

2. Removal of Photons.

The difficulty, however, lies in the assumptions. Let us first consider the effect of crystal thickness. The very advantage of the scintillation crystal is its increased efficiency; that is to say, it has many more gamma interactions than an equivalent volume of air. But if we increase the number of interactions, then n is not constant and equal to n_o but follows the usual "good" geometry attenuation law

$$n = n_o e^{-\mu x}$$

Therefore, for a crystal of thickness d,

$$E_T = \int_o^d n_o e^{-\mu x} \mu_a E_\gamma A dx$$

$$= n_o \mu_a E_\gamma A d \left(\frac{1 - e^{-\mu d}}{\mu d} \right) \qquad \text{(II-C-5)}$$

and

$$N = n_o \mu A \int_o^d e^{-\mu x} dx$$

$$\frac{\bar{I}^B}{\bar{I}^T} = \frac{\bar{I}^B_0}{\bar{I}^T_0} \qquad \text{(II-C-1)}$$

2. Presence of photons.

The difficulty, however, lies in the assumptions.
Let us first consider the effects of physical difference.
The next expansion of the multiplication symbol is the
increased efficiency that is to say, it has many more
terms interacting than an equivalent volume of air. But
it is because the number of interactions, when n is not
constant and equal to n^0 but follows the usual "bump"
secondary expansion law

$$n = n^0 e^{-\mu x}$$

Therefore, for a slabful of thickness x,

$$\bar{E}^A = \int_0^x n^0 e^{-\mu x} \bar{N}^B \bar{E}_\lambda \, dx$$

$$= n^0 \bar{N}^B \bar{E}_\lambda q \left(\frac{1 - e^{-\mu q}}{\mu q} \right) \qquad \text{(II-C-2)}$$

and

$$\bar{E} = n^0 t \int_0^x e^{-\mu x} \, dx$$

one satisfy the assumptions made in note item
$\frac{k}{\mu^2 \bar{N}}$ in slab/air-to air; and it be

$$N = n_o \mu A d \left(\frac{1 - e^{-\mu d}}{\mu d} \right) \qquad \text{(II-C-6)}$$

These equations reduce to (II-C-1) and (II-C-2) of course in the limit of small μd; i.e., for d small compared to $\frac{1}{\mu}$, the mean free path for scattering.

We note that $E_{AV} = \frac{E_T}{N}$ is unchanged by this correction and still equals $\frac{\mu_a}{\mu} E_\gamma$.

However the ratio $\frac{E_{T_1}}{E_{T_2}} = \frac{R_1}{R_2}$ is no longer strictly true if μd is not $<< 1$. That is

$$\frac{E_{T_1}}{E_{T_2}} = \frac{n_{o_1} \mu_{a_1} E_{\gamma_1} (1 - e^{-\mu_1 d})/\mu_1 d}{n_{o_2} \mu_{a_2} E_{\gamma_2} (1 - e^{-\mu_2 d})/\mu_2 d} \qquad \text{(II-C-7)}$$

and depending on crystal thickness and E_γ, we would not theoretically <u>expect</u> that our measurements would give the same dosage ratio as an air-wall ion chamber. The magnitudes of these corrections will be presented later and an evaluation of the expectation values obtained.

3. Non-monoergicity.

The second assumption, that of monoergic E_γ, is readily removable. We shall generalize our notation a bit: Let p_{ji} = percent abundance of i^{th} gamma ray from j^{th} source.

$$N = E^{\circ}_{Pbg} \left(\frac{1 - \beta_{-mg}}{\beta_{mg}} \right) \qquad \text{(II-C-8)}$$

These equations reduce to (II-C-5) and (II-C-6) of course in the limit of small β; i.e., for a small recovered to $\frac{1}{N}$, the mass transfer(pass for centering.

We note that $\Sigma^{Pb} = \frac{1}{N}$ is unchanged by this extraction and still equals $\frac{1}{N} \Sigma^{A}$.

However the ratio $\frac{\Sigma^{Pb}}{\Sigma^{T}} = \frac{\beta^{Pb}}{\beta^{T}}$ is no longer strictly true if β_{Pb} is not $<< 1$. Then it

$$\frac{\Sigma^{Pb}}{\Sigma^{T}} = \frac{\sigma^{Pb}_{a} N^{Pb} \Sigma^{T} (1 - e^{-\lambda T_{eq}})/\lambda T_{eq}}{\sigma^{T}_{a} N^{T} \Sigma^{T} (1 - e^{-\lambda T_{eq}})/\lambda T_{eq}} \qquad \text{(II-C-7)}$$

and depending on crystal thickness and σ^{Pb}, we would not theoretically recover that our measurements would find the same decay ratio as at all-well the absorber. The neutron-tubes of these extractions will be investigated later but an evaluation of the experimental points obtained.

3. Non-conservation.

The second assumption, that of conservation Σ^{Pb} is easily reasonable. We shall investigate our neutron a bit:

Let β^{Pb} = decay probability of T_{eq} times the time T_{eq} system.

$E_{\gamma_{ji}}$ = energy of i^{th} gamma ray from j^{th} source.

μ_{ji} = total linear attenuation coefficient corresponding to $E_{\gamma_{ji}}$.

$\mu_{a_{ji}}$ = linear absorption coefficient corresponding to $E_{\gamma_{ji}}$.

n_{o_j} = total number of photons/cm^2-sec incident from j^{th} source.

Then $n_{o_{ji}} = \frac{n_{o_j} p_{ji}}{\sum_i p_{ji}}$ = photons/cm^2-sec of i^{th} energy incident, (II-C-8)

and define $\bar{E}_{\gamma_j} = \sum_i (p_{ji} E_{\gamma_{ji}}) / \sum_i p_{ji}$ (II-C-9)

(For example the two γ's from Co^{60} have abundances of 100 percent each and energies of 1.17, 1.33 Mev.) If Co^{60} is j^{th} source considered, then

$$n_{o_{j1}} = \frac{n_{o_j}}{2}; \quad n_{o_{j2}} = \frac{n_{o_j}}{2}; \quad \bar{E}_{\gamma_j} = \frac{1.17 + 1.33}{1 + 1} = 1.25 \text{ Mev.}$$

Then for the i^{th} γ from the j^{th} source,

$$dE_{T_{ji}} = n_{o_{ji}} E_{\gamma_{ji}} \mu_{a_{ji}} A e^{-\mu_{ji} x} dx$$

$$dN_{ji} = n_{o_{ji}} \mu_{ji} A e^{-\mu_{ji} x} dx$$

and for the aggregate beam from j^{th} source,

ing for the attenuation power flow J_{qp} source.

$$dE^{jr} = \mu^{jr} k^{jr} \nu e^{-\alpha^{jr} x} dx$$

$$dE^{jr} = \mu^{jr} E^{jr} \nu^{jr} e^{-\alpha^{jr} x} dx$$

Then for the J_{qp} & from the J_{qp} source,

$$\sigma^{jr} = \frac{\delta}{\mu^{o}}; \; \mu^{jr} = \frac{\mu^{o}}{3}; \; E^{jr} = \frac{1.7 + 1.2}{1.7 + 1.2} = 1.22 \text{ Nev.}$$

J_{qp} source considered, then

(For example the two λ's from Co_{60} have abundances of 100 percent each and energies of 1.17, 1.33 Mev.) If Co_{60} is

$$\text{and define } \Sigma^{jr} = \sum_{i} (b^{ir} \nu^{jr}) \Big\backslash \sum_{i} b^{ir} \tag{II-5-9}$$

instead.

$$\text{Then } \mu^{o jr} = \frac{\sum_{i} b^{ir}}{\mu^{o} b^{jr}} = \text{photons/cm}^2\text{-sec of } J_{qp} \text{ source} \tag{II-5-8}$$

J_{qp} source.

$\mu^{o jr}$ = total number of photons/cm^2-sec incident from

to E^{jr}.

μ^{jr} = linear absorption coefficient corresponding

b^{jr} = point linear attenuation coefficient corresponding

E^{jr} = energy of J_{qp} photon and from J_{qp} source.

$$dE_{T_j} = \sum_i n_{o_{ji}} E_{\gamma_{ji}} \mu_{a_{ji}} A e^{-\mu_{ji} x} dx$$

$$dN_j = \sum_i n_{o_{ji}} \mu_{ji} A e^{-\mu_{ji} x} dx$$

Again integrating over the crystal thickness we obtain:

$$E_{Tj} = \sum_i n_{o_{ji}} E_{\gamma_{ji}} \mu_{a_{ji}} Ad \left(\frac{1 - e^{-\mu_{ji} d}}{\mu_{ji} d} \right) \qquad \text{(II-C-10)}$$

$$N_j = \sum_i n_{o_{ji}} \mu_{ji} Ad \left(\frac{1 - e^{-\mu_{ji} d}}{\mu_{ji} d} \right) \qquad \text{(II-C-11)}$$

$$\text{whence } E_{AV_j} = \frac{\sum_i n_{o_{ji}} E_{\gamma_{ji}} \mu_{a_{ji}} \left(\frac{1 - e^{-\mu_{ji} d}}{\mu_{ji} d} \right)}{\sum_i n_{o_{ji}} \mu_{ji} \left(\frac{1 - e^{-\mu_{ji} d}}{\mu_{ji} d} \right)} \qquad \text{(II-C-12)}$$

$$\text{and } \frac{E_{T_j}}{E_{T_k}} = \frac{\sum_i n_{o_{ji}} E_{\gamma_{ji}} \mu_{a_{ji}} \left(\frac{1 - e^{-\mu_{ji} d}}{\mu_{ji} d} \right)}{\sum_i n_{o_{ki}} E_{\gamma_{ki}} \mu_{a_{ki}} \left(\frac{1 - e^{-\mu_{ki} d}}{\mu_{ki} d} \right)} \qquad \text{(II-C-13)}$$

We now see that the correction for non-monoergicity results in several changes in procedure.

(a) Eq. (II-C-12) can be written:

$$E_{AV_j} = \frac{\sum_i n_{o_{ji}} E_{\gamma_{ji}} \frac{\mu_{a_{ji}}}{\mu_{ji}} (1 - e^{-\mu_{ji} d})}{\sum_i n_{o_{ji}} (1 - e^{-\mu_{ji} d})}$$

$$\Omega_{\pi}^{\pi} = \sum_{\pi}^{\pi} \Omega^{\pi} \Gamma_{\pi} \Gamma_{\pi} \Gamma_

There we see that $E_{\gamma_{ji}} \frac{\mu_{a_{ji}}}{\mu_{ji}} = E_{AV_{ji}}$, the value which would be picked off the curve of Figure 1, corresponds to $E_{\gamma_{ji}}$.

Therefore, in order to evaluate the intrinsic equivalence of anthracene to air by the "most nearly correct" theory available to date, we must <u>compute</u> E_{AV_j} for the j^{th} source from the curve, and compare it to the measured value. The value obtained will depend on crystal thickness d; we shall see presently how violently. Also, one can compute a "partially corrected" E_{AV_j} by omitting the terms in $\mu_{ji}d$; which also gives an idea of the effectiveness of crystal thickness attenuation. As we shall see in Section IV, the experimental results may then be compared with the "totally corrected" and "partially corrected" values. The theoretical values are presented in tabular form in Table (II-C-1) and are presented in graphical form along with the experimental results in Section IV, Figures 7 and 8.

<u>TABLE II-C-1</u>

Source	$\bar{E}_\gamma$ ×	E_{AV} (partially corrected)	E_{AV} (totally corrected) d = 6 mm	E_{AV} (totally corrected) d = 20 mm
Hg^{203}	280 Kev	72.1 Kev	72.1 Kev	72.1 Kev
Cs^{134}	698 Kev	271.5 Kev	265.9 Kev	266.5 Kev
Co^{60}	1.25 Mev	586. Kev	584. Kev	584. Kev
Na^{24}	2.07 Mev	1.109 Mev	1.028 Mev	1.037 Mev

×From formula (II-C-9).

There we see that $E_{\gamma}^{\gamma 2} \frac{e^{-\gamma 2 t}}{t^{\gamma 2}} = \Sigma^{\gamma 2}{}_{12}$, the value which would be picked off the curve of Figure 1, corresponds to $\Sigma^{\gamma 2}$.

Therefore, in order to evaluate the intrinsic equivalence of anticoncco to air by the "most nearly correct" energy available to date, we must determine $\Sigma^{\gamma 2}$ for the γ_{02} source from the curve, and compare it to the measured value. The value obtained will depend on crystal thickness di we shall see presently how critical. Also, one can compute a "partially corrected" $\Sigma^{\gamma 2}$ by omitting the terms in $b^{\gamma 2} g_i$ which also gives an idea of the effectiveness of crystal thickness attenuation. As we shall see in Section IV, the experimental results may then be compared with the "totally corrected" and "partially corrected" values. The theoretical values are presented in tabular form in Table (II-C-1) and are presented in graphical form along with the experimental results in Section IV, Figures 7 and 8.

TABLE II-C-1

Source	Σ^{γ}	$\Sigma^{\gamma 2}$ (partially corrected) d = 0 cm	$\Sigma^{\gamma 2}$ (totally corrected) d = 10 cm
Hg^{203}	280 Kev	73.1 Kev	73.1 Kev
Cs^{134}	606 Kev	471.8 Kev	468.9 Kev
Co^{60}	1.32 Mev	866. Kev	864. Kev
Na^{24}	2.77 Mev	1.109 Mev	1.099 Mev

from formula (II-C-8).

From this table we see that the correction for crystal thickness causes only slight changes (< 2 percent) in all but the sodium source, whose γ energies are separated widely. Figure 2 shows the decay schemes and necessary details for the computations involved. Figure A-1 (Appendix) furnishes the values of μ required. It is interesting to note how much more important crystal thickness would have been for the sodium iodide crystal with its far larger values of μ and rapid increase at low energy due to photo-effect.

(b) Returning now to our ratio of $\frac{E_{T_j}}{E_{T_k}}$, we see that if $\mu d \ll 1$ then $\frac{E_{T_j}}{E_{T_k}} = \frac{\sum_i n_{o_{ji}} E_{\gamma_{ji}} \mu_{a_{ji}}}{\sum_i n_{o_{ki}} E_{\gamma_{ki}} \mu_{a_{ki}}}$ and $\frac{E_{T_j}}{E_{T_k}} = \frac{R_j}{R_k}$ rigorously since the correction for non-monoergicity applies equally well to the ion-chamber! However, for μd not $\ll 1$, we will again have a difference in the observed ratio, and again, in <u>theory</u> alone, would not expect our measured dosage ratios to agree with those from the ion-chamber.

Accordingly, if the correction for μd is appreciable and our assumptions are reasonably correct, then our problem would seem insoluble. Hence, one must consider the theoretical magnitude of the expected deviation due to crystal thickness.

From this table we see that the correction for
crystal thickness causes only slight changes (< 2 percent)
in all but the motion spectra, where γ energies are
separated widely. Figure 2 shows the decay scheme and
necessary details for the computations involved. Figure
4-1 (Appendix) furnishes the values of α required. It is
interesting to note how much more important crystal thick-
ness would have been for the motion detector crystal with
its far larger values of α and right increase of low energy
due to photo-effect.

(*) Returning now to our ratio of $\frac{E_\gamma}{E_e}$, we see

that it is $<< 1$ when $\frac{E_\gamma}{E_e} = \frac{\sum_i n_{\gamma i} E_{\gamma i} k_{\gamma i}}{\sum_i n_{ei} E_{ei} k_{ei}}$ and $\frac{E_\gamma}{E_e} = \frac{E_\gamma}{E_e}$

rigorously since the correction for non-monoenergetic spectra
equally well to the ion-counter. However, for μd not $<< 1$,
we will again have a difference in the observed ratio, and
again, in theory alone, would not expect our measured
charge ratios to agree with those from the ion-chamber.

Accordingly, if the corrections for μd is appreciably
and our assumptions are reasonably correct, then our problem
would seem tractable. Again, one must consider the theoretical
magnitude of the expected deviation due to crystal thickness.

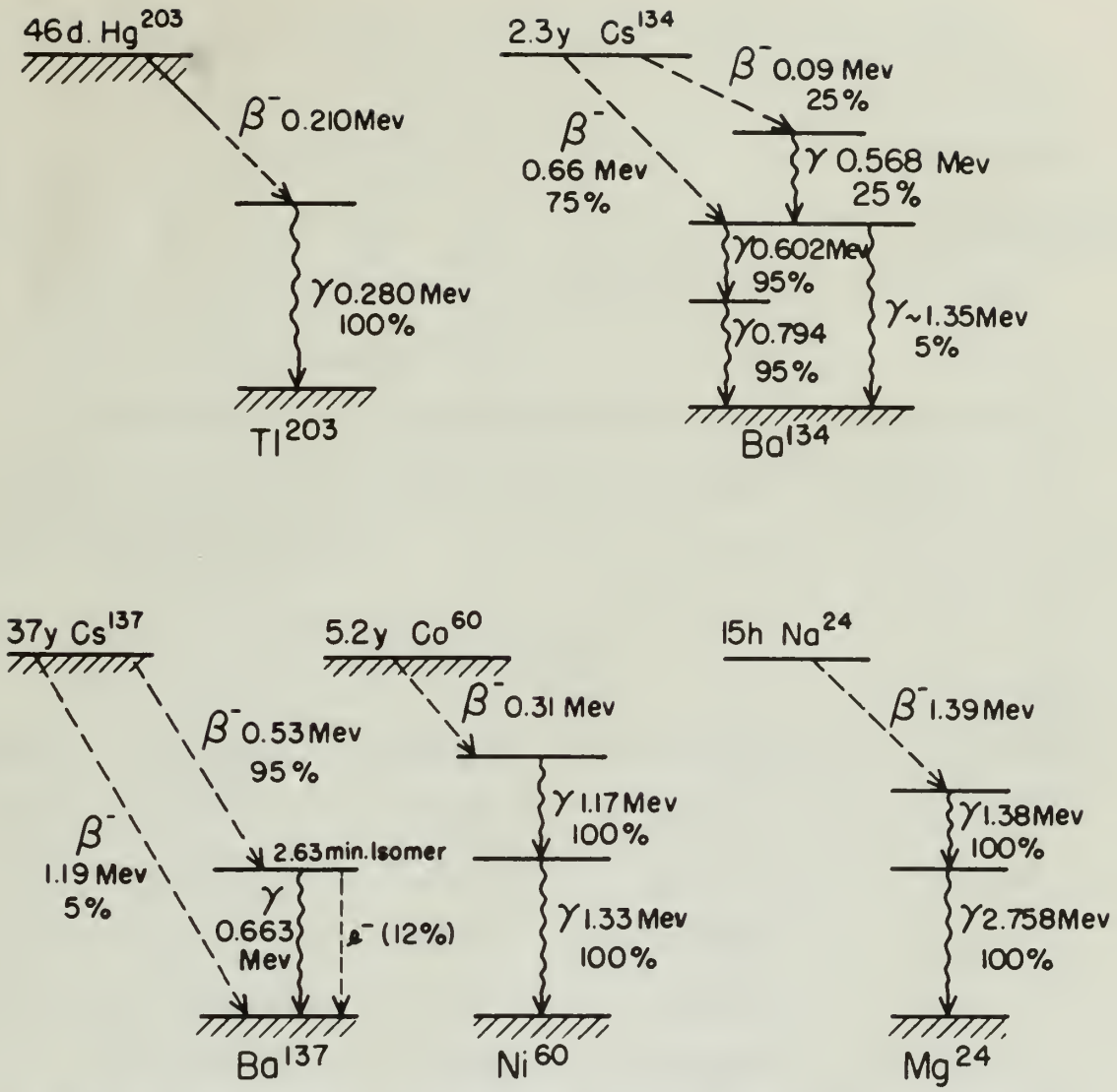

Note: Level separations schematic only; no energy scaling attempted.

Figure 2

ENERGY LEVEL DIAGRAMS FOR RADIO NUCLIDES
USED IN THIS INVESTIGATION.

(Reference: "Nuclear Data", Nat'l. Bureau of Standards Circ.499,1951)

A table of the correction factors($\frac{1 - e^{-\mu d}}{\mu d}$) is of value, for if they differ for each source by only a small amount, one might be able to assume a median value of the correction such that the true error over a given range would theoretically be expected to be less than a certain maximum within the limits of experimental error.

Considering average values of E_γ for the sources considered, except for the widely spread Na^{24} energies we obtain Table II-C-2.

TABLE II-C-2

d(mm)	Source	$\mu(cm^{-1})$	$1 - e^{-\mu d}$	$\frac{1 - e^{-\mu d}}{\mu d}$
6	Hg^{203}	0.143	0.082	0.956
6	Cs^{134}	0.098	0.0571	0.971
6	Co^{60}	0.074	0.0432	0.974
6	Na^{24} (1.38)	0.070	0.0412	0.981
6	Na^{24} (2.76)	0.0482	0.0284	0.983
20	Hg^{203}	0.143	0.249	0.871
20	Cs^{134}	0.098	0.178	0.909
20	Co^{60}	0.074	0.1377	0.931
20	Na^{24} (1.38)	0.070	0.1303	0.933
20	Na^{24} (2.76)	0.0482	0.0915	0.953

A table of the correction factors $\left(\frac{1 - e^{-\mu d}}{\mu d}\right)$ is of value, for if they differ too much another source by only a small amount, one might be able to assume a median value of the correction such that the true error over a given range would theoretically be expected to be less than a certain maximum within the limits of experimental error.

Considering average values of E^{λ} for the sources considered, except for the widely spread Ra_{Bp} energies we obtain Table II-C-2.

TABLE II-C-2

d(cm)	Source	$\mu(cm^{-1})$	$1 - e^{-\mu d}$	$\frac{1 - e^{-\mu d}}{\mu d}$
6	Ra_{ThD}	0.143	0.638	0.938
6	Cs_{134}	0.090	0.0971	0.971
6	Co_{60}	0.074	0.0432	0.974
6	Ra_{Bp} (1.76)	0.070	0.0413	0.975
6	Ra_{Bp} (2.76)	0.0625	0.0364	0.979
20	Ra_{ThD}	0.143	0.249	0.871
20	Cs_{134}	0.090	0.170	0.908
20	Co_{60}	0.074	0.1377	0.931
20	Ra_{Bp} (1.76)	0.070	0.1303	0.935
20	Ra_{Bp} (2.76)	0.0625	0.0918	0.954

From Table II-C-8, we see that it is possible to assume a "calibration factor" in the middle of the range of values of the factor $(\frac{1 - e^{-\mu d}}{\mu d})$ such that a certain percent accuracy can be expected. That is to say, if all experimental errors were zero, then if the dosage readings were "calibrated" by dividing by the median $(\frac{1 - e^{-\mu d}}{\mu d})$ factor, we would expect a certain percentage error for the several sources based solely on the theory developed to date:

(a) for the 6 mm crystal; assuming a calibration factor = 0.970, we see that the maximum error incurred for this range is about 1.4 percent.

(b) for the 80 mm crystal; assuming a calibration factor of 0.912 we can cover the whole range with a maximum error of 4.5 percent; or using 0.931 and eliminating the low end of the range we can obtain a maximum error of 2.3 percent.

The value or lack thereof of these considerations will be demonstrated in Section IV where theory and experimental results are compared.

Before leaving the theoretical development, let us consider two effects briefly mentioned above; the effect of plural scattering, and the effect of the leakage of energetic electrons from the confines of the crystal prior to expending all their energy into light output. These

From Table II-C-3, we see that it is possible to assume a "calibration factor" in the middle of the range of values of the factor $(1 - \frac{\delta_{-hq}}{\delta_{hq}})$ such that a certain percentage accuracy can be expected. That is to say, if all experimental errors were zero, then if this ideal value were "calibrated" by dividing by the median $(1 - \frac{\delta_{-hq}}{\delta_{hq}})$ factor, we would expect a certain percentage error for the measured spacings based solely on the theory developed in Paper

(a) For the 6 mm crystal; assuming a calibration factor = 0.970, we see that the maximum error incurred for this range is about 1.5 percent.

(b) For the 10 mm crystal; assuming a calibration factor of 0.978 we can adjust the whole range with a maximum error of 4.5 percent; or using 0.971 and eliminating the low end of the range we can obtain a maximum error of 2.1 percent.

The valid or lack thereof of these considerations will be demonstrated in Section IV where theory and experimental results are compared.

Before leaving the theoretical development, let us consider two effects briefly mentioned above: the effect of planar separation, and the effect of the lowering of

cannot be handled rigorously in an analytic manner, but a qualitative idea of their importance can be obtained by making some rather gross approximations. Sections D and E do this job in so far as the authors are able.

D. Plural Scattering Correction Approximation.

1. Effects of Plural Scattering.

The assumption has been made in the preceding theory that each photon suffers but one collision in the crystal. In possible justification of this assumption, let us examine more closely what it involves. To begin with, if a photon suffered another collision in the crystal, thus producing a second energetic electron and a corresponding output of light scintillation, it is clear that the resultant light from the second collision would not be a separate light pulse. The longest length of time possible between the two collisions in the thickest crystal is of the order of $\frac{2\ \text{cm}}{3 \times 10^{10}\ \text{cm/sec}} \sim 10^{-10}$ seconds while the resolving time of anthracene is $\sim 10^{-8}$ sec[8]. Therefore the light from the second collision increases the intensity of the light scintillation due to the first collision, and the photomultiplier contributes a pulse equal to that which it would have produced had the gamma lost in one collision all the energy that it lost in two collisions. Thus second collisions

cannot be handled rigorously in an analytic manner, but a qualitative idea of their importance can be obtained by making some rather crude approximations. Sections D and E do this job in so far as the authors are able.

E. Fluxal Restoring Correction Approximation.

1. Effects of Fluxal Restoring.

The assumption has been made in the preceding theory that each photon scatters but one collision in the crystal. In possible justification of this assumption, let us examine more closely what it involves. To begin with, if a photon scattered another collision in the crystal, thus producing a second energetic electron and a corresponding output of light scintillation, it is clear that the resultant light from the second collision would not be a separate light pulse. The longest length of time possible between the two scintillations in the thickest crystal is of the order of

$$\frac{2\ \text{cm}}{3 \times 10^{10}\ \text{cm/sec}} \sim 10^{-10}\ \text{seconds}$$

while the resolving time of the coincidence is $\sim 10^{-8}$ sec[3]. Therefore the light from the second scintillation increases the intensity of the light scintillation due to the first collision, and thus operates amplifier sometimes a pulse equal to that which it would have produced had the photon lost no energy collision all the energy that it lost in the collisions. Thus second collisions

do not increase the total counting rate but will increase the total energy measured and thus increase the measured average energy of the secondary electrons and the computed dosage over that which would be expected from the theory developed to date. Note that if it should prove to be of importance only for the Hg^{203} and the 20 mm crystal, then the low correction factor for this case in Table II-C-2 would be effectively increased and the range of error assuming a "calibration" factor of somewhat greater than 0.912, say 0.931, could be reduced (refer page 28). As will be seen in Section IV, an increase in average electron energy was noted as the crystal thickness increased; it is the purpose of this section to show whether the increase could or could not be due to second gamma collisions and whether it must be explained by another phenomenon; for instance, the leakage of energetic electrons from the crystal.

2. Analysis of Plural Scattering.

We shall assume some conditions which should be nearly optimum for second collisions to contribute appreciably to the energy absorption:

(a) Let n_o = number of photons/cm^2-sec incident on crystal, of area A.

E_γ = their energy.

μ = the linear attenuation coefficient at this E_γ.

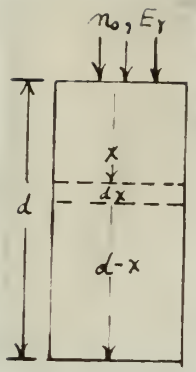

(b) Assume all primary collisions are such that the photons still go nearly in the forward direction.

(c) Assume photons still have energy E_γ and μ does not change.

Then the number of degraded photons produced in a thickness dx is equal to the number of electrons produced in $dx = n\mu A dx$ from formula (II-B-2). But $n = n_o e^{-\mu x}$, therefore the number of degraded photons produced in dx is $n' = n_o e^{-\mu x} \mu A dx$. Of these degraded photons, we know that $e^{-\mu(d - x)}$ of them will <u>not</u> have a collision between x and d, and therefore the fraction of the degraded photons which have a collision between x and d is $\left[1 - e^{-\mu(d - x)}\right]$. These are the photons which suffer at least two collisions in the crystal. Accordingly, the total number of photons which suffer at least two collisions in the crystal is $\int_o^d n'\left[1 - e^{-\mu(d - x)}\right] = n_o \mu A \int_o^d e^{-\mu x}(1 - e^{-\mu(d - x)})dx$ and the fractional number of incident photons which suffer at least two collisions, is

$$f = \mu \int_o^d (e^{-\mu x} - e^{-\mu d})dx$$

$$t = h \int_0^q (e^{-\alpha x} - e^{-hq}) dx$$

incident photons which suffer at least two collisions, is

$n^0 \sigma_T \int_0^q e^{-\mu x}(1 - e^{-h(q-x)}) dx$ and the fractional number of

least two collisions in the crystal is $\int_0^q \alpha_i \left[1 - e^{-\alpha(q-x)}\right] =$

accordingly, the total number of photons which suffer at

which suffer at least two collisions in the crystal.

between x and x + dx is $\left[1 - e^{-\alpha(q-x)}\right]$. Hence are the photons

fraction of the degraded photons which have a collision

will not have a collision between x and x', and therefore the

of these degraded photons, we have first $e^{-\mu(q-x)}$ of them

the number of degraded photons produced in dx is $n_1 = n^0 e^{-\mu x} \mu dx$.

$dx = \mu dx$ from Formula (II-B-1). But $n = n^0 e^{-\mu x}$; therefore

dx is equal to the number of fluorescent photons produced in

Then the number of degraded photons produced in a thickness

h does not change.

(c) Assume photons still have energy E^λ and

forward direction.

still be impinging solely in the

(b) Assume all primary radiations are such

that E^λ.

h = the linear attenuation coefficient at

$$f = \mu \left[\int_0^d e^{-\mu x} dx - e^{-\mu d} \int_0^d dx \right]$$

$$f = (1 - e^{-\mu d}) - \mu d e^{-\mu d} \qquad \text{(II-D-1)}$$

3. Conclusions Concerning Plural Scattering.

Now let us consider the energy for which μ is largest, i.e., E_γ = 0.280 Mev for Hg^{203}, with μ = 0.143 cm^{-1}, and the longest crystal used, i.e., d = 2 cm. This will give us the largest f which we will have to consider, since $\mu < 0.10$ cm^{-1} for all other sources used. For this case, under these assumptions, the fraction of all incident photons which suffer two collisions in the crystal is

$$f = (1 - e^{-0.286}) - (0.286)e^{-0.286}$$

$$= 0.249 - 0.215 = 0.034 = 3.4 \text{ percent.}$$

But we have chosen what we hope to be optimum assumptions for second collisions contributing to the energy absorption observed; viz:

(a) If the degraded photons do not (as is the case for some 90 percent of them according to Davisson[9]) go nearly in the forward direction and (as is actually the case for most of them) their energy is less because of the additional amount given to the electrons in the primary collision, then μ is greater; but from our geometry it is seen that d', the "in-crystal" distance remaining, is

$$f = \left[\int_0^a e^{-\mu x} dx - e^{-\mu a} \int_0^a dx \right]$$

$$f = (1 - e^{-\mu a}) - \mu a e^{-\mu a} \qquad \text{(II-C-1)}$$

3. Considerations Concerning Pinrel Scattering.

Now let us consider the energy for which μ is largest, i.e., $E^{\lambda} = 0.250$ Mev for Hg^{202}, with $\mu = 0.161$ cm^{-1}, and the longest crystal used, i.e., $d = 5$ cm. This will give us the largest f which we will have to consider, since $\mu < 0.10$ cm^{-1} for all other energies used. For this case, under these assumptions, the fraction of all incident photons which suffer two collisions in the crystal is

$$f = (1 - e^{-0.161})^2 - (0.805)e^{-0.161}$$

$$= 0.250 - 0.719 = 3.0\% = 3.4 \text{ percent.}$$

But we have chosen what we hope to be various assumptions for several collisions contributing to the energy absorption observed; viz:

(a) If the deflected photons do not (as in the case for some 30 percent of them) first undergo Raleigh(14) scattering, thus in effect; lose from our geometry it is quickly in the forward direction and (as is actually the case for most of them) their energy is less because of the additional amount given to the electrons in the primary collision, thus is effect; lose from our geometry it is

decreasing rapidly with increasing angle from the original direction; thus the product $\mu d'$ is nearly constant, and equal to μd, so f would not be materially affected.

(b) For those degraded photons which do not go nearly in the forward direction, since, as above, their energy is materially less than E_γ, the additional energy they could contribute in a second collision is less than they could have contributed in the primary collision, and thus the f = 3.4 percent would be greater than the actual percent increase in the total energy due to second collisions.

4. Justification of Analysis.

The true value of the percent increase in secondary electron energy due to second collisions would be extremely difficult to compute, if not impossible at the present stage of theoretical progress in the field of plural scattering, since we are concerned with a medium of small volume. It is felt that the above approximate analysis under gross assumptions provides a suitable overestimate of the increase in average and total secondary electron energy due to second collisions in the case of Hg^{203} radiation incident on the thick crystal, such that the true increase for this case is of the order of 3 percent or less. For the higher energy radiations for which μ decreases to <0.1 cm^{-1}, and for the thin (6 mm) crystal, the effect of second collisions

is therefore clearly inconsequential, and for the limiting case considered, the effect is of such magnitude that consideration of it is problematical.

E. Secondary Electron Leakage.

1. Analysis.

The final factor to be considered in the physical theory applicable to the problem is due to the magnitude of the crystal dimensions in comparison to the maximum range of energetic electrons in anthracene. A few representative values applicable here are calculated from Goodman[11]:

TABLE II-E-1

E(electron)	Maximum Range in Anthracene
145 Kev	0.15 millimeters
500 Kev	1.28 millimeters
1000 Kev	3.44 millimeters
1500 Kev	6.20 millimeters
2000 Kev	7.6 millimeters
2500 Kev	9.8 millimeters
2750 Kev	11.0 millimeters

The maximum energy obtainable by the electrons by

R(electron)	maximum range in hydrogen
165 Kev	0.15 millimeters
500 Kev	1.00 millimeters
1000 Kev	3.64 millimeters
1500 Kev	6.50 millimeters
2000 Kev	9.8 millimeters
2500 Kev	13.0 millimeters
3000 Kev	16.4 millimeters

The maximum energy obtainable by the electrons by

Compton collisions is given by the well-known formula[18]

$$E_{max} = \frac{E_\gamma}{1 + \frac{0.51}{2E_\gamma}} \qquad \text{(II-E-1)}$$

The maximum energies of secondary electrons from the various sources are:

TABLE II-E-2

Source	$E_{\gamma\ max}$	E_{max} (secondary electron)
Hg^{203}	280 Kev	146 Kev
Cs^{134}	794 Kev^{x}	600 Kev
Co^{60}	1.33 Mev	1.115 Mev
Na^{24}	2.76 Mev	2.525 Mev

$^{x}Cs^{134}$ has a 1.35 Mev gamma ray but of only 5 percent abundance.

Comparison of these two tables with the dimensions of the two crystals brings out a few interesting points.

(a) 6 mm crystal - cross section is a circle 30 mm in diameter. For this case, the minimum distance of travel for the secondary electrons is forward, which is the direction of the most energetic ones (head-on collision type). Since the electrons are produced all through the crystal, it is obvious that for the cobalt source and higher energies, an appreciable percentage of energetic electrons

Energy conservation is given by the well-known formula[14]

$$E_{max} = \frac{E_\gamma}{1 + \frac{0.51}{E_\gamma}} \qquad (II-3-1)$$

The maximum energies of secondary electrons from the various sources are:

TABLE II-3-2

Source	E_γ max	E_{max} (secondary electron)
^{85}Sr	860 Kev	746 Kev
^{137}Cs	784 Kev	620 Kev
^{60}Co	1.33 Mev	1.118 Mev
^{24}Na	1.76 Mev	1.368 Mev

^{137}Cs has a 1.33 Mev gamma ray but of only 2 percent abundance.

Comparison of these two peaks with the dimensions of the two crystals brings out a few interesting points.

(a) A one crystal - cross section is a circle 30 mm in diameter. For this case, the minimum distance of travel for the secondary electrons is *Zero*, which is the direction of the most energetic ones (head-on collision type). Since the electrons are produced all through the crystal, it is obvious that for the weakly energies, no appreciable percentage of energetic electrons

will pass out of the scintillator before expending all their energy in light production, such percentage increasing with energy.

(b) 20 mm crystal - cross section is a rectangle 10 mm by 20 mm. For this case the forward direction is the longest dimension of the crystal, and if we consider first only those electrons in the forward direction, then the leakage described above should only be important for the highest energy, i.e., Na^{24}, and should be <u>less</u> than for the 6 mm crystal. However, this crystal has a narrow horizontal dimension, such that many electrons <u>not quite</u> in the forward direction, but enough forward that they have considerable energy, will leak out the side faces before contributing all their energy to light. This is enhanced by the fact that the gamma beam is not truly parallel, due to the finite source-to-crystal distance (which was kept at least 10 times crystal dimensions) but diverges slightly, such that the most energetic electrons if produced near a side face, would be "aimed" to go out of the crystal. This effect would be negligible in the thin crystal due to its cross section.

2. Effect of Leakage.

Since the effects mentioned above would tend to decrease the energy converted into light and measured, one

will pass out of the scintillator before expending all their energy in light production, such particles interacting with energy.

(b) 30 mm crystal - cross section is a rectangle 10 mm by 30 mm. For this case the forward direction is the longest dimension of the crystal, and if we consider first only those electrons in the forward direction, then the leakage described above should only be important for the highest energy, i.e., Ra^{224}, and should be less than for the 8 mm crystal. However, this crystal has a shorter horizontal dimension, such that many electrons not going in the forward direction, but enough forward that they have considerable energy, will leak out the side front before contributing all their energy to light. This is enhanced by the fact that the beams is not truly parallel, due to the finite source-to-crystal distance (which can be at least 10 times crystal dimensions) but diverges slightly, such that the most energetic electrons if produced near a side face, would be "almost" to go out of the crystal. This effect would be negligible in the thin crystal due to its cross section.

3. Effect of Leakage.

Since the effects mentioned above would tend to decrease the energy converted into light and measured, the

would expect a decrease below the theoretical values both of E_{AV} and E_T ("dosage") due to this cause, in opposition to the increase expected due to plural scattering (Section II-D). Further, it would be expected to have more effect in the thin crystal than the thick, and to be of most concern for the higher energy gamma rays.

3. Solution to Leakage Problem.

A theoretical configuration to correct some of these ills suggested itself near the end of our experimentation. If one enclosed the crystal in a box of material of about the same density and composition of anthracene, say lucite for example, two effects could occur:

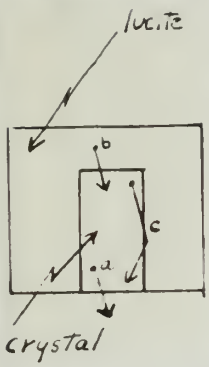

(a) and (b) On the average, for a number of electrons which leak out of the bottom of the crystal (a) producing a light pulse indicating an energy smaller than it actually had, there is a corresponding number (b) leaking <u>in</u> from the lucite top and producing a light pulse corresponding to the rest of the energy. Note that these two light pulse distributions are both random, therefore coincidence would be rare, and we would be increasing the number of pulses of low energy, thus decreasing the average electron energy measured, but increasing the dosage measured (since now little or none is <u>relatively</u> lost).

liquid or rare is relatively inert).

measured, but increasing the energy measured (since one of low energy, thus decreasing the average electron energy be true, and we would be increasing the number of pulses electrodynamics are both random, therefore coincidence would to the rest of the energy. Note that since two light pulse and producing a light pulse corresponding counter (b) leading to from the inside top of the crystal (a) producing a light pulse detecting an energy smaller than it actually has, there is a correspondence of electrons which just exit at the bottom

(a) and (b) On the average, for a number

For example, two effects could occur

the same density and composition of instrument, may locate If one measured the crystal in a box of material of about this suggested itself upon the need of our experimentation.

A theoretical modification to correct some of these

3. Solution to Leakage Problem.

be at most concern for the higher energy cosmic rays. to have more effect in the data captured than the former, and scattering (Section II-C). Further, it would be expected opposition to the increase expected due to plural both of $E_{\frac{1}{2}}$ and $E_{\frac{1}{4}}$ (Compare) due to this cause, in would expect a decrease below the theoretical values

(c) For electrons tending to stray out of the crystal sides, the dense lucite has nearly as much probability of scattering them back into the scintillator as scattering them further away, since the angle of incidence at the interface is small. This would not increase the number of pulses, since the same electron continues to produce the light pulse, having lost only a little energy in the lucite, but it would increase the amplitude of the light pulse over what it would be if the lucite were absent, thus reducing the effect of 1(b) above.

It should be noted that lucite on the bottom of the crystal has little effect since backscattering is small for all energies[24].

(d) It is impractical to try to decide, on the theoretical basis which of the effects (a) and (b) or (c) will be of greater importance, if either will. Section IV will show the result of an attempt to investigate this matter experimentally. It appears that in any event, at least 50 percent of the electrons which tried to get out of the sides would succeed, even with lucite "guard rails", so that experimental values below the theoretical should not be viewed with alarm. On the other hand, only the small effect of Section II-D would cause a value greater than the theoretical, so an appreciable excess above the

(a) For electrons impinging on every one of the crystal faces, the dense inelastic ions nearly as much probability of scattering them back into the semiconductor as scattering them further away, since the ratio of impedance of the interface is small. This would not increase the number of pulses, since the same electron continues to produce the light pulse, having lost only a little energy in the inelastic, but it would increase the resistance of the light pulse over what it would be if the inelastic were absent, thus reducing the effect of 1(b) above.

It should be noted that inelastic as the opposed has little effect since backscattering is small for all energies[4].

(d) It is important to try to decide, on the theoretical basis which of the effects (a) and (b) or (c) will be of greater importance, it either will. Section IV will show the result of an attempt to investigate this matter experimentally. It appears that in any event, at least 50 percent of the electrons which fail to get out of the plane would succeed, even with inelastic "giant pulse", so that experimental values below the theoretical should not be viewed with alarm. On the other hand, only the small effect of Section II-C would cause a ratio greater than the theoretical, so an experimental ratio above the

theoretical value would certainly be indicative of a major defect.

4. Conclusion of Theory.

This concludes the theoretical aspect of the problem in all the details which have been considered of major importance by the authors. The next section deals with the equipment used in the experiment, and the following section will compare the results obtained with the theory evolved in the five divisions of this section.

theoretical value would certainly be indicative of a major defect.

4. Conclusion of Theory.

This completes the theoretical aspect of the problem in all the details which have been considered of major importance by the authors. The next section deals with the equipment used in the experiments, and the following section will compare the results obtained with the theory evolved in the five divisions of this section.

III. EXPERIMENTAL EQUIPMENT AND PROCEDURE

A. Initial Equipment Configuration.

The first approach to presenting the output of the crystal-photomultiplier tube combination in terms suitable for evaluating its relation to dosage was to use the circuits of Figures 3 and 4. All of these components are standard units except the "integrating" circuit (Figure 4). This circuit's principle of operation is mentioned in reference (19), page 250. When it is operated as a counting rate meter, a one-shot multivibrator is placed in front of the "integrator" so that each count appears as a nearly square pulse, constant in amplitude. Under these conditions one can meet the requirements

$$\frac{1}{n} \gg T > 5R_1C_1 \qquad \text{(III-A-1)}$$

$$E \gg V > E_B \qquad \text{(III-A-2)}$$

$$C_2 > C_1 \qquad \text{(III-A-3)}$$

which are necessary for accurate operation of the circuit. In the above equations the nomenclature is defined in Figure 4. Since the detailed operation of this circuit as a counting rate meter is nowhere completely treated, it is felt worth while here to describe its operation in some detail. Referring to Figure 4, suppose a pulse of amplitude E volts appears at the input. In accordance with equation

III. [illegible]

A. Initial Equipment Specifications.

The first approach to presenting the output of the [illegible] photomultiplier tube examination in terms suitable for evaluating its relation to design was to use the circuits of Figures 3 and 4. All of these components are standard units except the "integrating" circuit (Figure 4). This circuit's principle of operation is mentioned in reference (18), page 220. When it is operated as a constant [illegible] meter, a rms-dust multivibrator is placed in front of the "integrator" so that each count appears as a nearly square pulse, constant in amplitude. Under these conditions one need use the inequalities

$$\frac{R}{T} \gg 1 > RF_0C' \qquad \text{(III-4-1)}$$

$$R \gg A > R_0 \qquad \text{(III-4-2)}$$

$$C_0 > C' \qquad \text{(III-4-3)}$$

which are necessary for accurate operation of the circuit. In the above notations the nomenclature is defined in Figure 4. Since the desired operation of this circuit as a counting rate meter is somewhat graphically pictured, it is felt worth while here to describe its operation in some detail. Referring to Figure 4, suppose a pulse of amplitude A volts appears at the input. It encounters [illegible]

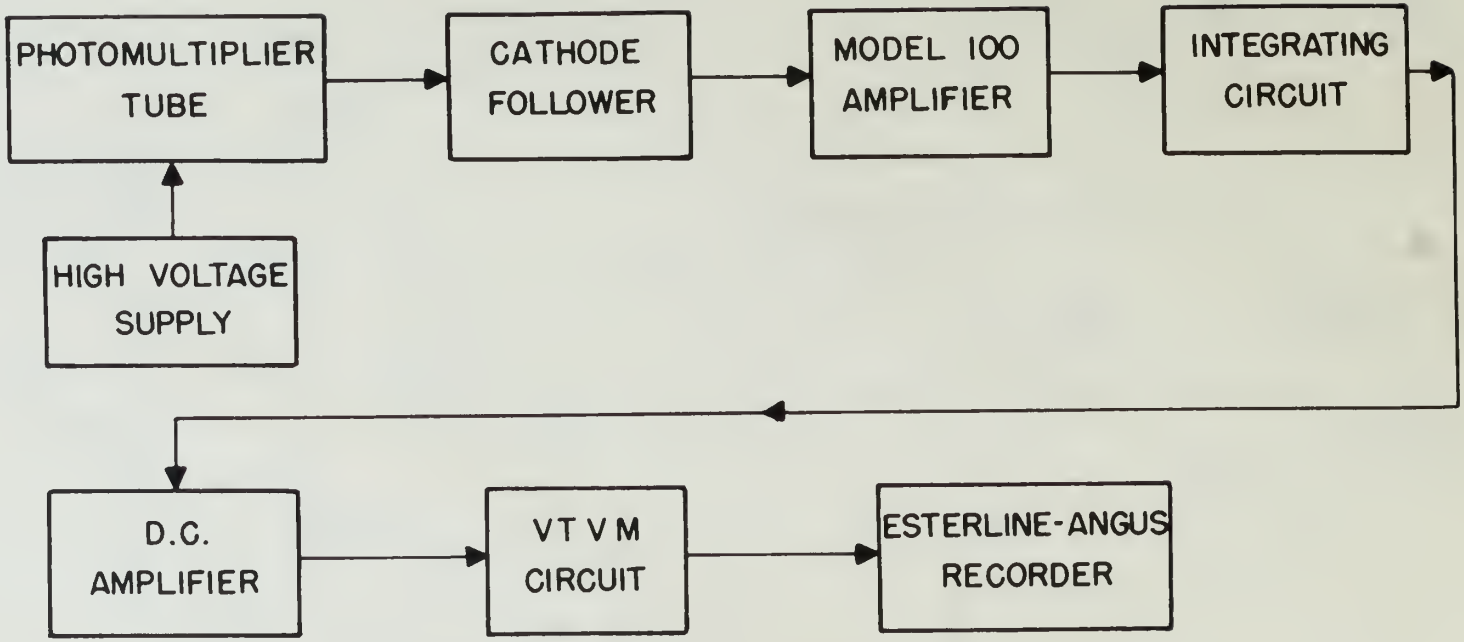

Notes:

(a) PM Tube is an RCA 5819 selected for good resolution.
(b) The Cathode Follower was used to match impedence between PM and Model 100.
(c) Model 100 Amplifier is a standard linear amplifier. See Ref. 19, page 166.
(d) See Figure 4 for circuit diagram of Integrating Circuit.
(e) Esterline-Angus Recorder was a Model AW (Serial No. 32315) 5Ma. D.C. Graphic Ammeter manufactured by the Esterline-Angus Co., Inc. of Indianapolis, Ind.

Figure 3

BLOCK DIAGRAM OF INITIAL EQUIPMENT USED TO "INTEGRATE" OUTPUT FROM PHOTOMULTIPLIER TUBE

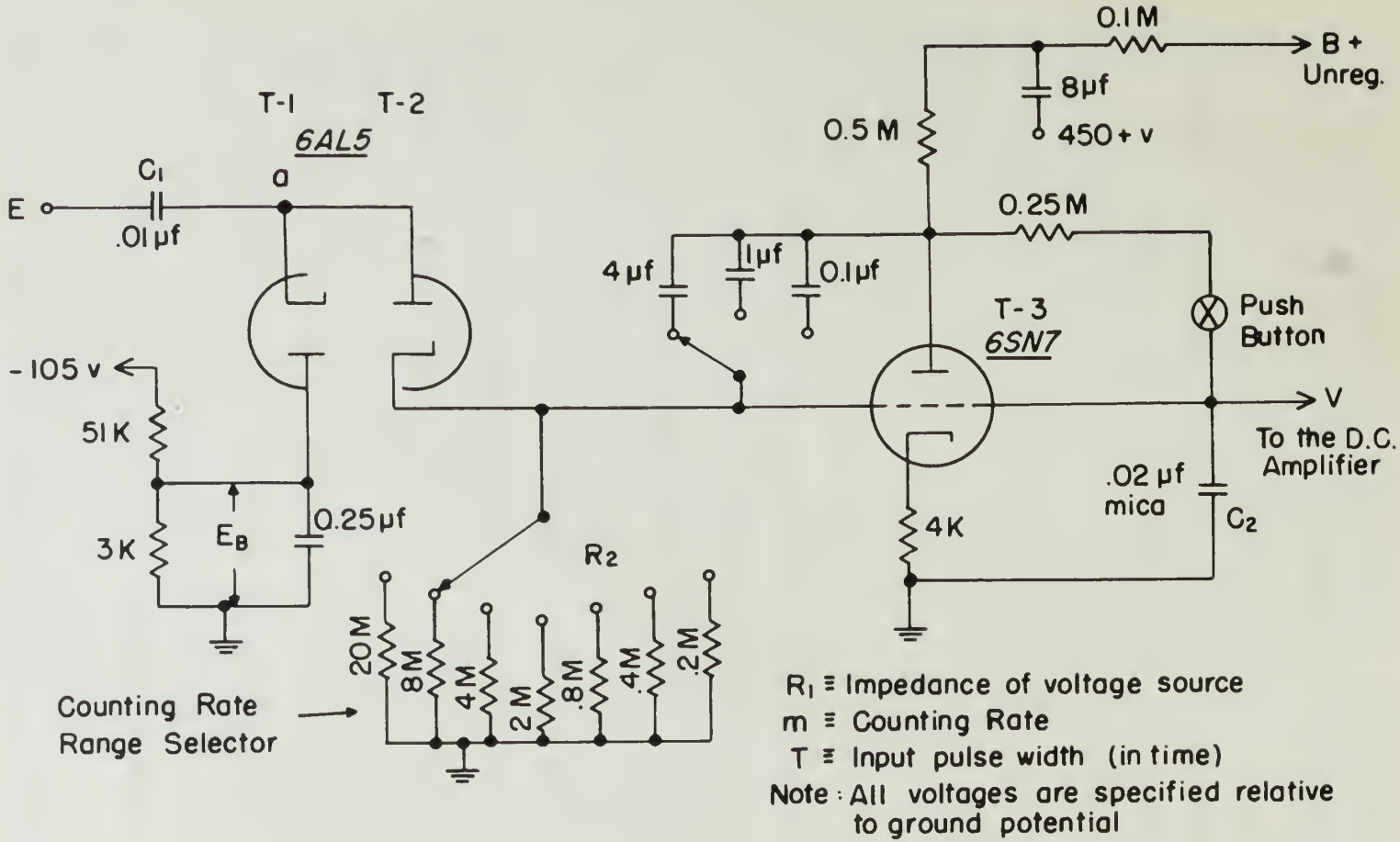

Figure 4

CIRCUIT DIAGRAM OF THE "INTEGRATOR"

(III-A-1), C_1 will be charged to the peak value (E - V). Since $C_2 >> C_1$ an amount of charge proportional to (E - V) (or to E if E >> V) will also be placed on C_2 through T-2 during T. It should be noted that T-3 and its associated circuitry serves only to increase the apparent size of C_2. At the end of the pulse T-2 no longer conducts while T-1 provides a path for the charge on C_1 to discharge to ground, thus returning point a to voltage E_B (some small negative voltage). Thus for each count a constant amount of charge is placed on C_2 which then gradually leaks off through R_2 with time constant R_2C_2 providing a smoothing action on voltage V. Thus V is a stable indication proportional to the counting rate. For further details on counting rate meters and their statistics see references (19) and (20).

In the present problem the application of this circuit, though superficially quite similar to that of the counting rate meter, is somewhat different. To get a measure of energy absorbed by the secondary electrons in the crystal one must sum over all pulse amplitudes, which are proportional to the energy of the electron causing the pulse[7,8] and over the number of pulses. Since, in theory, if the pulses are fed from the photomultiplier (after suitable amplification and clipping) directly to the "integrator" <u>each</u> pulse should deposit a charge on C_2

"integrator" such pulse should deposit a charge on C^2 suitable amplification and clipping) directly to the if the pulses are fed from the photomultiplier (after pulse[7,8] and over the number of pulses. Since, in theory, are proportional to the energy of the electron causing the the crystal one must sum over all pulse amplitudes, which measure of energy absorbed by the secondary electrons in counting rate meter, is somewhat different. To get a circuit, though superficially quite similar to that of the

In the present problem the application of this meters and their statistics see references (19) and (20). the counting rate. For further details on counting rate voltage V. Thus V is a stable indication proportional to with time constant R_2C_2 providing a smoothing action on is placed on C_2 which then gradually leaks off through R_2 voltage). Thus for each count a constant amount of charge time returning point a to voltage E_2 (some small negative provides a path for the charge on C_1 to discharge to ground, At the end of the pulse T-2 no longer conducts while T-1 circuitry serves only to increase the equipment size of C_2. during T. It should be noted that T-3 and its associated (or to E if E >> V) will also be placed on C_2 through T-2 Since $C_2 >> C_1$ an amount of charge proportional to (E - V) (III-4-1), C_1 will be charged to the peak value (E - V).

proportional to (E - V) or E if E >> V. Now, since $V = mq_2R_2$ or mC_1ER_2 [19], this voltage, V, should be proportional to the total energy per unit time of the secondary electrons in the crystals. Referring to Section II-B we see that this corresponds to formula (II-B-4), in that $E_T \propto m\mu_a E_\gamma$.

Unhappily, there are factors at work which make this circuit quite unsuitable. Extensive time was devoted to showing experimentally that this was indeed true. It is also easy to show theoretically.

The first difficulty arises in that the spectra of pulses used as input to this circuit range in magnitude from some very small value up to a maximum determined by the energy of the gamma rays of the radioactive source being used and the amplification required. Thus over the lower portion of the spectra E may be comparable with or even less than V. If E is comparable with V the charge going into C_2 is now proportional to (E - V). Thus, the smaller pulses will not be weighted enough according to their true amplitude. If E < V the pulse will not be recorded at all.

The second difficulty arises if there is any overshoot on the input pulse. If the overshoot goes more negative than E_B, then T-1 will conduct, charging C_1 in such a manner that point a will be left positive relative to ground when

T-1 stops conducting after the overshoot voltage becomes less negative than E_B. Thus if the overshoot went negative greater than an amount $(E_B + V)$ an additional charge will be put on C_g, though small in magnitude.

There are, then, two sources of error, one tending to decrease the measured dosage while the other tends to increase it. Both of these errors were observed in this equipment and after very extensive experimentation using both pulse generators and radioactive sources, it was concluded that the circuit could not be operated at a satisfactory level of accuracy for research on this problem.

Since the amount of error introduced by overshoot is very sensitive to E_B it was found that, for a <u>particular</u> spectrum, E_B could be adjusted to give a reasonable value, but if any other source with either a different differential pulse height distribution or maximum pulse height were used error, of course, again was introduced. Furthermore, it was necessary to "know the answer to get the answer" by adjustment of E_B.

It is possible, of course, to remove the overshoot in the pulse and still retain the amplitude; however this solves nothing since the error due to small values of E enters. This error, also, is a function of the differential pulse height distribution of the spectra used.

The conclusion that this "integrating" principle is not sufficiently accurate for research purposes is well borne out by Glass and Hurst at Oak Ridge who after much investigation evolved a very complex circuit[?] which was satisfactory for dosage indications; however, due to its complexity, it was extremely difficult to keep the unit in routine operation.

This discussion is not to be construed as concluding that this instrument cannot be made accurate enough to be used for survey purposes or other more routine dosage measurements. It appears quite probable that one could develop such an instrument, though its relative cost compared to common survey instruments would render its practicability questionable.

B. Final Equipment Configuration.

1. New Approach to the Problem.

Having experienced such difficulty with the equipment described above, it was decided to abandon further attempts in that general line in view of the length of time remaining to the authors at this institution, and to attack the feasibility problem from the standpoint of physics with an entirely different approach. We have seen above that the initial equipment was intended to average the product of

number of electrons produced per unit time and the energy of each. The final equipment decided upon gives readings from which this figure can be calculated; thus, as mentioned in the introduction, the human being has replaced part of the electronics.

2. Description of the New Approach.

The final equipment is shown in block diagram in Figure 5. All of the parts are standard instruments available at this institution. An identical configuration has been and is being used by Dr. G. J. Hine in his gamma ray spectrometer studies with a sodium iodide crystal[11]. Let us see what changes were made from the initial configuration and indicate the purpose of each component part:

(a) No change was made in the photomultiplier tube and mount, except for the obtaining of a "good" 5819 tube known to have good resolution, which we will see is required in energy calibration for this method. The high voltage supply was the same one, except that it was replaced late in the experiment by a more stable one, this change producing no effect in the results. All through the data runs on which our results are based, the high voltage supply to the photomultiplier was set at 740 volts.

(b) In order to get a higher gain for the small pulses from the low energy source (Hg^{203}) the preamplifier was changed from a cathode follower to a stage of gain of about 10.

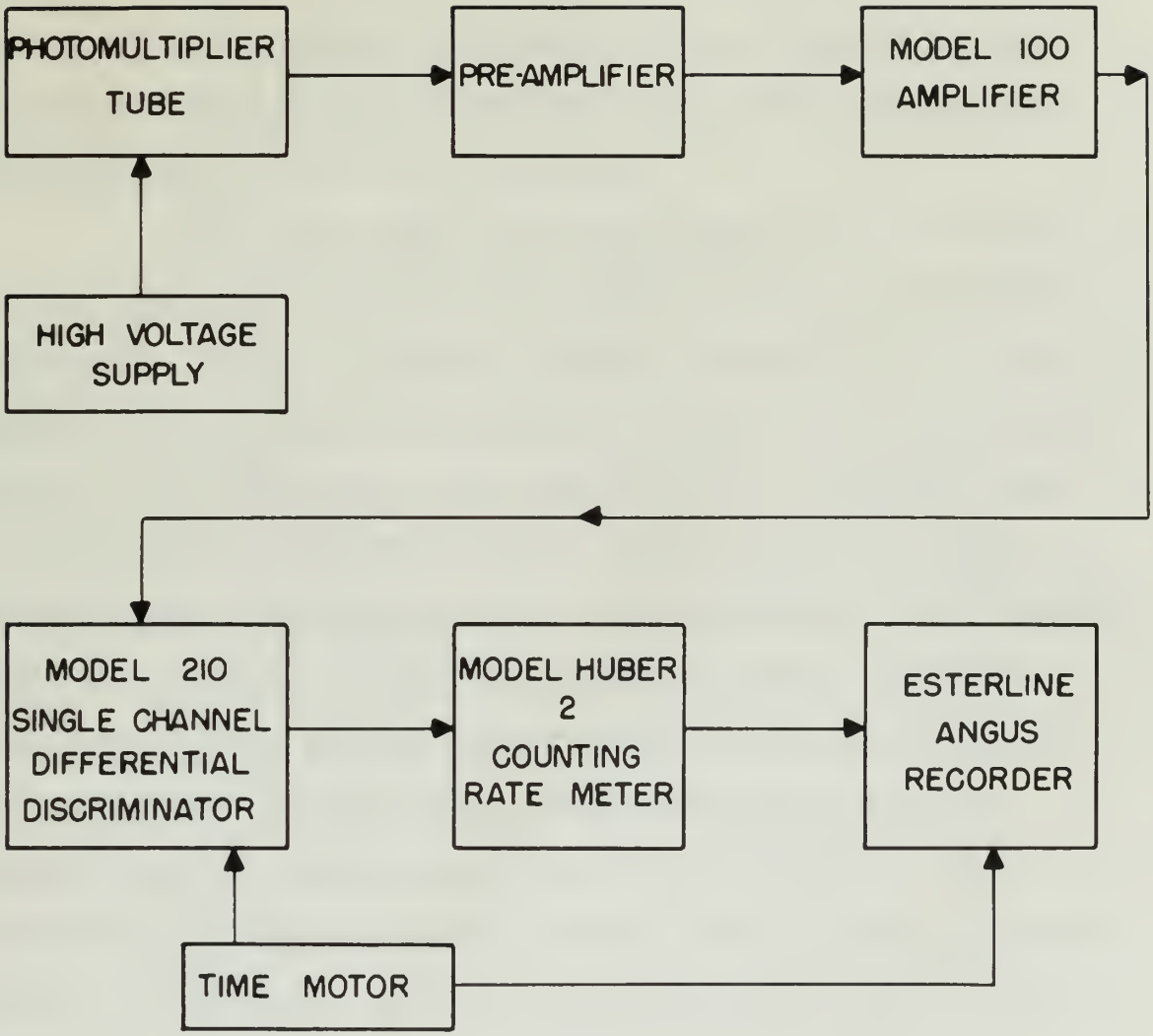

Note: See Section III - B for Description of Operation.

Figure 5

BLOCK DIAGRAM OF FINAL ELECTRONIC EQUIPMENT

(c) The Model 100 amplifier was unchanged, except that it was operated at lower gains for the higher energy sources, so that the output never exceeded 95 volts. Output voltages above 100 volts are unreliable due to the overloading of this type amplifier.

(d) The output from the Model 100 was now led into a Model 210 single channel differential discriminator with window width of about 2 volts. The exact value of window width is of extreme importance and will be discussed later. The Model 210 window position was controlled with a motor-driven rheostat which swept the ranges of 0-96 volts in approximately an hour and 10 minutes. This rheostat and its dial were carefully calibrated using a calibrated voltmeter, pulse generator with variable amplitude signal and Techtronix synchroscope. The calibration curve is included in Appendix B as Figure B-1. It was found that discriminator did not work properly below a value of window center = 2.6 volts, and all data taken were begun at this minimum.

(e) The output from the Model 210 discriminator was then fed into a Model Huber-2 Counting Rate Meter, with internal calibration for scales of 5000 cpm, 10,000 cpm, 20,000 cpm, which were the only scales used. Before each run, the CRM was carefully zeroed and each scale calibrated on 3600 cpm (line 60 cycle AC).

(c) The Model 100 amplifier was unchanged, except that it was operated at lower gains for the higher energy sources, so that the output never exceeded 95 volts. Output voltages above 100 volts are unreliable due to the overloading of this type amplifier.

(d) The output from the Model 100 was fed into a Model 310 single channel differential discriminator with window width of about 5 volts. The exact value of window width is of extreme importance and will be discussed later. The Model 310 window position was controlled with a motor-driven potentiometer which swept the range of 0-95 volts in approximately an hour and 10 minutes. This potentiometer and its dial were carefully calibrated using a calibrated voltmeter, pulse generator with variable amplitude signal and Tektronix oscilloscope. The calibration curve is included in Appendix B as Figure B-1. It was found that discriminator did not work properly below a value of window center = 3.3 volts, and all data taken were begun at this minimum.

(e) The output from the Model 310 discriminator was then fed into a model Hyper-X Counting Rate Meter, with internal calibration for scales of 5000 cps, 10^4,000 cps, 20^4,000 cps, which were the only scales used. Before each run, the CRM was carefully warmed and each scale calibrated on 3800 cps (time 30 cycle AC).

(f) Finally, the CRM output was displayed on an Esterline-Angus 5 ma recorder, with motor feed connected to the motor of the motor-driven dial so that stopping of discriminator rheostat motor also stopped Esterline-Angus tape feed.

3. Mounting of Gamma Sources.

The sources of gamma radiation were supported above the crystal using the usual laboratory stand with an extension arm so that the stand members were at least 40 cm from the vertical line between source and crystal, to minimize the effects of scattering by adjacent equipment. The sources were of various strengths uncalibrated except for the 428 μc Co^{60} and 904 μc of Ra. They were placed at various distances, which were measured to ±0.5 mm, such that convenient CRM scales were available. These distances were recorded, and were reproducible in the main.

4. Phototube Mounting.

A word about the phototube mounting shown in Figure 6 is next necessary. The voltage divider for supplying dynode voltages is contained in the metal box containing the 5819 socket.

The resistors are arranged to give a 40 percent greater voltage rise from cathode to first dynode than from dynode to dynode the rest of the way, other steps being equal. This arrangement provides better collection of

(f) Finally, the CO2 output was displayed on
an Esterline-Angus S ca recorder, with motor fuel connected
to the motor of the motor-driven dial so that stepping of
discriminator resonator motor also stepped Esterline-Angus
tape feed.

3. Counting of Gamma Quanta.

The sources of gamma radiation were supported above
the crystal using the usual laboratory stand rig in position
in so that the stand mounted vers el least 40 cm from the
vertical line between source and crystal, to minimize the
effects of scattering by adjacent equipment. The sources
were of various strengths quantitatively except for the 60
Be Co^{60} and 30% Be of Ba. They were placed at various
distances, which were measured to ±0.5 mm, such that
convenient CPM rates were available. These distances
were recorded, and were reproducible in the data.

4. Pulseheight Sounting.

A word about the pulseheight measuring system in Figure
6 is more necessary. The voltage divider for supplying
dynode voltages is enclosed in the metal box containing
the BNC sockets.

The resistors are arranged to give a dy percent
greater voltage rise from anodes to first dynode than
from dynode to dynode the rest of the way, which gives
equal. This arrangement provides better collection of

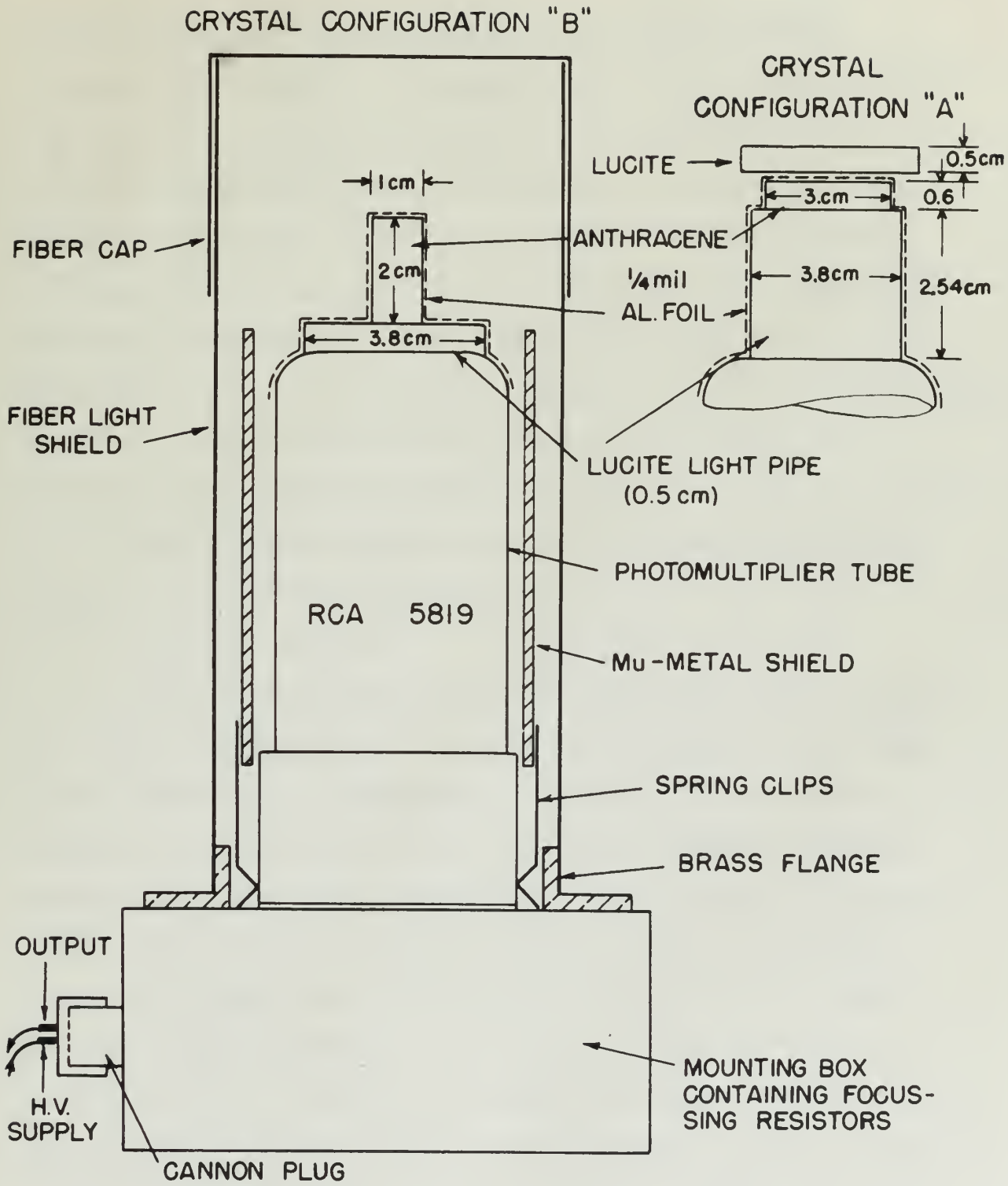

Figure 6

DETAILS OF SCINTILLATION COUNTER CONSTRUCTION

cathode emitted electrons and improves resolution[22]. A cardboard light shield is placed over the entire phototube and crystal assembly, and over all, a black cloth is draped. A low background obtainable is considered proof that light-tightness is nearly perfect. Cardboard was used in place of brass to minimize any "scattering-in" of soft gamma rays from the light shield. It was also found that movement of iron apparatus in the vicinity affected the output considerably. A mu-metal shield was therefore installed as shown in Figure 6 and magnetic effects disappeared.

The crystal configurations "A" and "B" as shown in Figure 8 will be discussed later.

5. Data Taken.

We shall outline in brief now what data were obtained and what information can be obtained therefrom. With each source and crystal configuration, a gain on the Model 100 amplifier was chosen such that the largest pulses from the crystal were just below the maximum window height. A minute source (practically weightless point-source) of Cs^{137} was used to calibrate the window center voltage to kilovolts energy at this particular gain and phototube high voltage. This was done by placing the calibration source directly on top center of the anthracene crystal (which was covered with 1/4 mil (1.7 mg/cm^2) aluminum foil) and observing the

cathode emitted electrons and improves resolution[EC]. A cardboard light shield is placed over the entire phototube and crystal assembly, and over all, a black cloth is draped. A low background obtainable is demonstrated proof that light-tightness is nearly perfect. Cardboard was used in place of brass to minimize any "scattering-in" of soft gamma rays from the light shield. It was also found that movement of iron apparatus in the vicinity affected the output considerably. A mu-metal shield was therefore installed as shown in Figure 8 and negligible effects disappeared.

The crystal configurations "A" and "B" as shown in Figure 9 will be discussed later.

2. Data Taken.

We shall outline in brief how what data were obtained and what information can be obtained therefrom. With each source and crystal configuration, a path on the Model 100 multiplier was chosen such that the largest pulses from the crystal were just below the maximum window height. A source (preferably weightless point-source) of Cs^{137} was used to calibrate the window counter voltage to kilovolts energy at this particular gain and phototube high voltage. Data was done by placing the collimated source directly on the center of the multicrystal crystal (which was covered with 1/4 mil (1.7 mg/cm^2) aluminum foil) and observing the

position of the window center for the Cs^{137} conversion electron peak (625 Kev line spectrum of e^-). A representative peak is shown in Figure B-2. This method has also been used by other investigators[23]. It was determined experimentally that this thickness of aluminum foil caused no error in the energy calibration, since tripling the thickness of the foil caused no detectable shift in the position of the Cs^{137} peak. Then with calibration source removed and sample source in place on its stand, by letting the motor sweep the discriminator rheostat through the range of energies of the particular spectrum, a curve of the number of pulses per energy interval (window width converted into Kev by Cs^{137} calibration being the energy interval and termed herein ΔE) versus their energy at the center of the interval was obtained. That is, a curve of $\frac{dN}{dE}\Delta E$ (cts/min) versus E(Kev) was the directly plottable output of the equipment. Finally, for each spectrum, a run was made sans source to determine background to be subtracted.

Now we see that ΔE, the window width in Kev, is of supreme importance where the absolute number of counts in the entire spectrum is desired, since an increase in E causes an increase in the ordinate ($\frac{dN}{dE}\Delta E$) and when obtaining the integral counting rate by measuring the area under the curve and dividing by ΔE as is further explained in Section

IV, ΔE must be known to the accuracy desired in the integral counting rate. This major difficulty, as will be discussed, is an intrinsic fault of a differential discriminator since it is difficult to measure and even more difficult to keep constant or reset to the same value when it drifts off due to the usual changes in a complicated multivibrator instrument due to tube age, temperature, and line voltage variations. It is th<u>e major</u> source of error in our experiments regarding dosage, but is of little or no importance in the measurements involving E_{AV}, as shown in Section IV. Changes in ΔE <u>were</u> observed to occur <u>during</u> several runs, but these were recognizable from experience and such runs were discarded and repeated.

Now that we have seen what the final equipment was, and what quantity it measured, we shall spend Section IV in examining what knowledge can be extracted therefrom and how our results thus obtained compare with the theory evolved in Section II.

IV, Δt must be large of the accuracy desired in the
integral computed here. This major difficulty, is still
to be resolved, is an inevitable result of a differential
characteristic since it is difficult to measure and very
more difficult to keep constant or reset to the same value
when it drifts off due to the usual changes in a complicated
multivibrator instrument due to tube age, temperature, and
like voltage variations. It is to be noted however by error
in our approximate integrating device, but is of little or
no importance in the servomechanism involving Δt, be shown
in Section IV. Changes in Δt were observed to occur during
several runs, but these were recognizable from inspection
and such runs were discarded and repeated.

Now that we have seen what the final equipment was,
and what quantity it measured, we shall spend Section II in
examining what knowledge can be extended theoretical and how
our results bore checked ourselves with the theory evolved
in Section II.

IV. EXPERIMENTAL RESULTS AND COMPARISON WITH THEORY

A. General Mathematical Procedure and Preliminary Results.

1. Obtaining E_{AV} and Dosage from Experimental Measurements.

We have seen in the preceding section that the directly plottable output of the final equipment was $\frac{dN}{dE}\Delta E$ vs E, in the previous notation. If now the ordinate of each point on the curve is multiplied by its abscissa, we obtain a curve of $E\frac{dN}{dE}\Delta E$. In order to plot this on the same sheet a scale factor is usually used. All of the spectra shown in Appendix B (Figures B-3 through B-12) are of this type and on each is shown scale factor and window width (ΔE).

Having plotted these curves, one next uses a planimeter and obtains the area under each one. Each curve was planimetered at least 5 times and an average area used in further computations. The accuracy of this operation was better than 1 percent.

Thus we have two areas:

$$(a) \qquad \int_0^{E_{max}} \left(\frac{dN}{dE}\Delta E\right) = \Delta E \int_0^{E_{max}} \left(\frac{dN}{dE}\right) dE$$

IV. EXPERIMENTAL RESULTS AND COMPARISON WITH THEORY

A. General Mathematical Procedure and Preliminary Results.

1. Obtaining $\frac{dE}{dx}$ and Energy Loss Experimental Measurements.

We have seen in the preceding section that the directly plottable output of the final equipment was $\frac{dN}{dE}\Delta E$ vs E. In the previous notation. If now the ordinate of each point on the curve is multiplied by its abscissa, we obtain a curve of $E\frac{dN}{dE}\Delta E$. In order to plot this on the same sheet a scale factor is usually used. All of the spectra shown in Appendix B (Figures B-1 through B-12) are of this type and on each is shown scale factor and window width (ΔE).

Having plotted these curves, one next uses a planimeter and obtains the area under each one. Each curve was planimetered at least 5 times and an average area used in further computations. The accuracy of this operation was better than 1 percent.

Then we have the expression

$$(a) \qquad \int_{0}^{E_{max}} \left(\frac{dN}{dE}\Delta E\right) = \Delta E \int_{0}^{E_{max}} \left(\frac{dN}{dE}\right) dx$$

[since ΔE = constant for each run (III-B-5)]

$$\int_0^{E_{max}} \left(\frac{dN}{dE}\Delta E\right) dE = \Delta E \times N \quad \text{Kev} \times \text{counts/min.}$$

$$\text{(b)} \quad \int_0^{E_{max}} \left(E\frac{dN}{dE}\Delta E\right) dE = \Delta E \int_0^{E_{max}} \left(E\frac{dN}{dE}\right) dE$$

$$= \Delta E \times E_T \qquad \frac{\text{Kev} \times \text{Kev}}{\text{minute}}$$

That is, (a) is the total number of counts/minute in the spectrum multiplied by the window width in Kev; and (b) is the total energy absorption by secondary electrons measured in the crystal multiplied by the window width in Kev. If now we divide (b) by (a) we obtain the average secondary electron energy, and notice that is is independent of ΔE:

$$E_{AV} = \frac{\Delta E \times E_T}{\Delta E \times N} = \frac{E_T}{N}$$

However, if we are interested in the dosage, which is in turn related to the total energy absorbed by the secondary electrons, we find that we must know ΔE accurately.

It should be noted that the integration carried out was from zero to E_{max}. Since this required a somewhat arbitrary extrapolation of each curve to zero, the area under the extrapolated curves and the area under the

under the extrapolated curves and the area under the
tapering extrapolation of each curve to zero, the area
has been taken to E_{max}; since this resulted a somewhat

It should be noted that the integration carried out
electrons, we find that we must know ΔE accurately.
turn related to the total energy absorbed by the secondary
However, if we are interested in the change, which is in

of ΔE:

$$\beta_A = \frac{\Delta E \times E}{\Delta E \times E_\lambda} = \frac{E}{E_\lambda}$$

secondary electron energy, and notice that is is independent
Ker. If now we divide (B) by (A) we obtain the average
measured in the crystal multiplied by the stopping width in
(A) is the total energy absorption by secondary electrons
in the spectrum multiplied by the stopping width in Kev and

$$= \Delta E \times E_\lambda \qquad \frac{\text{Kev x Cts}}{\text{minute}}$$

Zone Ia, (A) is the total number of counts/minute

$$(A) \qquad \int_0^{E_{max}} \left(\frac{dN}{dE}\Delta E\right) dE = \Delta E \int_0^{E_{max}} \left(\frac{dN}{dE}\right) dE$$

$$\int_0^{E_{max}} \left(\frac{dN}{dE}\Delta E\right) dE = \Delta E \times E \quad \text{Kev x counts/min}$$

[since ΔE = constant for each run (III-3-1)]

unextrapolated curves was measured. The figures for both are plotted in Figures 7 and 8 and it is seen from Figure 8 that the extrapolation gives a point which is lower by a constant percentage. Thus, for ease in comparison, only the unextrapolated curve areas are considered hereafter, in that they involve no arbitrary extrapolation assumptions.

Returning now to (b), and assuming we know ΔE in Kev exactly, we see that we have measured the total energy of the secondary electrons per minute; i.e., the rate of energy absorption of the whole crystal from the gamma beam. How then can we convert this to "dosage"? To begin with, it is necessary to know the mass of crystal in which the absorption occurred. The crystals are therefore weighed:

Thin (6 mm crystal) = 5.023 gms.

Thick (30 mm crystal) = 6.098 gms.

Thus we obtain the energy absorption rate in terms of Mev/min-gm anthracene. But the roentgen can be expressed as 5.24×10^7 Mev/gm-air. Since we expect from Figure 1 that Compton effect predominates in the range considered, the only difference between air and anthracene lies in the number of scattering centers per gram; that is, the number of electrons per gram, which was computed in Appendix A:

$n = 3.007 \times 10^{23}$ electrons/gm air

$n = 3.18 \times 10^{23}$ electrons/gm anthracene.

Thus by multiplying our energy absorption rate in Mev/min-gm anthracene by $\frac{3.007}{3.18}$ and dividing by $\frac{5.24 \times 10^{7} \text{ Mev}}{\text{gm air}}$, we can obtain dosage rate in roentgens per minute; or more conveniently by a time correction, in milliroentgens per hour.

It must be remembered that we assumed that ΔE was known exactly. This assumption is not experimentally valid as has been mentioned in Section III-B; the result of its variation from run to run will be shown later in this section.

The possible correction for crystal thickness mentioned in Section II-C has not been made at this point. Refer to Section IV-C for the experimental merit thereof.

It should finally be noted that the decay of Na^{24} ($T_{1/2}$ = 15 hrs) during the 1 hour runs was accounted for by correcting the observed counting rates prior to plotting.

2. Preliminary Results and Selection of Crystal Configurations.

Before proceeding with measurements with all sources, it was desired first to see the gross effects of crystal configuration change with different conditions, such as length of light pipe, thickness of crystal, lucite plate on top of crystal and type of reflector. Many runs were

$n = 3.007 \times 10^{23}$ electrons/gm-atom

$p = 3.18 \times 10^{23}$ electrons/gm-atom.

Then by multiplying our density equation with $\frac{3.007}{3.18}$ and dividing by $\frac{6.64 \times 10^{7}}{60 \text{ sin}}$, we can obtain charge rate in coulombs per minute per gram-atom, or more conveniently by a slow conversion, in milliampheres per hour.

It must be remembered that we assumed that $\Delta\Sigma$ was known exactly. This assumption is not satisfactorily valid as has been mentioned in Section III-B; the result of its violation from run to run will be shown later in this section.

The possible correction for crystal imperfections mentioned in Section II-D has not been made at this point. Refer to Section IV-C for the experimental work thereof.

It should finally be noted that the theory of $Hg_{24}(T\lambda)_2$ = Ig pro) during the 3 hour runs was accounted for by correcting the observed counting rates prior to plotting.

3. Preliminary Results and Selection of Crystal Configurations.

Before proceeding with experiments with all crystals, it was desired first to see the gross effects of crystal configuration changes with different crystals, such as length of light path, thickness of crystal, inertia time on top of crystal and type of reflector. Many runs were

made with the cobalt and mercury sources under many configuration changes, and evaluation of them was made by comparison of spectral shapes. We will not bore the reader with enumeration of all these runs. The important effects noted are shown in Figures 9 and 10. In general, it was discovered that:

(a) Some light pipe was advantageous in that the light was distributed more evenly over the photo cathode, though length of light pipe was not an important factor. The light pipe also facilitated fitting the crystals to the curved top of the photomultiplier tube.

(b) A 1/4 mil (0.00025 in) aluminum foil reflector in smooth contact with all top and side crystal faces was very satisfactory.

(c) Figures 9 and 10 show that the spectral shape from cobalt was little affected by crystal thickness, while the mercury spectrum was more peaked for the thin crystal. In order to be sure that the geometry, and not the different <u>crystal</u>, was responsible for this difference, a run was made with the thick crystal on its side, with the 10 mm dimension vertically oriented. As Figure 10 clearly shows, the geometry was the cause of spectral shape change.

made with the object and material numbers under many
configurations exactly, and evaluation of them was made
by comparison of spectral outputs. We will not deal the
reader with enumeration of all these runs. The important
effects noted are shown in Figures 9 and 10. It seemed
it was discovered that:

(a) Some light pipe was extraneous in that
the light was distributed more evenly over the photo cathode.
Energy resolution of light pipe was not an important factor.
The light pipe also facilitated fitting the crystals to
the curved top of the photomultiplier tube.

(b) A 1\4 mil (0.00025 in) aluminum foil
reflector in smooth contact with all but one side crystal
cases was very satisfactory.

(c) Figures 9 and 10 show that the spectral
shape from source was little affected by crystal thickness,
while the accuracy therefore was more needed for the thin
crystal. In order to do more than "count", and not
the different energies, was responsible for this difference.
A run was made with the thick crystal on its face, with
the ID on the channels partially retained. In Figure 12
clearly shows, the feature was the cause of spectral shape
change.

Figure 9

PRELIMINARY DATA ON COBALT-60
SECONDARY ELECTRON SPECTRUM

Curves normalized to same counting rate in "valley" to show magnitude of effect of crystal thickness.

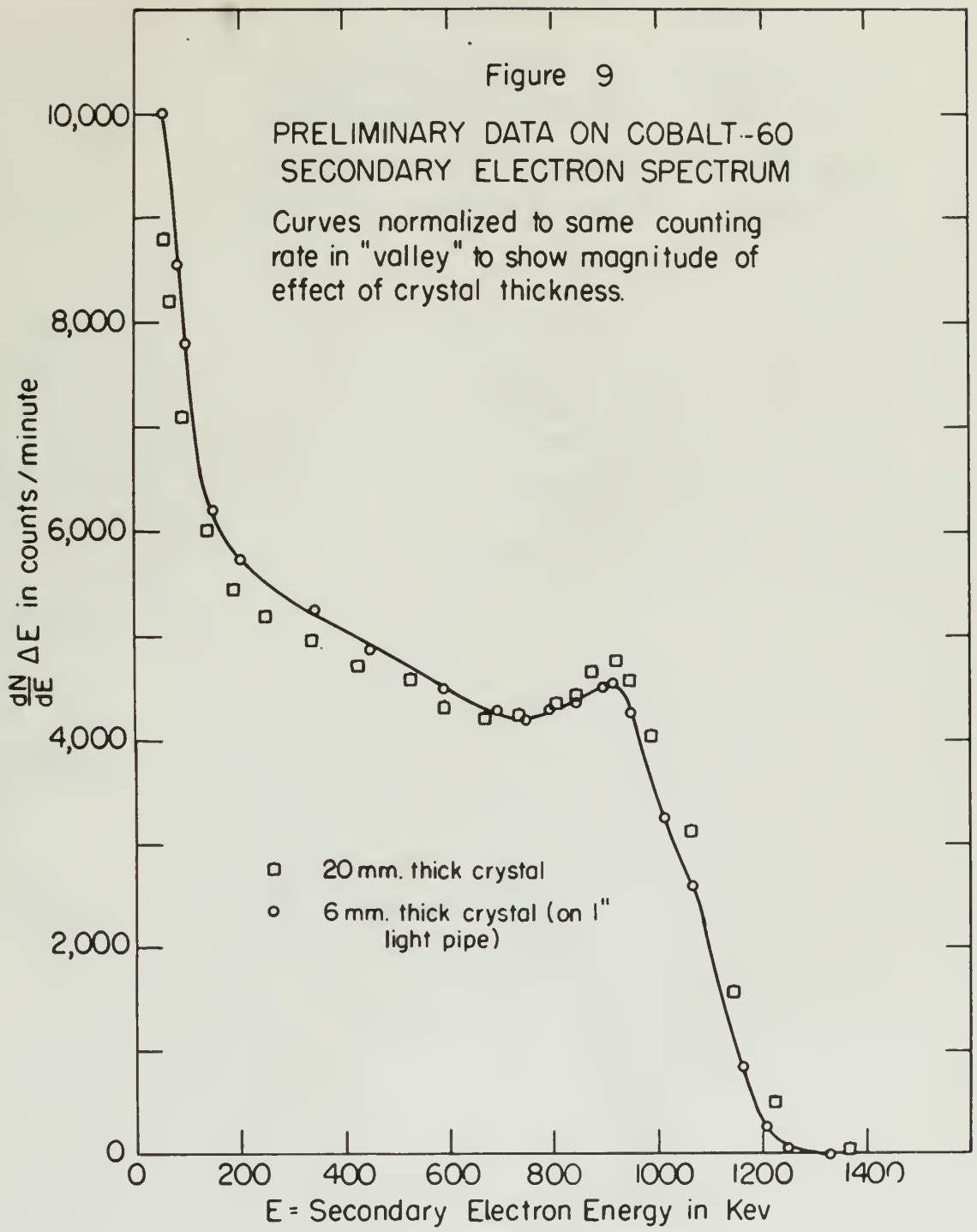

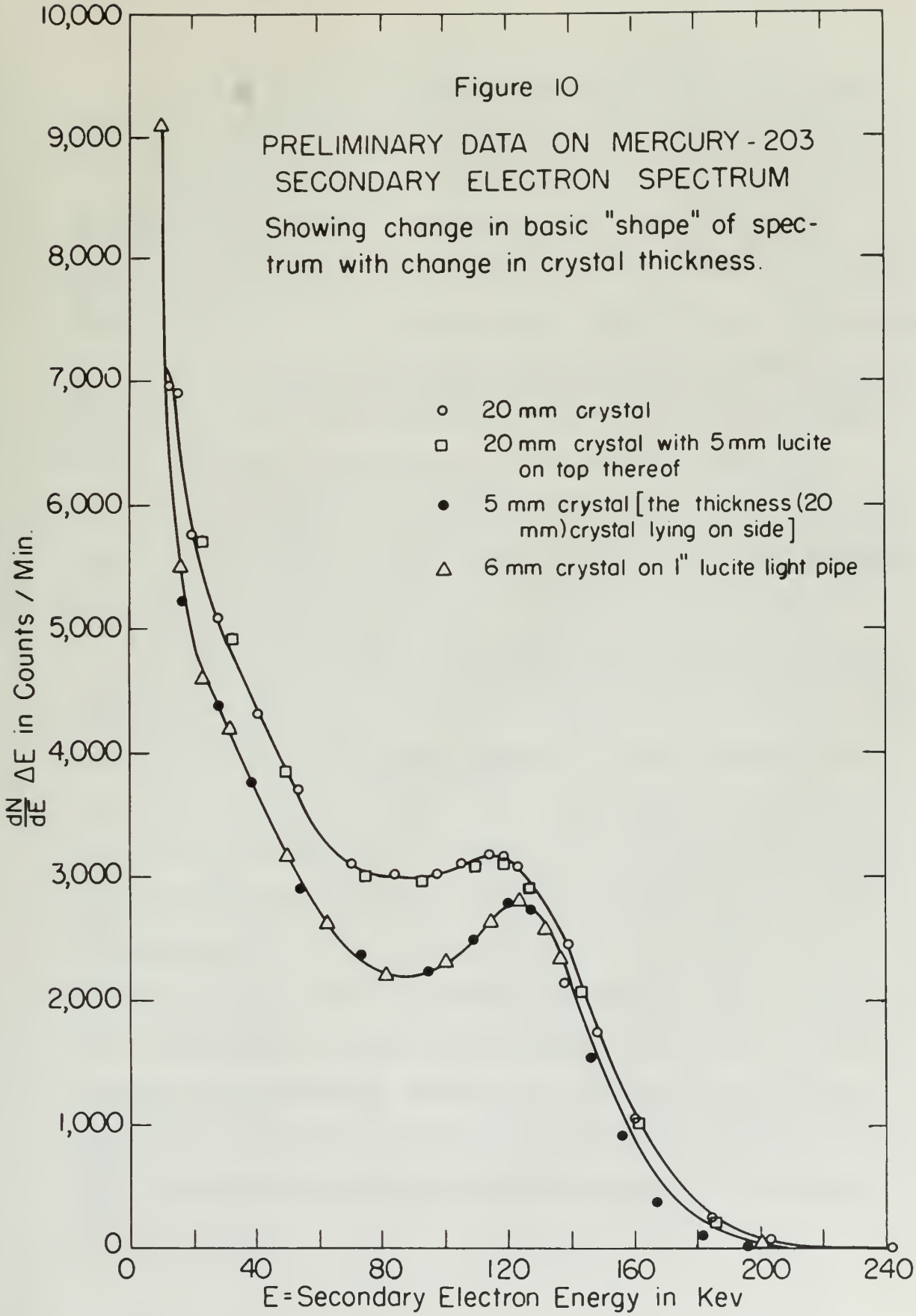
Figure 10
PRELIMINARY DATA ON MERCURY - 203
SECONDARY ELECTRON SPECTRUM
Showing change in basic "shape" of spectrum with change in crystal thickness.
20 mm crystal
20 mm crystal with 5 mm lucite on top thereof
5 mm crystal [the thickness (20 mm) crystal lying on side]
6 mm crystal on 1" lucite light pipe
dN/dE ΔE in Counts / Min.
E = Secondary Electron Energy in Kev
10,000
9,000
8,000
7,000
6,000
5,000
4,000
3,000
2,000
1,000
0
0
40
80
120
160
200
240

(d) Finally we see that the lucite plate atop the thick crystal made no difference to either spectrum.

Therefore, in order to obtain results chiefly dependent upon crystal thickness, the obviously most important variable, configurations "A" and "B" were chosen (Figure 6), with "A" involving the 6 mm crystal, "B" involving the 80 mm crystal. As a last determination, occasioned by the results with "A" and "B", another run was made with sodium using "B" enclosed in a 13 mm thick lucite box. This configuration is not shown; the results are described below. The results of all runs on "A" and "B" are included in Figures B-3 through B-12.

A point of general interest, before proceeding with specific results, is the general shape of all spectra. One should note that the large number of small pulses is not due to background or noise since each curve has been corrected therefor. The tailing off at high energies is due to phototube resolution and the statistical variation of emission from the photo cathode, as is borne out by the shape of the Cs^{137} conversion electron "line", Figure B-2. The curves showing the greatest difference in spectra between configurations "A" and "B" are those for sodium, where we see that the thicker crystal gave a much higher $E\frac{dN}{dE}\Delta E$ value at the high end of the spectrum. Finally,

(4) Finally we see that the Debye plate edge
the think crystal made no difference to either spectrum.

Therefore, in order to obtain results directly
dependent upon crystal thickness, the objectively most
important variable, configurations "A" and "B" were chosen
(Figure 6), with "A" involving the 3 mm crystal, "B" involving
the 30 mm crystal. As a last determination, associated by
the results with "A" and "B", another run was made with
section mating was replaced by a 13 mm Debye Scherrer Box.
This configuration is not shown; the results are described
below. The results of all runs on "A" and "B" are included
in Figures 3-3 through 3-12.

A point of general interest, before proceeding with
specific results, is the general shape of all spectra. One
should note that the large number of small values is not
due to background or noise since each curve has been
corrected therefor. The falling off at high energies is
due to photoelectron recoil and the statistical variation
of emission from the photo cathode, as is borne out by
the shape of the Cs_{137} conversion electron "line", Figure
3-2. The curves showing the greatest difference in spectra
between configurations "A" and "B" are those for sodium
where we see that the thicker crystal gave a much higher
$\frac{dE}{dE}$ value at the high end of the spectrum. Finally,

the peak is termed a "Compton Peak" and corresponds to the most probable energy obtained in Compton collisions; qualitatively, it appears where it should be, somewhat below the maximum energy of Compton electrons as computed by formula (II-B-1).

B. Average Secondary Electron Energy Results and Theory Correlation.

1. Presentation of Results.

The tabulation of Table II-C-1 is repeated here, with experimental values added. These data are also displayed in Figures 7 and 8, in which the logarithmic plot is included to show the relative deviation of the points from the theoretical curve.

TABLE IV-B-1

Source	$\bar{E}_\gamma$	Crystal Conf.	E_{AV} (exper)	E_{AV} (theoretical) Partially Corr.	Totally Corr.
Hg^{203}	280 Kev	A	68.8 Kev	72.1 Kev	72.1 Kev
Cs^{134}	608 Kev	A	250 Kev	271.5 Kev	268.9 Kev
Co^{60}	1.25 Mev	A	506 Kev	586. Kev	584. Kev
Na^{24}	2.07 Mev	A	800 Kev	1.109 Mev	1.028 Mev
Ra	~1.06 Mev	A	422 Kev	-	-
Hg^{203}	280 Kev	B	71.6Kev	72.1 Kev	72.1 Kev
Cs^{134}	608 Kev	B	258 Kev	271.5 Kev	268.5 Kev
Co^{60}	1.25 Mev	B	555 Kev	586. Kev	584. Kev
Na^{24}	2.07 Mev	B	841 Kev	1.108 Mev	1.037 Mev
Ra	~1.06 Mev	B	456 Kev	-	-

the peak is termed a "Compton Peak" and corresponds to the most probable energy obtained in Compton collisions; qualitatively, it appears where it should be, somewhat below the maximum energy of Compton electrons as computed by formula (II-3-1).

b. Inverse Compounder Electron Energy Results and Theory Correlation.

1. Presentation of Results.

The tabulation of Table II-C-1 is repeated here, with experimental values added. These data are also displayed in Figures 7 and 8, in which the logarithmic plot is included to show the relative deviation of the points from the theoretical curve.

TABLE IV-B-1

Source	E_γ	Crystal Const.	N_{EY} (meter)	E_{EY} (Experimental) Partially Corr.	Totally Corr.
Co^{57}	120 Kev	1	69.3 Kev	72.1 Kev	72.1 Kev
Cs^{134}	604 Kev	A	480 Kev	571.4 Kev	588.9 Kev
Co^{60}	1.18 Mev	A	808 Kev	808. Kev	824. Kev
Na^{24}	1.37 Mev	A	900 Kev	1.10 Mev	1.028 Mev
Ra	~1.08 Mev	A	480 Kev	-	-
Co^{57}	120 Kev	B	71.0Kev	72.1 Kev	72.1 Kev
Cs^{134}	604 Kev	B	480 Kev	571.4 Kev	588.9 Kev
Co^{60}	1.18 Mev	B	808 Kev	808. Kev	824. Kev
Na^{24}	1.37 Mev	B	841 Kev	1.10 Mev	1.028 Mev
Ra	~1.08 Mev	B	480 Kev	-	-

The experimental values tabulated are from the unextrapolated curves as was mentioned in IV-A-1. In addition to the data plotted above, another Na^{24} source was obtained, which happened to be stronger than the source for which values are tabulated in Table IV-B-1, and had to be placed at three times the previous distance used for sodium. This source was run on configuration "B" and on "B-1", the latter being "B" encased in a lucite box (13 mm thick) on sides and top, seeking the effect mentioned in II-E-3(c). The spectral curves for these runs are not included since they appear nearly the same as Figures B-9 and B-10. The values of E_{AV} and dosage obtained from them, however, differ appreciably. Data obtained:

Configuration	E_{AV}
"B"	908 Kev
"B-1"	971 Kev

The increase in E_{AV} for "B" over that shown in Table IV-B-1 is attributable to the change in distance, since by Section II-E, the leakage would be less with a more parallel gamma beam; i.e., for the greater distance. The maximum divergence of the beam from the vertical was 7.9° for the shorter distance and only 0.95° for the longer distance. Accordingly, for comparing the effect of the lucite box (B-1) to the earlier sodium data

The experimental values tabulated are from the unsophisticated curves as was mentioned in IV-4-1. In addition to the data listed above, another E_{84} source was obtained, which appeared to be stronger than the source T-- which values are tabulated in Table IV-6-1, and had to be placed at three times the previous distance used for scaling. This source was run on configurations "g" and on "5-12", the latter being "a" covered in a lucite box (1) mm thick) on sides and top, leaving the effect mentioned in II-3-3(a). The spectral curves for these runs are not included since they present nearly the same as Figures 3-8 and 3-10. The values of E_{γ} and decays obtained from them, however, differ appreciably, they obtained:

Configuration	E_{γ}
"g"	903 Kev
"5-12"	891 Kev

The increase in E_{γ} for "g" over that given in Table IV-6-1 is attributable to the change in distance, since by Problem II-8, the leakage would be less with a more parallel beam (i.e., for the greater distance. The maximum divergence of the beam from the vertical was 1.3° for the shorter distance and only 0.85° for the longer distance. Accordingly, for correcting the effect of the lucite box (5-1) to the earlier reading data

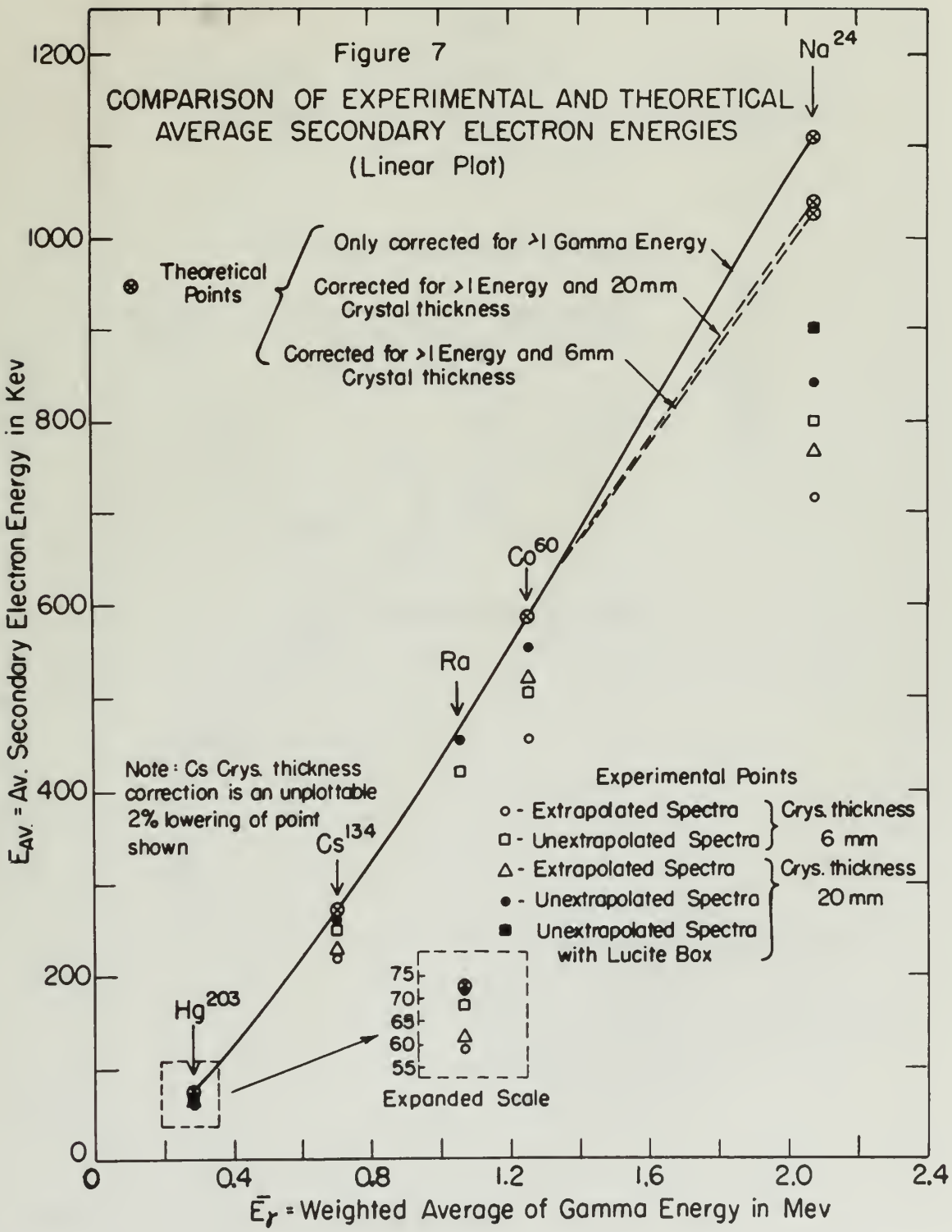
Figure 7
COMPARISON OF EXPERIMENTAL AND THEORETICAL AVERAGE SECONDARY ELECTRON ENERGIES
(Linear Plot)
Theoretical Points
Only corrected for >1 Gamma Energy
Corrected for >1 Energy and 20mm Crystal thickness
Corrected for >1 Energy and 6mm Crystal thickness
Na24
Co60
Ra
Cs134
Hg203
Note: Cs Crys. thickness correction is an unplottable 2% lowering of point shown
Experimental Points
o - Extrapolated Spectra
□ - Unextrapolated Spectra
Crys. thickness 6 mm
Δ - Extrapolated Spectra
● - Unextrapolated Spectra
■ Unextrapolated Spectra with Lucite Box
Crys. thickness 20 mm
75
70
65
60
55
Expanded Scale
$E_{Av.}$ = Av. Secondary Electron Energy in Kev
$\bar{E}_\gamma$ = Weighted Average of Gamma Energy in Mev
0
200
400
600
800
1000
1200
0.4
0.8
1.2
1.6
2.0
2.4

Figure 8

COMPARISON OF EXPERIMENTAL AND THEORETICAL AVERAGE SECONDARY ELECTRON ENERGIES

(Logarithmic Plot)

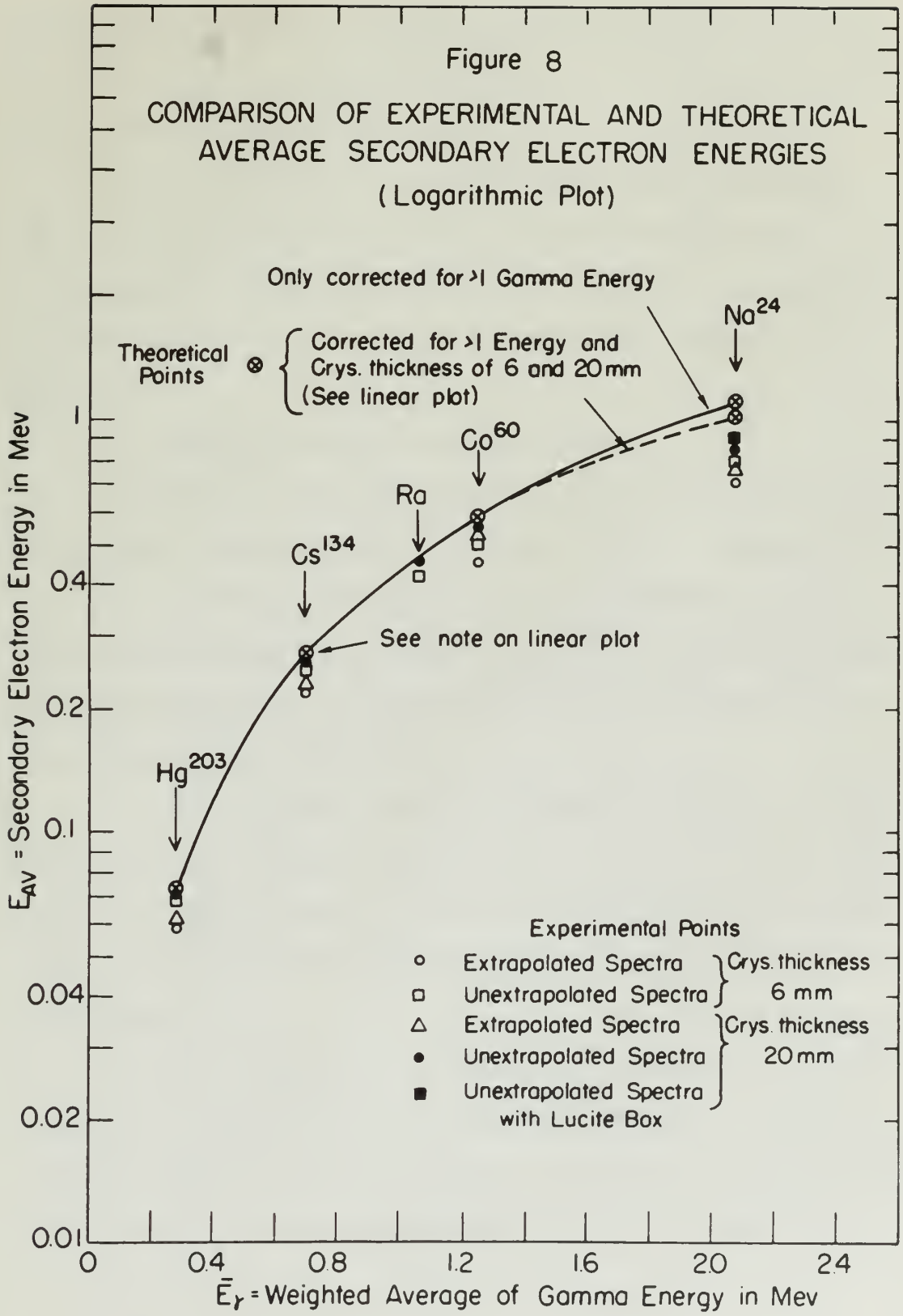

(which are plotted in Figures 7 and 8), E_{AV} for "B-1" was corrected to that distance with a linear approximation and plotted as $971 \times \frac{841}{908} = 900$ Kev.

The values of $\overline{E}_{\gamma}$ for Ra are obtained by fitting the E_{AV} points obtained to the curve connecting the corresponding points for the other sources. Comment on the value of $\overline{E}_{\gamma}$ obtained for Ra will be reserved for Section V.

2. Interpretation and Evaluation.

A number of very interesting results are obtainable from a close inspection of Figures 7 and 8. Figure 8 is probably of more value, since its logarithmic ordinate scale presents constant ratios or percent difference as constant distances. These points are enumerated for clarity and easy reference:

(a) First, we note that all measured E_{AV} are below the theoretical values. This is in agreement with Section II-E-3(d) page 38, and substantiates the belief that plural scattering was of little importance in our crystals.

(b) Secondly, all of the values for the thick crystal are above those for the thin crystal. This is as predicted in II-E-2, page 36. Of course, this conclusion is the result of one measurement on each configuration

is the result of one measurement on each configuration
as predicted in II-E-2, page 36. Of course, this consistency
crystal are *given* those for the thin crystal. This is
(b) *Second*, all of the values for the thick
crystals.

that plural scattering was of little importance in our
Section II-E-3(d) page 38, and substantiates the belief
below the theoretical values. This is in agreement with
(a) *First*, we note that *all* measured $\Sigma^{\lambda\lambda}$ are

clarity and easy reference:
constant distances. These points are enumerated for
scale presents constant ratios or percent differences as
property of more value, since its logarithmic ordinate
from a close inspection of Figures 7 and 8. Figure 8 is
a number of very interesting results are obtainable

1. Interpretation and Evaluation.

Section V.
the value of $\bar{E}^{\lambda}$ obtained for Pa will be preserved for
corresponding points for the other sources. Comment on
the $\Sigma^{\lambda\lambda}$ points obtained by the curve connecting the

The values of $\bar{E}^{\lambda}$ for Pa are obtained by fitting
and plotted as $571 \times \frac{908}{511} = 900$ Kev.
was corrected to that distance with a linear approximation
(which are plotted in Figure 7 and 8), $\Sigma^{\lambda\lambda}$ for "E-1"

for each of 5 sources, and there is a finite chance that this could be a coincidence. However, if we considered that there should be equal values for thick and thin crystal and that probability and randomness were the cause of one being higher than the other, then the chance of all of the thick crystal values being greater than the thin crystal values is, of course, $(\frac{1}{2})^5 = \frac{1}{32}$. True, we may have had the one chance in 32 occurring; only further experimentation by other parties will tell. However, the authors feel strongly that this is a physical phenomenon explainable by Section II-E-2.

(c) Next we see that the "totally corrected" curve is closest to the experimental results; and that for low energies, the experimental points are very close to the theoretical, differing from it by a nearly constant ratio for energies less than 1 Mev, with a slight increase in error at Co^{60}, and a considerable increase in error for the energetic gammas of Na^{24}, as also manifested by the spectral shape, as noted in Section IV-A-2 (page 58). The trend away from the theoretical curve at high energies is in conformity again with Section II-E; and further substantiation to the argument regarding electron leakage and its correction, per Section II-E-3, is the rise of the sodium point with configuration B-1. This indicates that

the effect of "scattering-in" of II-B-3(c) predominates over the "compensating" effect of (a) and (b), same section.

Thus, the majority of our theory is confirmed. In general, the anthracene crystal is "air-equivalent", but crystal geometry must be considered in designing a scintillation dosimeter for gamma energies above 1.25 Mev, since the effects of secondary electron leakage become increasingly important with increasing energy, and these effects are apparently the ones which cause a deviation from true air equivalence. Round crystals of about 20 mm diameter and 20 mm in thickness, surrounded with a lucite cylinder of wall thickness of ~10 mm would appear to be the best geometry, and experimentation therewith is recommended.

C. Attempt at Dosage Evaluation.

1. Procedure.

In order to evaluate the dosages as obtained from the integration of the curves as described in Section IV-A-1, a Keleket dosimeter was obtained. The calibration curves for this chamber are included in Appendix B as Figures B-13 and B-14. The dosimeter was placed in the crystal's position and runs made on all sources for a number of

hours necessary to obtain a reasonable reading on the scale of 200 mr. The dosimeter run on Na^{24} with its short half-life was corrected back to the zero time of the discriminator run by the easily derivable formula:

$$R_o = \frac{D\lambda}{(e^{-\lambda t_1} - e^{-\lambda t_2})} ;$$

in which D = total (less background) dosage measurement, λ = decay constant, t_1 = time of beginning dosimeter exposure, t_2 = time of ending exposure, R_o = dose rate at zero time (beginning of discriminator run). A similar formula was used to convert the reading on 46.5 day Hg^{203} back an interval of some 10 days to the day of its discriminator run.

The dosage exposure runs required a good deal of exposure time, as is seen from the dose rates below. For this reason, it was not possible to take enough exposures to get a low statistical standard deviation, as may be seen by Table IV-C-1, and, as will be shown, the variation of window width made further attempts impractical.

2. Comparison of Computed Dosage and Measured (Dosimeter) Dosage.

As has been mentioned before, the window width ΔE (in volts) varied from run to run in spite of careful

$$\frac{\partial}{\partial t}$$

setting of zero sets on the differential discriminator. It should be noted that ΔE in Kev is also a function of the position of the Cs^{137} peak, and is therefore subject to a small error due to the statistical variations therein. In computing the data set forth in Table IV-C-1 by the method of Section IV-A-1, E in Kev was computed using a window width of 1.8 ± 0.1 volts, a conservative estimate of the error. From Table IV-C-1, it can be seen that only qualitative conclusions can be drawn: The computed dosage rate generally agrees with the measured rate within 10 percent. In general, it may be said that this electronic difficulty eliminates the possibility of using this equipment to measure dose rate, though the value of the equipment in establishing the air-equivalence of anthracene is not affected by the difficulty and the results of IV-B above are perfectly valid.

TABLE IV-C-1

Source	Crystal Conf.	Dosage× ΔE (mr/hr×Kev)	ΔE(Kev)	Calc. Dosage (mr/hr)	Observed (Dosimeter) Dosage (mr/hr)
Hg^{203}	A	5.45	5.7[illegible]±0.3	0.953±0.050	0.944±0.2
Hg^{203}	B	5.53	7.[illegible]±0.4	0.770±0.043	0.944±0.2
Cs^{134}	A	49.1	15.5 ±0.8	3.18 ±0.16	3.[illegible]4 ±0.7
Cs^{134}	B	58.7	18.6 ±1.0	3.16 ±0.18	3.84 ±0.7
Co^{60}	A	633	36.6 ±[illegible].0	17.3 ±0.9	14.7 ±0.3
Co^{60}	B	4[illegible]6	33.0 ±1.8	1[illegible].93 ±0.7	14.7 ±0.3
Na^{24}	B	1880	72.8 ±4.0	[illegible]5.8 ±1.4	31.5 ±[illegible].2
Na^{24}	B-1	2080	73.6 ±4.0	[illegible]8.3 ±1.5	31.5 ±[illegible].2
Ra	A	384	43.1 ±[illegible].4	8.9 ±0.5	9.19 ±1.3
Ra	B	517	54.3 ±[illegible].9	9.5 ±0.5	9.19 ±1.3

Because of this wide scatter of comparative results, no attempt has been made to include an evaluation of the correction factors of II-C-3(b). Before such could be done, a method of accurate window width determination would be required (see Section V).

The reader is now referred to the following section for a summary of findings and additional interpretation and discussion thereof.

Species	Symmetry	Frequency (cm^{-1})	Intensity	$\Delta\nu_{1/2}$	Total Cross Section (cm²/molecule)	Observed Cross Section (cm²/molecule)
H_2O	A	3652	0.1	5.0	0.7×10^{-20}	0.044×10^{-20}
H_2O	B	3756	0.1	5.0	1.0×10^{-20}	0.044×10^{-20}
CH_4	A	2917	0.3	10.0	14.4×10^{-20}	3.14×10^{-20}
CH_4	B	3019	0.6	10.0	28.8×10^{-20}	3.14×10^{-20}
CO	A	2143	0.1	10.0	1.4×10^{-20}	1.47×10^{-20}
CO	B	2158	0.1	10.0	1.4×10^{-20}	1.47×10^{-20}
N_2O	B	2240	0.3	10.0	4.3×10^{-20}	2.2×10^{-20}
N_2O	A	2563	0.3	10.0	4.3×10^{-20}	2.2×10^{-20}
O_3	A	1042	0.3	10.0	4.3×10^{-20}	0.44×10^{-20}
O_3	B	1110	0.6	10.0	8.6×10^{-20}	0.44×10^{-20}

Because of their wide overlap of temperature sensitive regions, only one band needs to be included in evaluation of the temperature factors of II-C-1(f). Before such could be done, a method of accurate atomic line intensities would be required (see Section V).

The reader is now referred to the following section for a summary of findings and additional interpretation and discussion thereof.

V. SUMMARY AND RECOMMENDATIONS

A. General Conclusions.

From the experimental results as given in detail in Section IV it can be concluded that:

1. Anthracene is essentially air-equivalent in the energy range considered, except as noted in (2) and (3) below.

2. Deviations from air-equivalence will be experienced at higher gamma energies if the scintillating medium is not large enough to eliminate electron leakage; or at the lower gamma energies if the crystal is so large that plural scattering becomes appreciable.

3. Electron leakage can be minimized by surrounding the crystal with a "reflecting" material similar in composition to the anthracene.

4. Dosage measurements made with the scintillation counter were consistent with those made by an ionization chamber, subject to the inaccuracy imposed by indeterminacy in differential discriminator window width.

5. It appears to be very difficult to construct an electronic circuit to display the scintillator output directly in terms of dosage. A circuit was used which gave this indication indirectly.

7. [illegible] and [illegible]

4. [illegible]

[illegible] any [illegible] shall be [illegible] Section 17 [illegible]

1. [illegible] [illegible] [illegible] [illegible] [illegible] [illegible] [illegible] [illegible] [illegible] [illegible] below.

2. [illegible] [illegible] [illegible] [illegible] [illegible] [illegible] [illegible] [illegible] [illegible] [illegible]

6. As described in Section IV-B-1, a value of 1.06 Mev for the weighted average energy ($\overline{E}_\gamma$) of the gamma rays from a radium source with 0.5 mm platinum filtration was obtained. This is consistent with the results of Hine[24], who obtained 1.04 Mev, but somewhat higher than a computed value of 0.84 Mev using the spectrum given by Ellis and Aston[25] and using data from Davisson[9] to compute the effect of Pt filtration. Other spectra mentioned in the literature would give values agreeing more closely with the results obtained herein, but since the value of the weighted average gamma ray energy of a spectrum as complex as radium is in doubt, nothing further can properly be concluded here.

B. Recommendations for Future Investigations.

Since crystal size at higher energies is important further work should be done in getting more detailed quantitative information on the effect. These data will be important to workers using the scintillation counter at energies above ~1.5 Mev.

In order to make the system using the differential discriminator give indication of dosage accurate enough for research purposes, a method of determining the exact window width must be devised. Two such methods are suggested:

(a) Use of a scaler-timer circuit in conjunction with the equipment used by the authors; with discrimination level of scaler matched to the lower level of the differential discriminator. In this way, ΔE can be determined by comparison with the measurement of $\Delta E \times N$ (Section IV-A).

(b) Use of a vacuum tube voltmeter with recording equipment, to monitor ΔE in volts directly across the particular resistor in the differential discriminator which provides the voltage difference ΔE. After this has been accomplished more work can be done on comparing the dosage given by the scintillation counter with that given by the air ionization chamber.

In order to utilize the scintillation detector as a practical instrument for indicating dosage a simple electronic circuit must be designed to sum the photomultiplier output over the number of pulses and pulse heights. One approach is to rectify the output taken directly from the photomultiplier tube to avoid overshoot difficulties. Ter-Pogossian[1] and the Sloan-Kettering Institute[26] have developed two such circuits but no information has been published concerning their accuracy, or other characteristics.

In conclusion, the authors wish to express their sincere thanks to Dr. Robley D. Evans for his invaluable counsel, advice, and encouragement throughout the whole of

(a) Use of a zener-diode circuit to synchronize with the equipment used by the operator the electrolysis level of zener reduced to the lower level of the differential discriminator. In this way, ΔI can be increased by combination with the measurement of ΔI = 0 (section II-1).

(b) Use of a vacuum tube voltmeter with reversible movement, to measure ΔI in volts directly across the particular resistor in the differential discriminator which contains the voltage difference ΔE. After this has been accomplished more work can be done on evaluating the change given by the potentiometer corrected with that given by the air ionization chamber.

In order to utilize the polarization technique as a practical instrument for locating damage a simple electronic circuit must be designed to put the potentiometer output over the reading of values and value criteria. The requirement is to rectify the output using diversity from the oscillating type to avoid overshoot difficulties. Therefore[11] and the Glaser-Wetherby Institute[10] have developed the most circuits that an interesting has been published concerning their accuracy, or close correspondence.

In conclusion, the authors wish to express their sincere thanks to Dr. Martin C. Brown for his invaluable counsel, advice, and encouragement throughout the whole of

this work; to Dr. Gerald J. Hine for his original suggestion of the problem, infinite patience and day-by-day guidance without which little success would have been possible; to Mr. Norman Rudnick for his aid in developing a reasonable theory; to all the personnel of the Radioactivity Center, M.I.T. for their cooperation at all times: Mr. Joel B. Bulkley and Mr. Sidney G. Millen; and finally to Mrs. Grace Rowe for her competent draftsmanship in reproducing the figures included.

APPENDIX A

COMPUTATION METHODS FOR σ, σ_a, τ, K

APPENDIX A

APPENDIX A

COMPUTATIONS FOR ATTENUATION AND ABSORPTION COEFFICIENTS

1. For air, the required information is available from Goodman[11] and its accuracy in σ and σ_a was checked by recomputing σ and σ_a from ${}_e\sigma$ and ${}_e\sigma_a$ as given in reference (12). In these computations, the percentage by weight of air was used as follows:

Nitrogen	75.8 percent
Oxygen	23.22 percent
CO_2	0.05 percent
Rare gases	0.93 percent

This gave a figure of 3.007×10^{23} electrons per gram, in agreement with Lea[13], which when combined with ${}_e\sigma$ and ${}_e\sigma_a$ and density in gms/cm^2 gives σ and σ_a in cm^{-1}.

2. For anthracene and sodium iodide no ready-made curves were available and each coefficient had to be calculated by the use of appropriate formulas, taking the weight percentage of each element into account.

APPENDIX V

CALCULATIONS FOR EXCITATION AND DEEXCITATION COEFFICIENTS

Anthracene ($C_{14}H_{10}$)

Percent hydrogen by weight = 5.61

Percent carbon by weight = 94.39

Electrons per gram calculation: N = Avogadro's number

H: $0.0561 \text{ gms} \times \frac{1 \text{ mole}}{1 \text{ gm}} \times \frac{6.02 \times 10^{23} \text{ atoms}}{\text{mole}} \times \frac{1 \text{ electron}}{\text{atom}} = 0.0561N$

C: $0.9439 \times \frac{1 \text{ mole}}{12 \text{ gms}} \times \frac{6.02 \times 10^{23} \text{ atoms}}{\text{mole}} \times \frac{6 \text{ electrons}}{\text{atom}} = \frac{0.471N}{0.5281N}$

Therefore electrons/gm = 3.18×10^{23}

ρ = density of anthracene = 1.25 gms/cc.

Sodium iodide

Percent Na by weight = 15.3

Percent I by weight = 84.7

Similar computation to anthracene gives 2.572 elect/gm.

ρ = density of sodium iodide crystal = 3.667 gm/cc.

Thus for these two crystals, knowing the electrons/gm and ρ, we obtain ${}_e\sigma$ and ${}_e\sigma_a$ from reference (12), and compute σ and σ_a as a function of E_γ.

The computation of τ and κ is a bit more difficult. First let us consider the photoelectric effect. Lea[13] gives an empirical photoelectric relation:

$$\tau/\rho = 0.0089 \frac{Z^{4.1}}{A} \lambda^n$$

where λ is the gamma wavelength in angstroms; and tabulates

Antimony ($^{121}Sb^{123}$)

Fermi Velocity of metal = 3.02

Fermi Energy of metal = 3.78

Electrons per free molecule: 3 = Avogadro's number

In $0.0367 \text{ gm} \times \frac{1 \text{ gm}}{1 \text{ mole}} \times \frac{6.02 \times 10^{23} \text{ atoms}}{\text{mole}} \times \frac{3 \text{ electrons}}{1 \text{ atom}} = 0.0663$

Or $0.0659 \times \frac{1 \text{ mole}}{12 \text{ gm}} \times \frac{6.02 \times 10^{23} \text{ atoms}}{\text{mole}} \times \frac{3 \text{ electrons}}{\text{atom}} = \frac{0.1978}{0.0736}$

Therefore electrons/cc = 2.69×10^{22}

k = Density of molecules = 1.01 gm/cc.

Boiling Point

Pressure in mm mercury = 12.3

Pressure 1 in metals = 12.4

Electric resistivity at temperature given $(.320$ ohm$/cm$.

k = density of boiling point crystal = 3.884 gm/cc.

Then for known the hysteria, pressure the electrons/cc and γ,

we obtain σ_{α} and σ_{α}^{β} then relations (21), and compute σ_{α}

and σ^{β} as a function of ζ^{λ}.

The conversion of λ and K in mix zone different.

Plate 7cm on monitor the thermometric effect. $Fig(13)$

Steps in monitor thermometric negation

$$\lambda\lambda\beta = 0.0000 \frac{\beta}{\sigma^{-1}}$$

Above T is the Fermi sensitivity in temperature and resistance

values of n and of the coefficient of λ^n for various elements:

Element	Coefficient	n
H	0.009	3.05
C	1.150	3.05
Na	7.200	2.85

Therefore for anthracene, weighting each coefficient by the percent abundance of the element, we obtain

$$(\tau/\rho)_{anth} = \left[(0.0561)(0.009) + (0.9439)(1.15)\right] \lambda^{3.05}$$

$$= \frac{2.067 \times 10^{-6}}{E_\gamma^{3.05}} \text{ cm}^{-1} \qquad (E_\gamma \text{ in Mev})$$

This weighting method was applied as a check to a determination of τ/ρ for air and the value obtained was in agreement with published values of τ for air[11].

We notice that the value of n in λ^n is not given for iodine, and it was therefore not possible to use the above method completely for sodium iodide.

$$(\tau/\rho)_{Na} \text{ by Lea formula} = \frac{2.644}{E_\gamma^{2.85}} \times 10^{-5} \quad \frac{\text{cm}^2}{\text{gram}}$$

From Victoreen[14] we find

$$(\tau/\rho)_I = 1140\,\lambda^3 - 1163\,\lambda^4 \qquad \lambda \text{ in angstroms.}$$

$$= \frac{2.17 \times 10^{-3}}{E_\gamma^3} - \frac{2.73 \times 10^{-5}}{E_\gamma^4} \quad \frac{\text{cm}^2}{\text{gram}}$$

values of a and of the coefficients of f_{xy} for various elements:

Element	Coefficients	a
Si	0.004	3.09
Cr	1.130	3.09
Fe	1.000	3.09

Therefore for calculating weighting mass coefficient for the various elements of the element, we obtain

$$(\mu/\rho)_{comp} = \left[(0.0001)(0.003) + (0.8430)(1.12)\right] f_{3.09}$$

$$= \frac{1.00 \times 10^{-4}}{\lambda^{3.09}} \quad \text{cm}^2\text{/gm}$$

This weighting scheme was applied to a curve by a determination of μ/ρ for λ_E and the value obtained was in agreement with published values of λ for air[11].

To derive (1-3 the value of a in λ_E is now given the letter, and is now therefore not "specific" to mass the whole method consistently for weighing lambda.

$(\mu/\rho)_{Si}$ by the formula $= \frac{1.00}{\lambda^{3.09}} + 3.09 \quad \frac{\text{cm}^2}{\text{gm}}$

Pure Electrons[12] we find

$(\mu/\rho)^1 = 1100\ \lambda_E - 1100\ \gamma_E$ λ in Angstroms.

$$= \frac{1.17 \times 10^{-3}}{\lambda^3} - \frac{1.11 \times 10^{-3}}{\lambda^4} \quad \frac{\text{cm}^2}{\text{gm}}$$

Then by the usual weighting,

$$(\tau/\rho)_{NaI} = (0.153)(\tau/\rho)_{Na} + (0.847)(\tau/\rho)_{I}$$

from which formula τ_{NaI} was computed.

Finally, K was computed for both crystals by use of a lead standard curve. Lead was chosen because its theoretical pair production curve has been well checked by experimentation. A Project Rand report[15] tabulates the atomic pair production coefficient σ_{pp} for lead where $K = \frac{N}{A}\rho\,\sigma_{pp}$, N being Avogadro's number, ρ the density, and A the mass number.

Then from Kine[16]

$$K/\rho \propto N \sum_i p_i \frac{Z_i^2}{A_i}$$

where p_i = percent, by weight, of constituents.

$$\text{Therefore } \frac{(K/\rho)_{lead}}{(k/\rho)_x} = \frac{\frac{Z_{lead}^2}{A_{lead}}}{\left(\sum_i p_i \frac{Z_i^2}{A_i}\right)_x}$$

$$\text{whence } K_x = \rho_x \frac{K_{lead}}{\rho_{lead}} \frac{A_{lead}}{Z_{lead}^2} \left[\sum_i p_i \frac{Z_i^2}{A_i}\right]_x$$

Substituting from above, to obtain K_x in terms of Rand values:

$$(T/P)_{ref} = (0.120)(T/P)_{in} + (0.880)(T/P)_{1}$$

Then solid formula T_{Ref} was determined.

Finally, K was computed for both materials by use of a load adjusted curve. Load was chosen because its theoretical fair precipitation curve has been well mapped by experimentation. A [helium test result][3,4] validates the steady state conduction coefficient C_{ss} for load where $K = \frac{1}{n} \sum C_{ss}$ being Incendary's number, i the density, and i the mean number.

Then term [line][2,6]

$$K/\gamma \propto \pi \sum_{i} \rho_i^2 \frac{i^2}{n^2}$$

where λ^2 = thermal diffusivity of materials.

$$\text{Therefore } \frac{(K/\gamma)_{mod}}{(K/\gamma)_{ref}} = \frac{\frac{\rho_{mod}^2}{n^2}}{\left(\sum \rho_i^2 \frac{i^2}{n^2}\right)_{ref}}$$

$$\text{assume } K^2 = \frac{\rho_{mod}^2}{K_{ref}} \frac{i_{mod}^2}{i_{ref}} \left[\sum \rho_i^2 \frac{i^2}{n^2}\right]_{ref}$$

Substituting free above, to obtain K^2 in terms of load values:

$$K_x = \rho_x N \sigma_{pp} \frac{\left[\sum_i p_i \frac{Z_i^2}{A_i}\right]_x}{Z_{lead}^2}$$

For anthracene the constants evaluate to give

$$(K)_{anth} = 3.22 \times 10^{-3} \sigma_{pp} \text{ cm}^{-1}$$

For sodium iodide, we obtain

$$(K)_{NaI} = 8.27 \times 10^{-3} \sigma_{pp} \text{ cm}^{-1}$$

From these computations, the values of μ and μ_a were calculated for use in Section II. The variation of μ with E_γ is shown in Figure A-1, for anthracene and sodium iodide.

$$K^{\chi} = k_{\chi} d^{\frac{1}{2}} \frac{\left[\sum \frac{p_i x_i^2}{\sum p_i x_i}\right]}{\sum p_i x_i}$$

The relationship for anomalous scattering is given

$$(K)^{anom} = 1.11 \times 10^{-2} d^{\frac{1}{2}} \sin^{-1}$$

For medium lattice, we obtain

$$(K)^{met} = 0.27 \times 10^{-1} d^{\frac{1}{2}} \sin^{-1}$$

These three equations, the values of $\frac{1}{2}$ for γ^{χ} were calculated for use in section IX. The variation of $\frac{1}{2}$ with E_{γ}^{χ} is shown in Figure 4-1, for reference and section table.

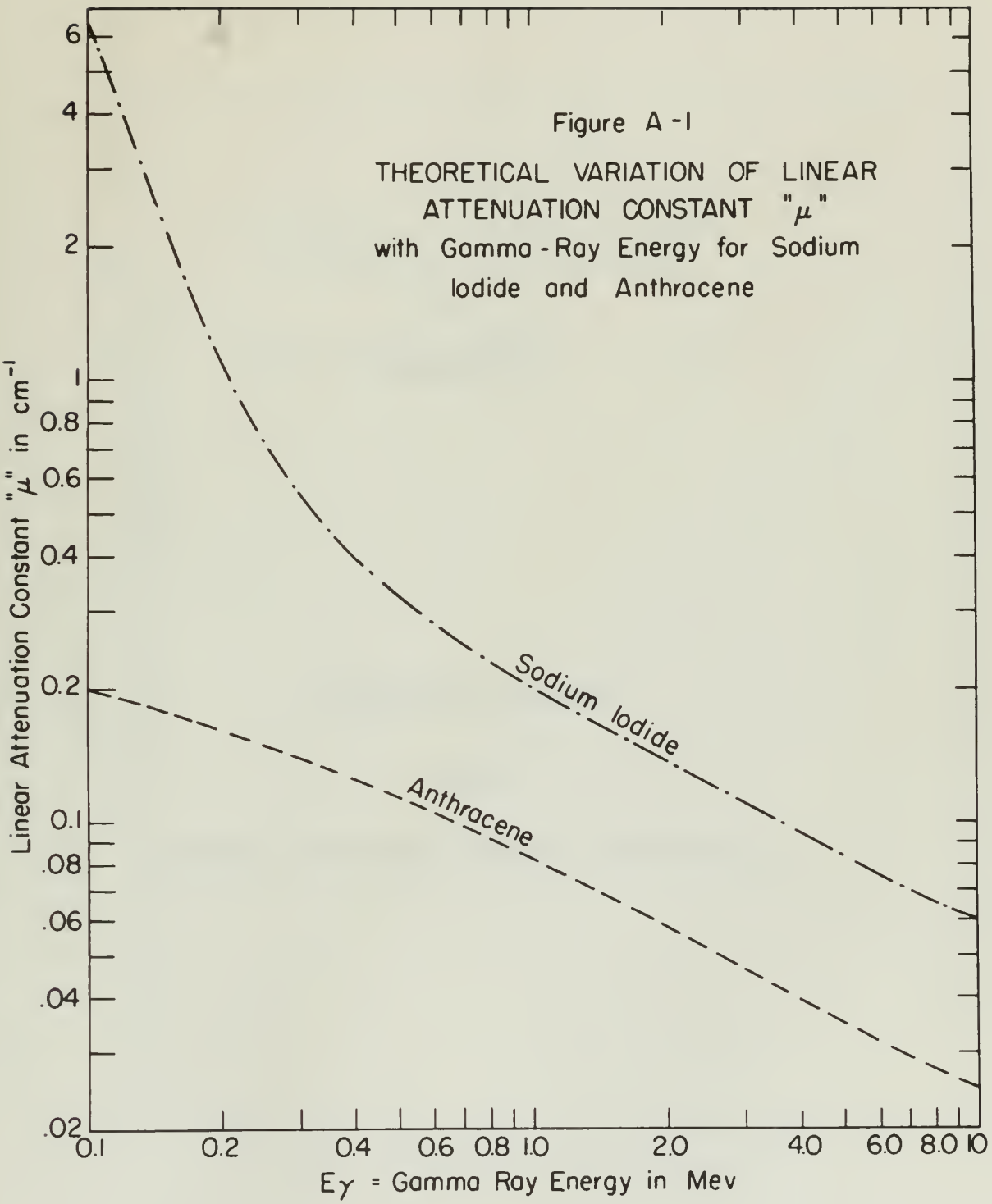
Figure A-1
THEORETICAL VARIATION OF LINEAR ATTENUATION CONSTANT "μ" with Gamma-Ray Energy for Sodium Iodide and Anthracene
Linear Attenuation Constant "μ" in cm⁻¹
6
4
2
1
0.8
0.6
0.4
0.2
0.1
.08
.06
.04
.02
Sodium Iodide
Anthracene
0.1
0.2
0.4
0.6
0.8
1.0
2.0
4.0
6.0
8.0
10
Eγ = Gamma Ray Energy in Mev

APPENDIX B

CALIBRATION CURVES

AND

SECONDARY ELECTRON SPECTRAL DISTRIBUTIONS

Figure B-1

CALIBRATION OF SINGLE CHANNEL
DIFFERENTIAL DISCRIMINATOR
Model 210

Window Width = $\frac{(\Delta E)}{\text{gain factor}}$ = 1.8 volts

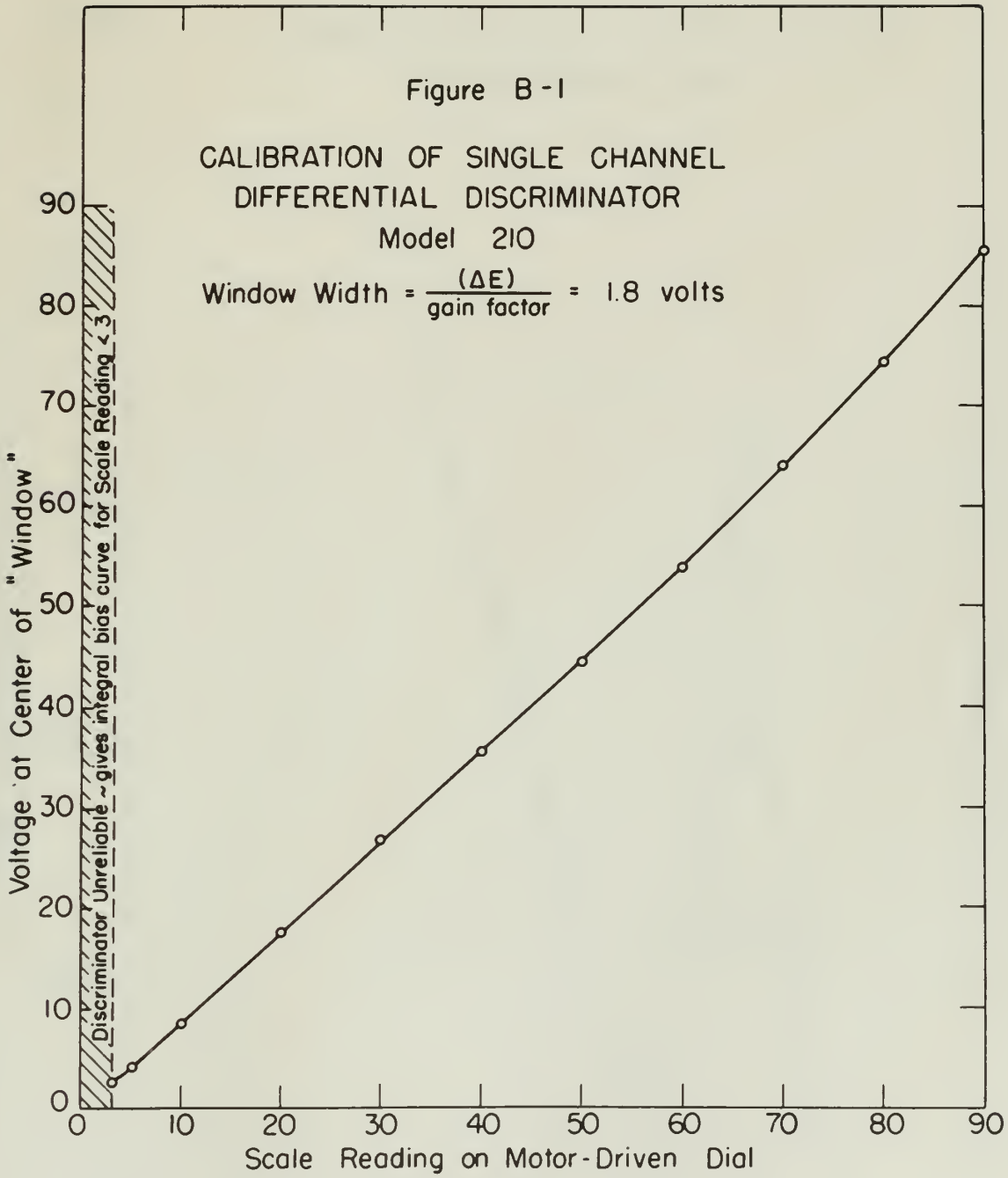

Figure B - 2

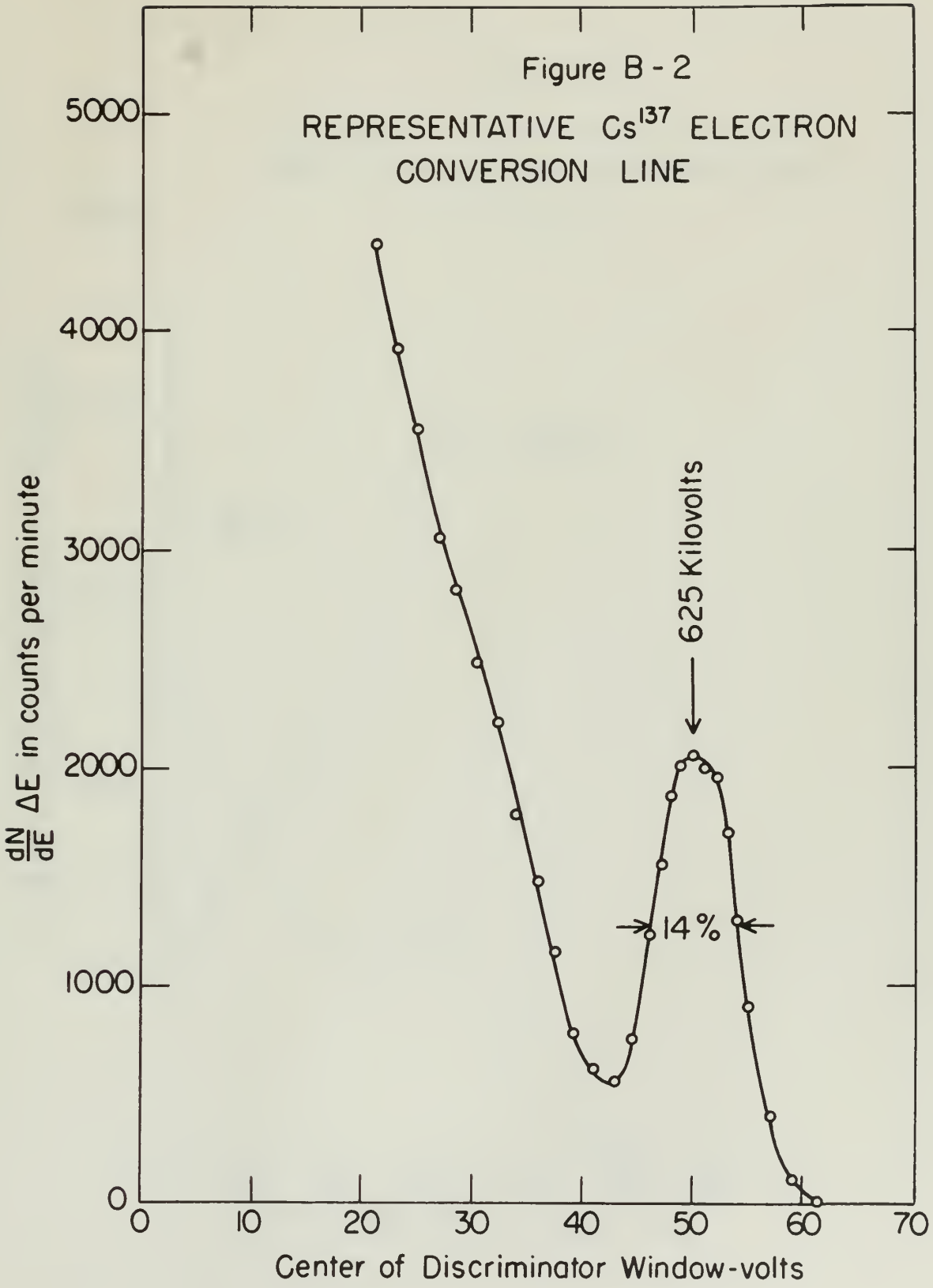
REPRESENTATIVE Cs137 ELECTRON CONVERSION LINE
5000
4000
3000
2000
1000
0
dN/dE ΔE in counts per minute
625 Kilovolts
14 %
0
10
20
30
40
50
60
70
Center of Discriminator Window-volts

Figure B-3

SECONDARY ELECTRON SPECTRUM OF Hg^{203} USING CRYSTAL CONFIGURATION "A"
(ΔE = 5.72 Kev)

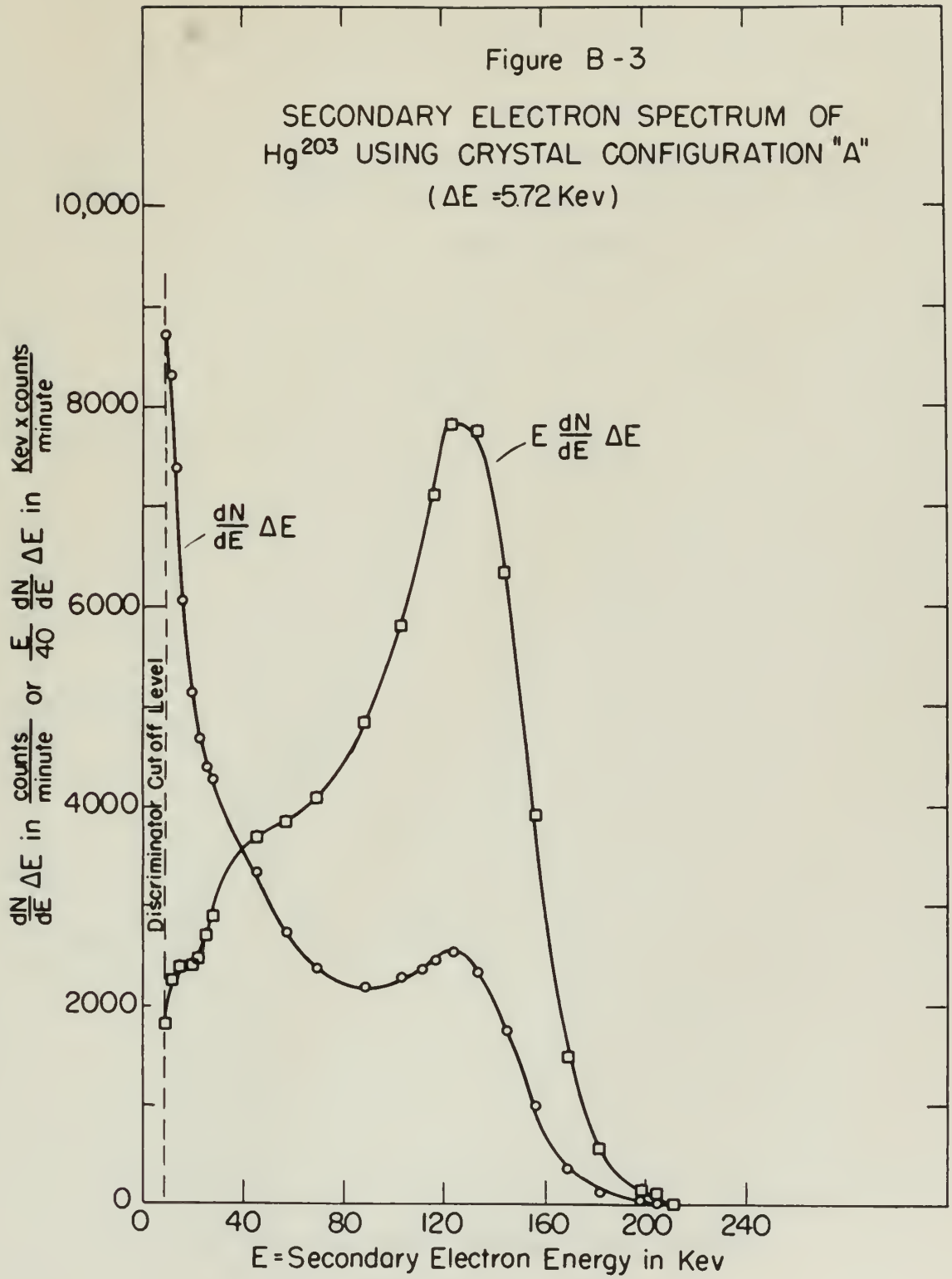

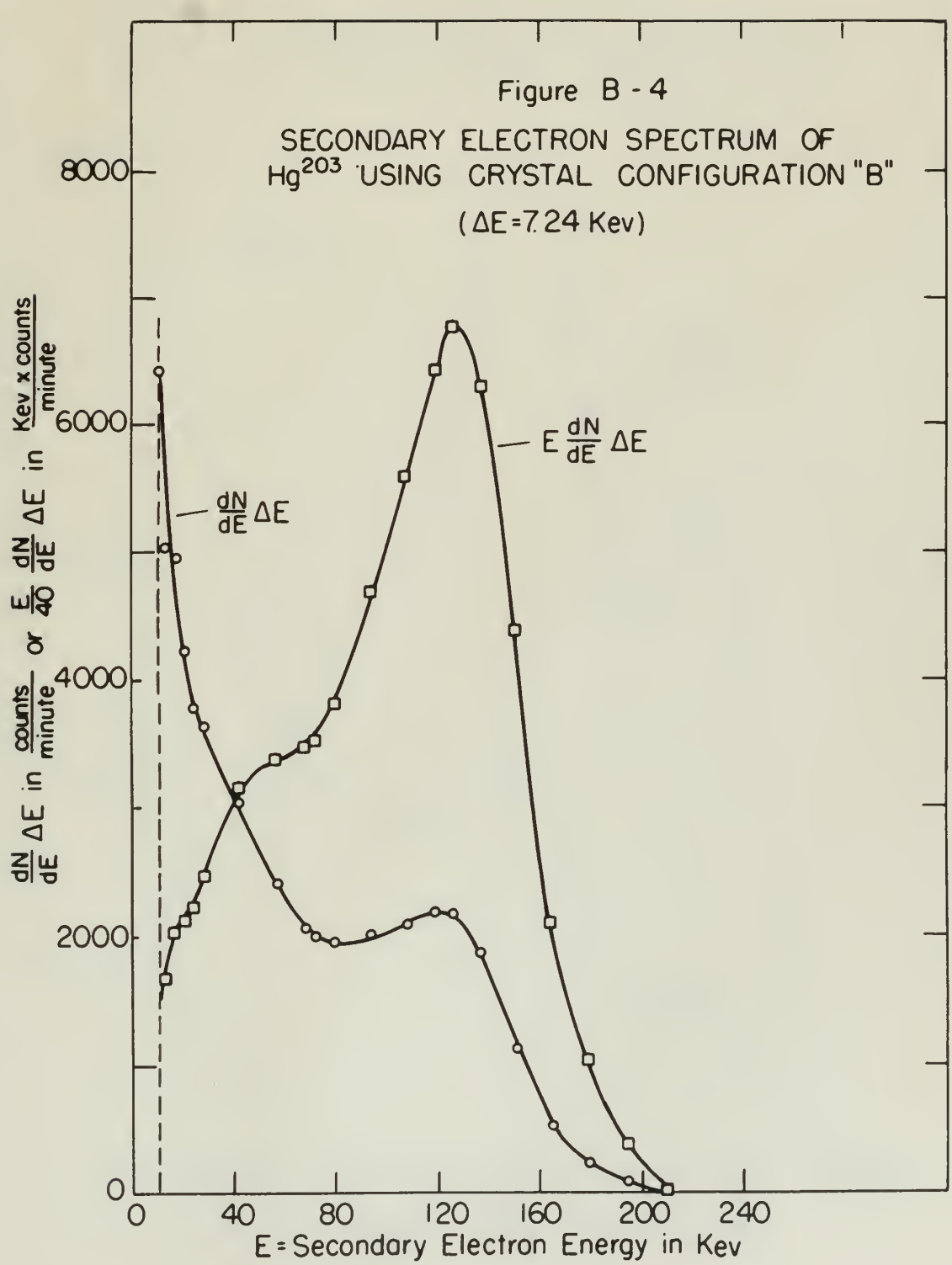
Figure B - 4
SECONDARY ELECTRON SPECTRUM OF
Hg203 USING CRYSTAL CONFIGURATION "B"
(ΔE=7.24 Kev)
8000
6000
4000
2000
0
0
40
80
120
160
200
240
E = Secondary Electron Energy in Kev
dN/dE ΔE in counts/minute or E/40 dN/dE ΔE in Kev x counts/minute
dN/dE ΔE
E dN/dE ΔE

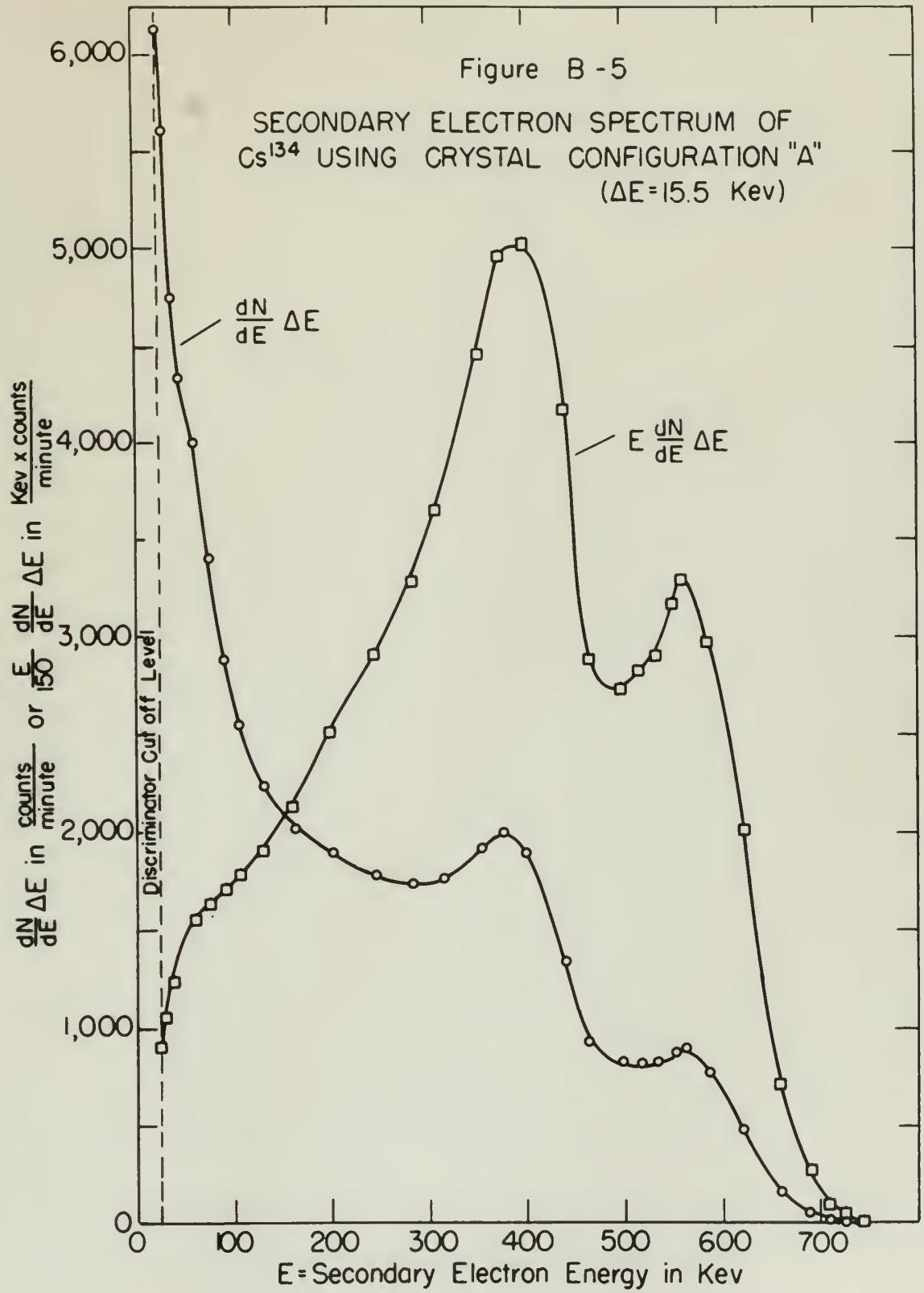
Figure B-5
SECONDARY ELECTRON SPECTRUM OF
Cs^{134} USING CRYSTAL CONFIGURATION "A"
(ΔE=15.5 Kev)
$\frac{dN}{dE}\Delta E$
$E\frac{dN}{dE}\Delta E$
Discriminator Cut off Level
$\frac{dN}{dE}\Delta E$ in $\frac{counts}{minute}$ or $\frac{E}{150}\frac{dN}{dE}\Delta E$ in $\frac{Kev \times counts}{minute}$
E = Secondary Electron Energy in Kev
0
1,000
2,000
3,000
4,000
5,000
6,000
100
200
300
400
500
600
700

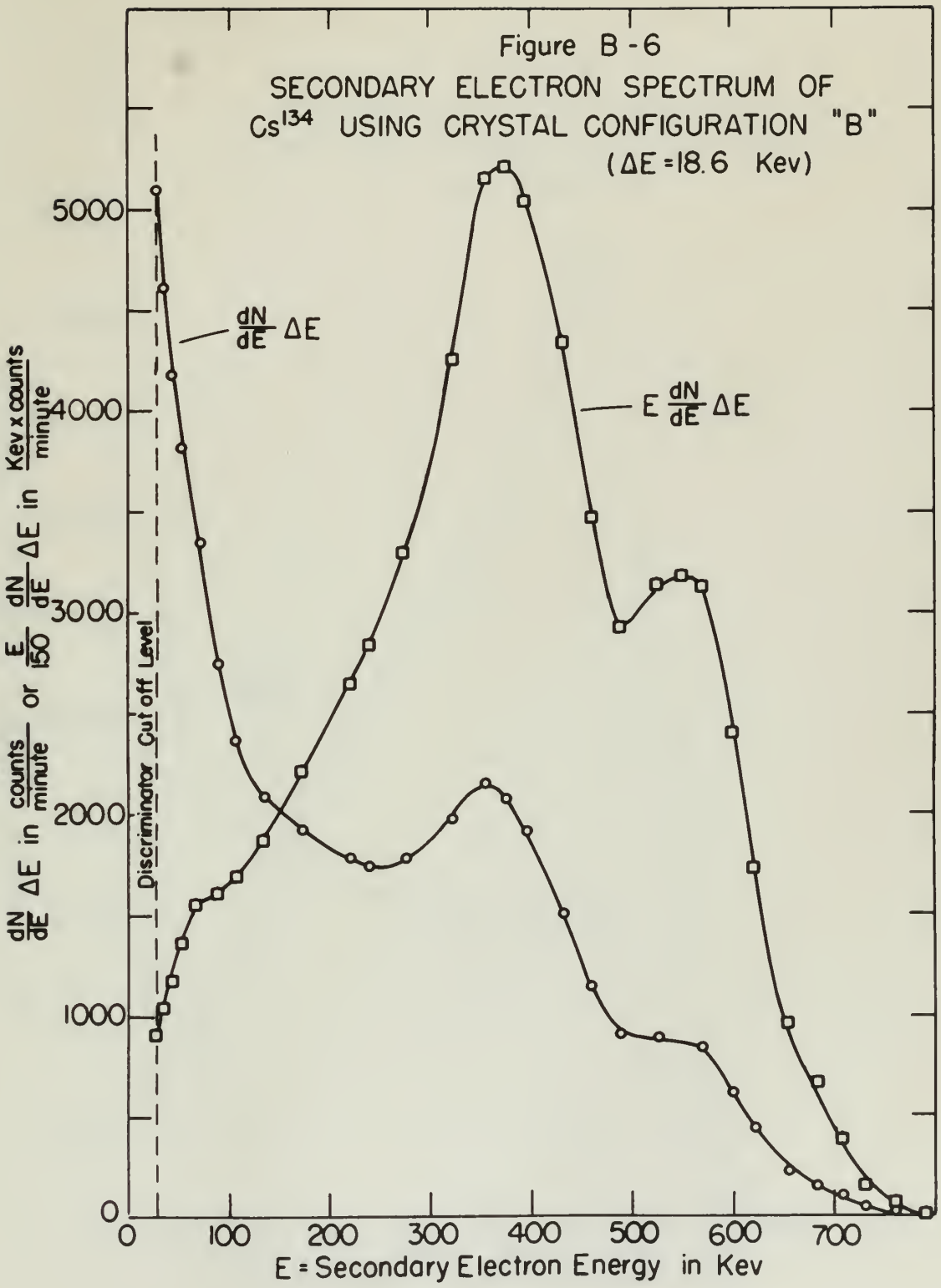
Figure B-6
SECONDARY ELECTRON SPECTRUM OF
Cs134 USING CRYSTAL CONFIGURATION "B"
(ΔE = 18.6 Kev)
dN/dE ΔE
E dN/dE ΔE
Discriminator Cut off Level
dN/dE ΔE in counts/minute or E/150 dN/dE ΔE in Kev x counts/minute
E = Secondary Electron Energy in Kev
0
1000
2000
3000
4000
5000
0
100
200
300
400
500
600
700

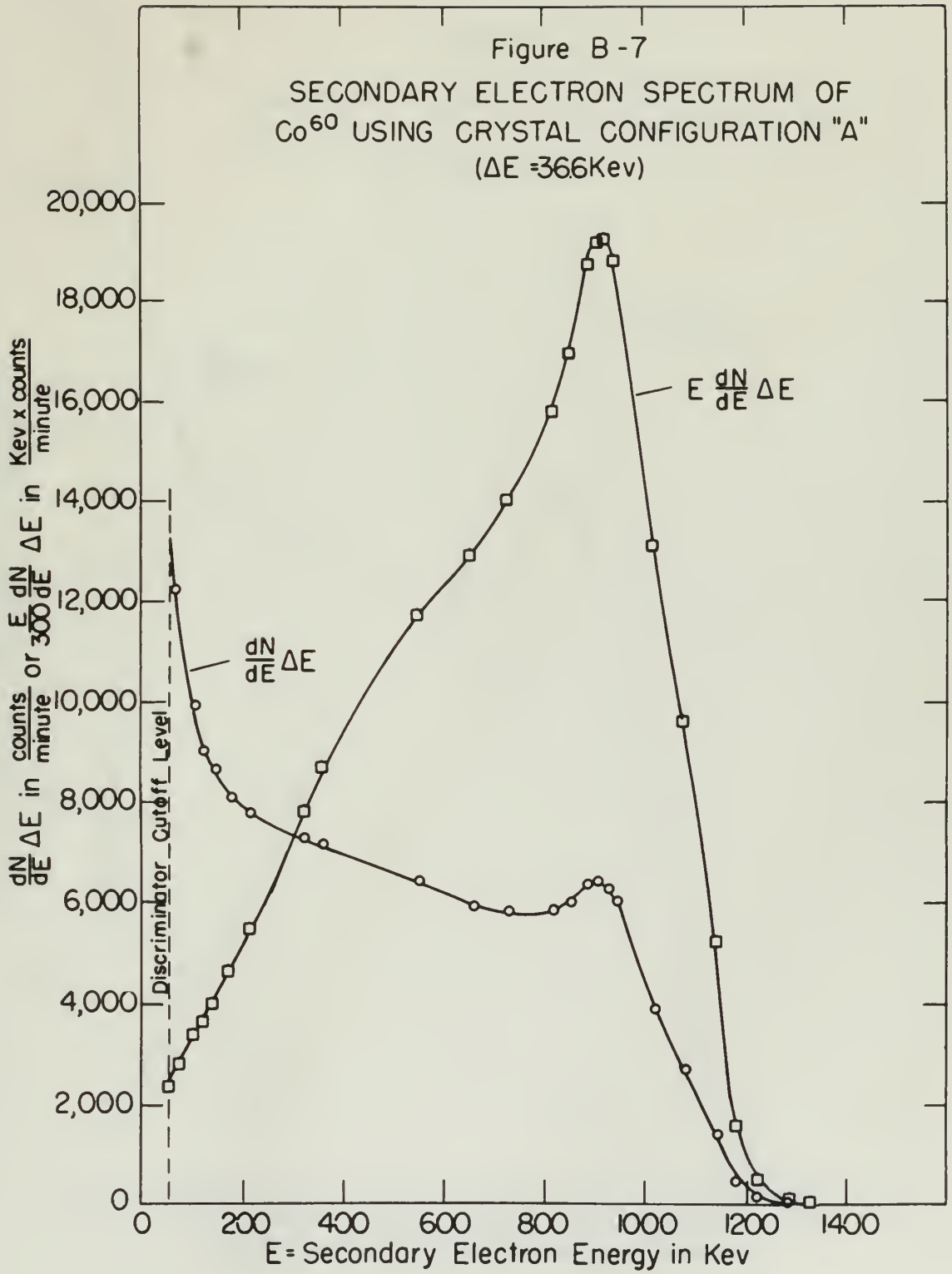
Figure B-7
SECONDARY ELECTRON SPECTRUM OF
Co60 USING CRYSTAL CONFIGURATION "A"
(ΔE =36.6Kev)
20,000
18,000
16,000
14,000
12,000
10,000
8,000
6,000
4,000
2,000
0
0
200
400
600
800
1000
1200
1400
E = Secondary Electron Energy in Kev
dN/dE ΔE in counts/minute or E/300 dN/dE ΔE in Kev x counts/minute
E dN/dE ΔE
dN/dE ΔE
Discriminator Cutoff Level

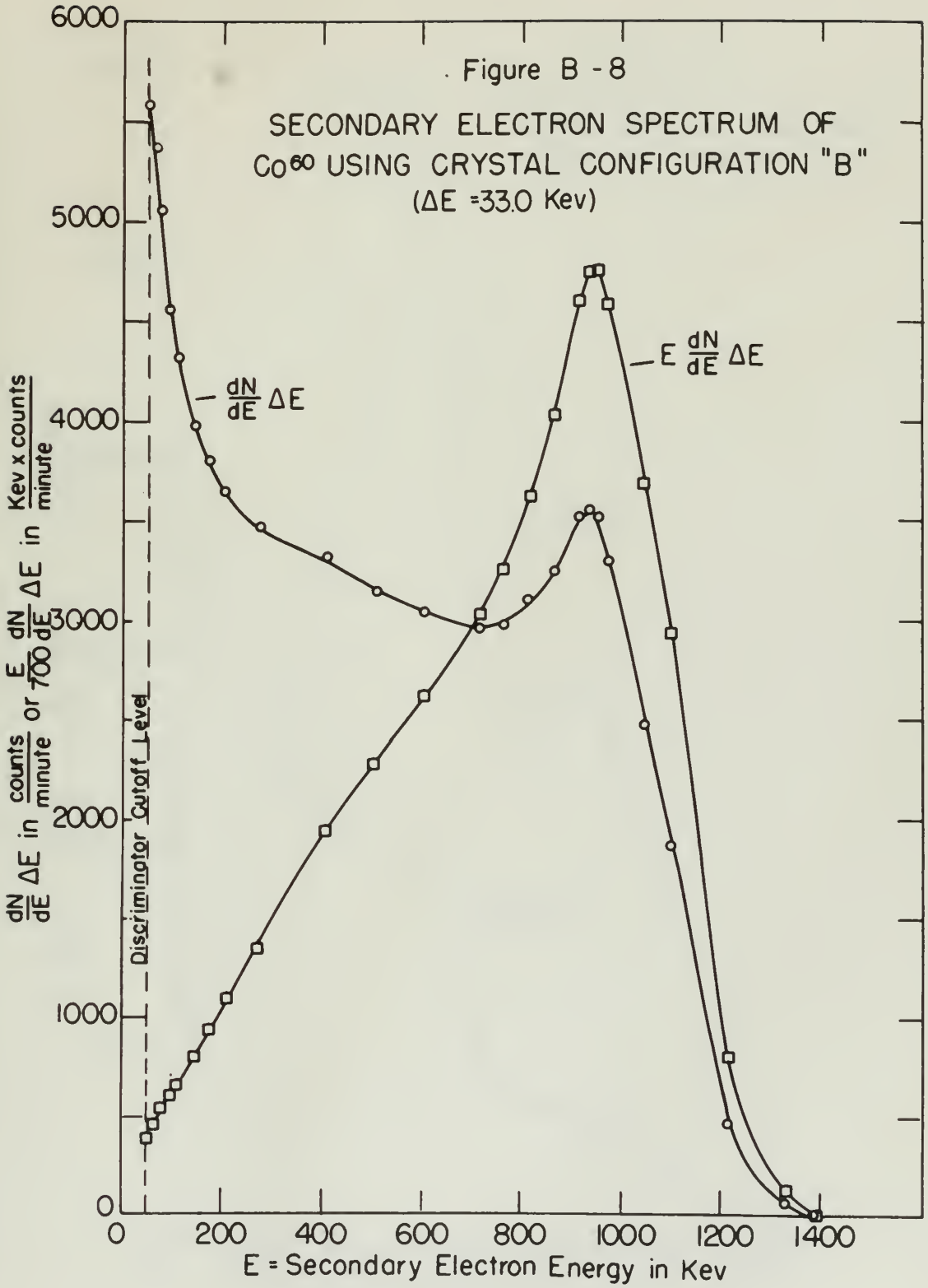
Figure B - 8
SECONDARY ELECTRON SPECTRUM OF
Co60 USING CRYSTAL CONFIGURATION "B"
(ΔE =33.0 Kev)
6000
5000
4000
3000
2000
1000
0
0
200
400
600
800
1000
1200
1400
E = Secondary Electron Energy in Kev
dN/dE ΔE in counts/minute or E/700 dN/dE ΔE in Kev x counts/minute
Discriminator Cutoff Level
dN/dE ΔE
E dN/dE ΔE

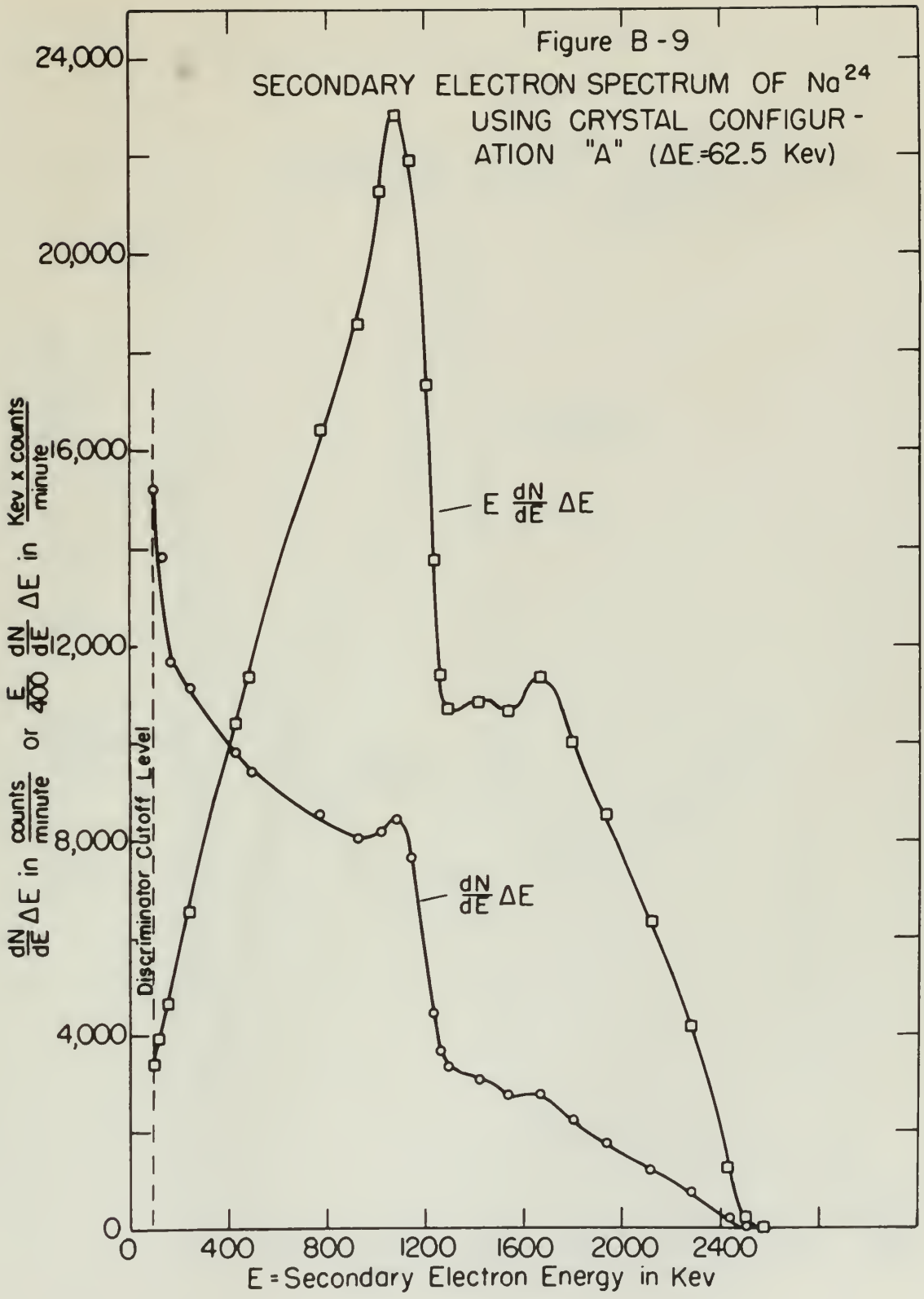
Figure B-9
SECONDARY ELECTRON SPECTRUM OF Na24 USING CRYSTAL CONFIGURATION "A" (ΔE=62.5 Kev)
24,000
20,000
16,000
12,000
8,000
4,000
0
0
400
800
1200
1600
2000
2400
E = Secondary Electron Energy in Kev
dN/dE ΔE in counts/minute or E/400 dN/dE ΔE in Kev x counts/minute
Discriminator Cutoff Level
E dN/dE ΔE
dN/dE ΔE

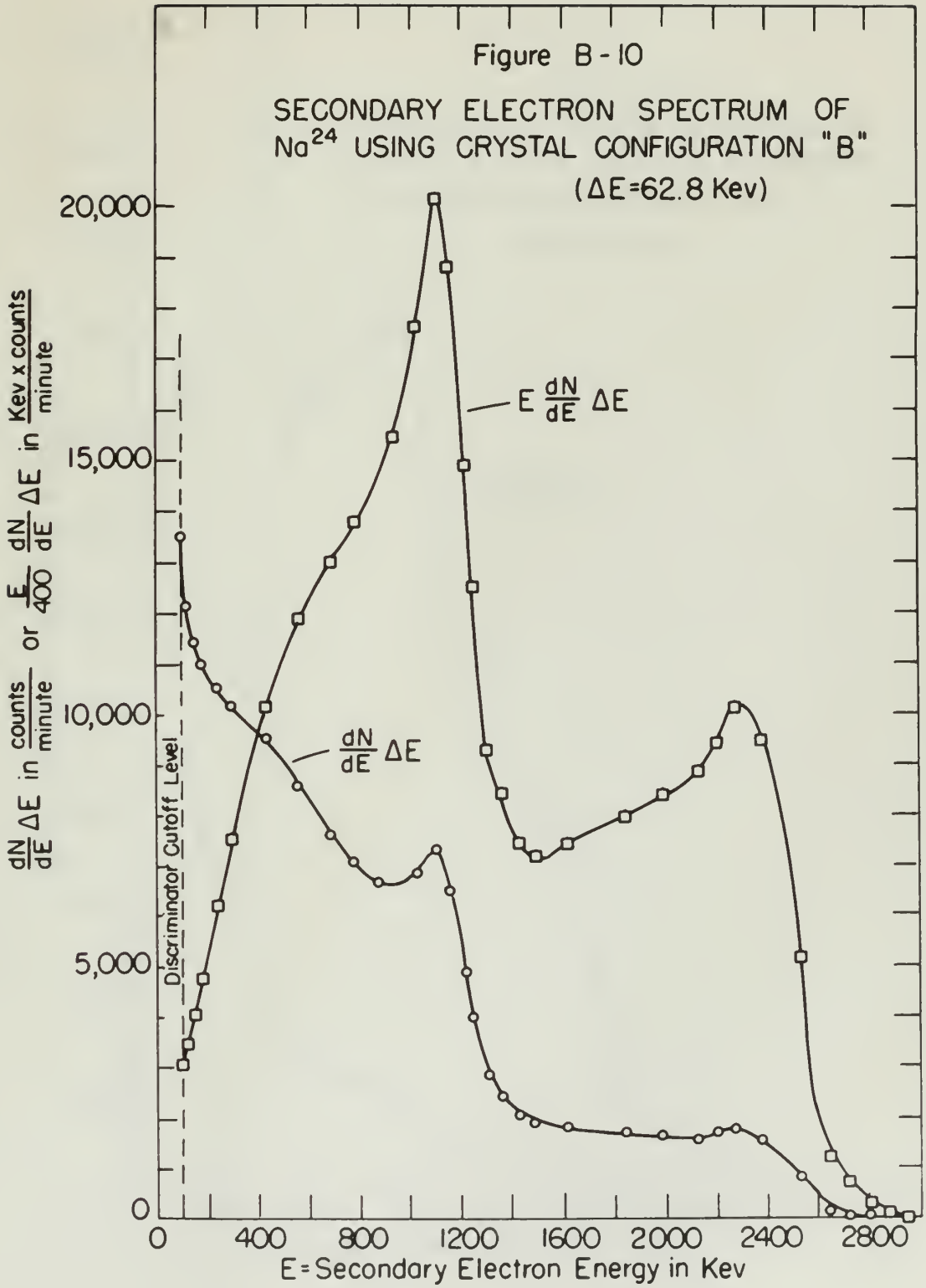
Figure B - 10
SECONDARY ELECTRON SPECTRUM OF
Na24 USING CRYSTAL CONFIGURATION "B"
(ΔE=62.8 Kev)
20,000
15,000
10,000
5,000
0
0
400
800
1200
1600
2000
2400
2800
E = Secondary Electron Energy in Kev
dN/dE ΔE in counts/minute or E/400 dN/dE ΔE in Kev x counts/minute
E dN/dE ΔE
dN/dE ΔE
Discriminator Cutoff Level

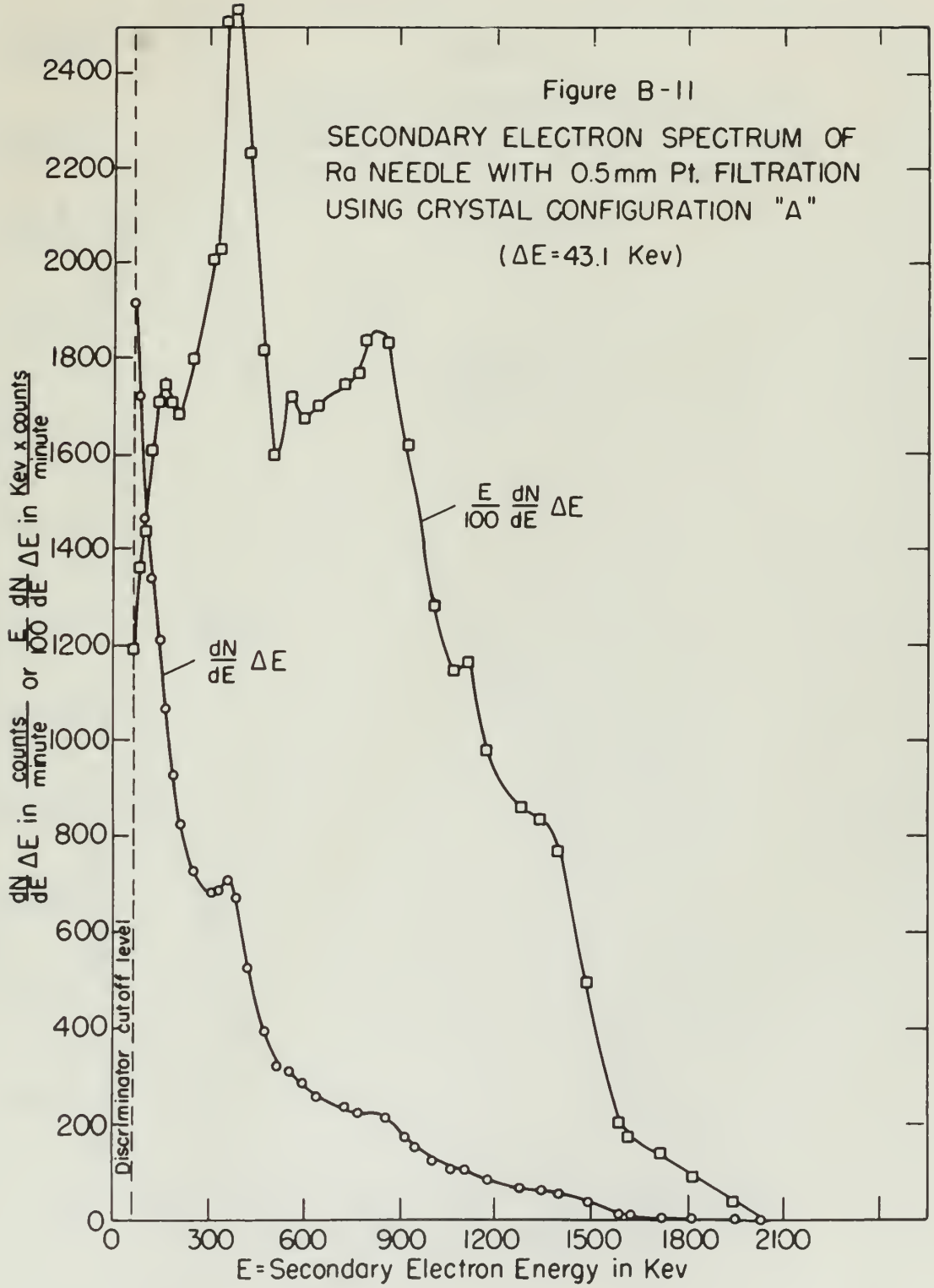
Figure B-11
SECONDARY ELECTRON SPECTRUM OF
Ra NEEDLE WITH 0.5mm Pt. FILTRATION
USING CRYSTAL CONFIGURATION "A"
(ΔE=43.1 Kev)
$\frac{E}{100}\frac{dN}{dE}\Delta E$
$\frac{dN}{dE}\Delta E$
Discriminator Cutoff level
$\frac{dN}{dE}\Delta E$ in $\frac{counts}{minute}$ or $\frac{E}{100}\frac{dN}{dE}\Delta E$ in $\frac{Kev \times counts}{minute}$
E=Secondary Electron Energy in Kev
0
200
400
600
800
1000
1200
1400
1600
1800
2000
2200
2400
0
300
600
900
1200
1500
1800
2100

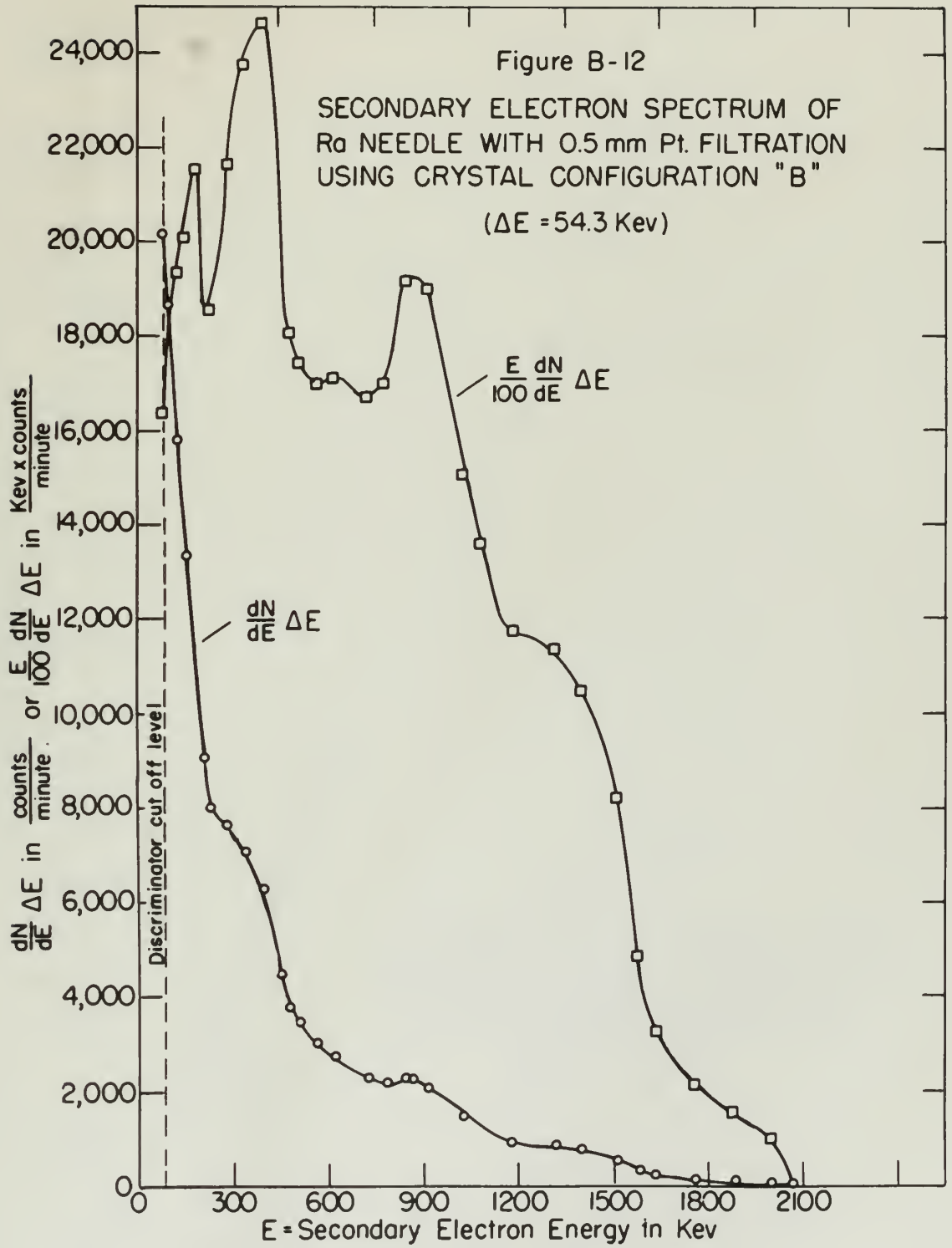
Figure B-12
SECONDARY ELECTRON SPECTRUM OF
Ra NEEDLE WITH 0.5 mm Pt. FILTRATION
USING CRYSTAL CONFIGURATION "B"
(ΔE = 54.3 Kev)
$\frac{E}{100}\frac{dN}{dE}\Delta E$
$\frac{dN}{dE}\Delta E$
Discriminator cut off level
$\frac{dN}{dE}\Delta E$ in $\frac{counts}{minute}$ or $\frac{E}{100}\frac{dN}{dE}\Delta E$ in $\frac{Kev \times counts}{minute}$
E = Secondary Electron Energy in Kev
0
2,000
4,000
6,000
8,000
10,000
12,000
14,000
16,000
18,000
20,000
22,000
24,000
300
600
900
1200
1500
1800
2100

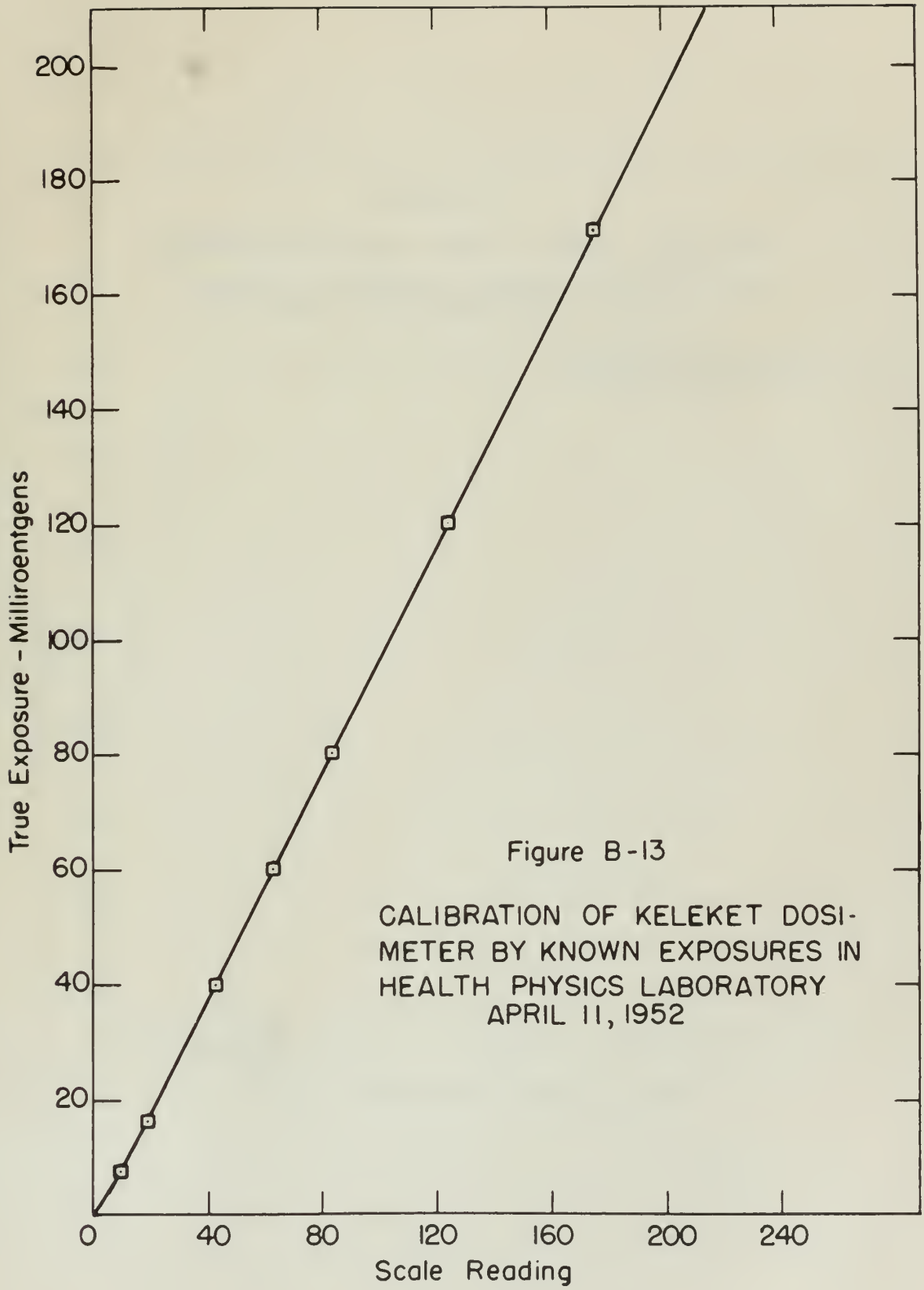

Figure B-13

CALIBRATION OF KELEKET DOSIMETER BY KNOWN EXPOSURES IN HEALTH PHYSICS LABORATORY APRIL 11, 1952

Figure B - 14

CORRECTION FACTOR FOR KELEKET DOSIMETER

(corrects for variation in response to lower gamma ray energies). As distributed by manufacturer.

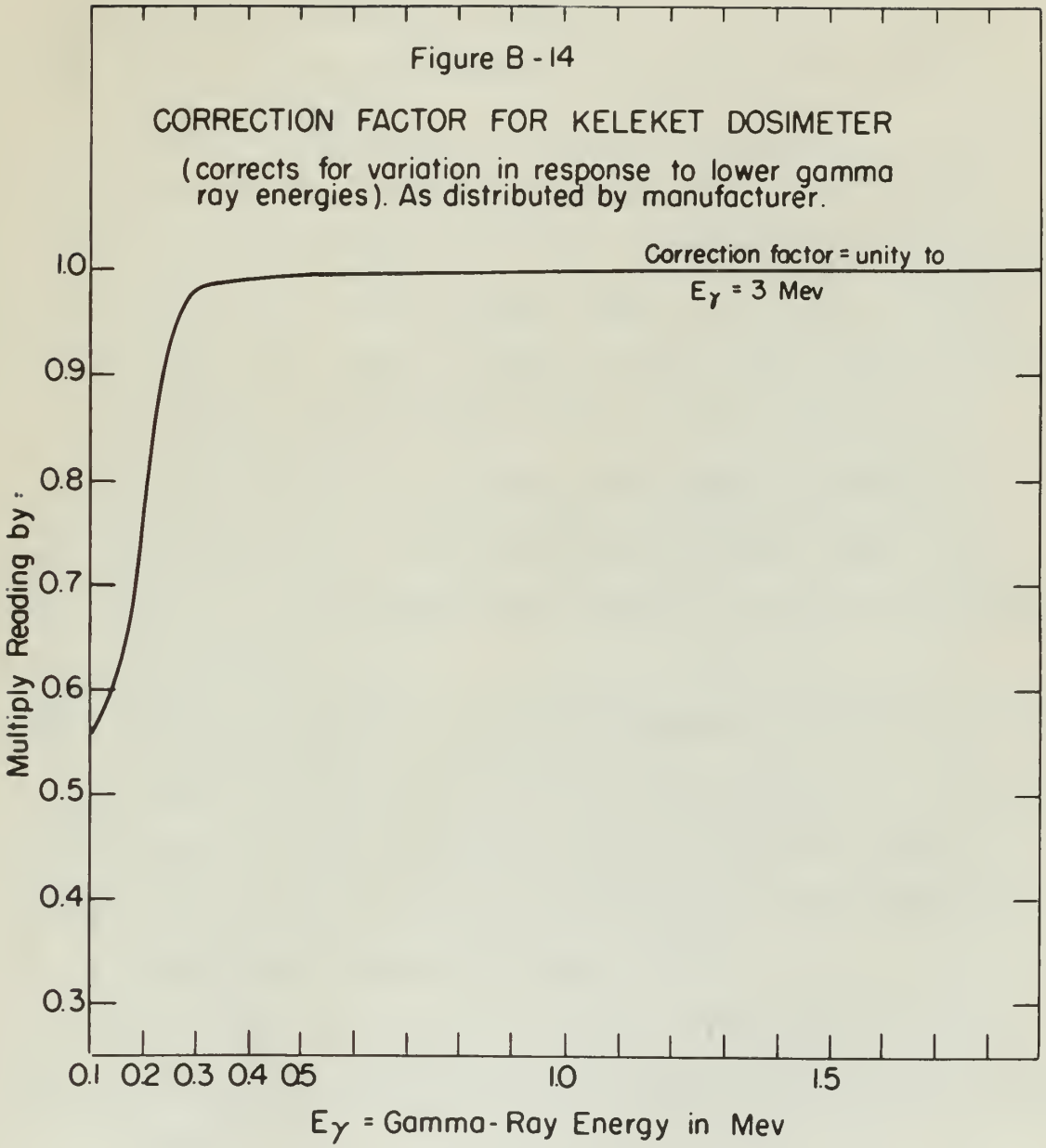

BIBLIOGRAPHY

1. Ittner, W. B., III, Ter-Pogossian, M.; Nucleonics 10, No. 2, February 1952.
2. Glass, F. M., and Hurst, G. S.; Rev. Sci. Inst. 23, 67 (1952).
3. Evans, R. D.; Nucleonics 1, No. 2?, October 1947.
4. Gray, L. H.; Proc. Roy. Soc. (London) 156A, 578 (1936).
5. Gray, L. H.; Proc. Cambr. Phil. Soc. 40, 72 (1944).
6. LNSE, Mass. Inst. of Tech., Tech. Report No. 55, Jan. 1952.
7. Hopkins, J. I.; Phys. Rev. 77, 406 (1950).
8. Hopkins, J. I.; Rev. Sci. Inst. 22, 29 (1951).
9. Davisson, C. L. M.; MIT Ph. D. Thesis, 1948.
10. Evans, R. D.; Unpublished chapter on gamma interactions, May 1951.
11. Goodman, C.; "Science and Engineering of Nuclear Power", Vol. 1, Addison and Wesley Press, 1947.
12. Kine, G. J.; Nucleonics 7, No. 4, October 1950.
13. Lea, D. E.; "Action of Radiation on Living Cells", Cambridge University Press, 1946.
14. Victoreen, J. A.; Jour. Appl. Phys. 14, 95 (1943).
15. Latter, R., and Kahn, H.; "Project Rand" Report R-170, 1949.
16. Kine, G. J.; Nucleonics 10, No. 1, January 1952.
17. Whitcher, S. L.; Nucleonics 10, No. 4, April 1952.
18. Fluharty, R. G.; Nucleonics 3, No. 1, July 1948.

BIBLIOGRAPHY

19. Elmore, W. C., and Sands, M.; "Electronics", McGraw-Hill (1949).

20. Kip, A., Bousquet, A., Evans, R. D., and Tuttle, W.; Rev. Sci. Inst. 17, No. 9, 343 (1946).

21. Kine, G. J.; LNSE, MIT Progress Report, 29 Feb. 1952.

22. MIT, Eng. Memo. No. 18, Servomechanism Lab., page 4 (1951).

23. Taylor, C. J., Jentschke, W. K., Remley, M. E., Eby, F. S., and Kruger, P. G.; Phys. Rev. 84, 1034 (1951).

24. Kine, G. J.; Phys. Rev. 81, 755 (1951).

25. Ellis, C. D., and Aston, G. H.; Proc. Roy. Soc. 129A, 180 (1930).

26. Sloan-Kettering Institute, New York, N. Y., Electrometer Circuit Model 204.

27. Rossi, B. B., and Staub, H. H.; "Ionization Chambers and Counters; Experimental Technique of", McGraw-Hill (1949).